

# Grid-friendly Dispatch Strategy of PV Generation System with Battery Energy Storage



A Dissertation Submitted in Partial Fulfillment of the Requirements  
for the Degree of Doctor of Philosophy in Electrical Engineering  
Department of Electrical Engineering  
FACULTY OF ENGINEERING  
Chulalongkorn University  
Academic Year 2019  
Copyright of Chulalongkorn University

กลยุทธ์การจัดสรรกำลังการผลิตที่เป็นมิตรกับโครงข่ายไฟฟ้าของระบบผลิตไฟฟ้าพลังงาน  
แสงอาทิตย์ร่วมกับการกักเก็บพลังงานด้วยแบตเตอรี่



วิทยานิพนธ์นี้เป็นส่วนหนึ่งของการศึกษาตามหลักสูตรปริญญาวิศวกรรมศาสตรดุษฎีบัณฑิต  
สาขาวิชาวิศวกรรมไฟฟ้า ภาควิชาวิศวกรรมไฟฟ้า  
คณะวิศวกรรมศาสตร์ จุฬาลงกรณ์มหาวิทยาลัย  
ปีการศึกษา 2562  
ลิขสิทธิ์ของจุฬาลงกรณ์มหาวิทยาลัย

Thesis Title                      Grid-friendly Dispatch Strategy of PV  
    Generation System with Battery Energy Storage  
By                                      Mr. Sarute Srisontisuk  
Field of Study                      Electrical Engineering  
Thesis Advisor                      Associate Professor NAEBBOON  
    HOONCHAREON, Ph.D.

---

Accepted by the FACULTY OF ENGINEERING, Chulalongkorn  
University in Partial Fulfillment of the Requirement for the Doctor of  
Philosophy

..... Dean of the FACULTY OF  
ENGINEERING  
(Professor SUPOT TEACHAVORASINSKUN,  
Ph.D.)

DISSERTATION COMMITTEE

..... Chairman  
(Professor DAVID BANJERDPONGCHAI,  
Ph.D.)

..... Thesis Advisor  
(Associate Professor NAEBBOON  
HOONCHAREON, Ph.D.)

..... Examiner  
(Associate Professor SURACHAI  
CHAITUSANEY, Ph.D.)

..... Examiner  
(Associate Professor KULYOS  
AUDOMVONGSEREE, Ph.D.)

..... External Examiner  
(Professor Issarachai Ngamroo, Ph.D.)

..... External Examiner  
(Somphop Asadamongkol, Ph.D.)

ศรุต ศรีสันติสุข : กลยุทธ์การจัดสรรกำลังการผลิตที่เป็นมิตรกับโครงข่ายไฟฟ้าของระบบผลิตไฟฟ้าพลังงานแสงอาทิตย์ร่วมกับการกักเก็บพลังงานด้วยแบตเตอรี่. (Grid-friendly Dispatch Strategy of PV Generation System with Battery Energy Storage) อ.ที่ปรึกษาหลัก : รศ. ดร. แนนบุญ หุนเจริญ

แนวโน้มการเพิ่มขึ้นของโรงไฟฟ้าพลังงานแสงอาทิตย์ลดความทนทานด้านเสถียรภาพของระบบไฟฟ้า เพราะการลดลงของความถี่และความสามารถเชิงอัตราการผลิตหรือลดกำลังผลิตไฟฟ้าของระบบในการจัดการกับปัญหาดังกล่าวอันเนื่องมาจากสัดส่วนโรงไฟฟ้าพลังงานแสงอาทิตย์ที่เพิ่มสูงขึ้น ผู้ดูแลระบบและโรงไฟฟ้าแสงอาทิตย์ควรพิจารณาปรับปรุงการเดินเครื่องผลิตไฟฟ้าสำหรับผู้ดูแลระบบ ค่าวิกฤตความสามารถเชิงอัตราการผลิตหรือลดกำลังผลิตไฟฟ้าที่สัมพันธ์กับสัดส่วนโรงไฟฟ้าพลังงานแสงอาทิตย์สามารถนำมาใช้ประโยชน์เพื่อกำหนดขอบเขตค่าสุดของความสามารถเชิงอัตราการผลิตหรือลดกำลังผลิตไฟฟ้า เพื่อรองรับเหตุไม่คาดหมายกรณีอุปกรณ์ถูกปลดออกจากระบบ 1 ชิ้น และการรบกวนอื่นที่คาดการณ์ไว้ ในการศึกษานี้ ผลการทดสอบแสดงว่าระบบสามารถปฏิบัติงานได้อย่างปลอดภัยที่สัดส่วนโรงไฟฟ้าพลังงานแสงอาทิตย์สูงถึงร้อยละ 40 เมื่อค่าวิกฤตความสามารถเชิงอัตราการผลิตหรือลดกำลังผลิตไฟฟ้าอยู่ระหว่าง 0.05-0.09 ต่อหน่วยต่อนาที ในกรณีเดียวกัน หากสัดส่วนขนาดของการรบกวนที่คาดการณ์ไว้ของกำลังผลิตรวมของโรงไฟฟ้าแสงอาทิตย์มีค่าต่ำกว่า 0.3 จะไม่มีความจำเป็นต้องจำกัดอัตราการผลิตหรือลดกำลังการผลิตของโรงไฟฟ้าแสงอาทิตย์ในแต่ละโรง สำหรับเจ้าของโรงไฟฟ้าแสงอาทิตย์ กลยุทธ์การจัดสรรกำลังการผลิตที่เป็นมิตรกับโครงข่ายไฟฟ้า สามารถชดเชยการลดลงของรายได้จากการขายพลังงานด้วยรายได้ส่วนเพิ่มที่มาจากค่าบริการควบคุมโหลดและความถี่ ยิ่งไปกว่านั้น วิธีที่นำเสนอซึ่งหลีกเลี่ยงการจำกัดที่ไม่จำเป็นของพลังงานไฟฟ้าที่ได้จากแสงอาทิตย์ โดยนำไปใช้ให้บริการควบคุมโหลดและความถี่ และบริการสนับสนุนเชิงความถี่ และหลีกเลี่ยงการเสื่อมสภาพของแบตเตอรี่ โดยการใช้กำลังผลิตสำรองภายในแทนเพื่อการสนับสนุนเชิงความถี่ ในภาพรวม เมื่อทำเช่นนี้ ส่งผลให้ความมั่นคงเชิงความถี่ของระบบดีขึ้นร้อยละ 16.6 ขณะที่สมรรถนะโรงไฟฟ้าแสงอาทิตย์มีค่าดัชนีการทำตามสัญญาขายไฟล่วงหน้าหนึ่งวันที่ร้อยละ 94.3 และค่าดัชนีการทำตามสัญญาการควบคุมโหลดและความถี่ที่ร้อยละ 73.88 ตามลำดับ

สาขาวิชา วิศวกรรมไฟฟ้า

ลายมือชื่อนิติ

ปีการศึกษา 2562

ลายมือชื่อ อ.ที่ปรึกษาหลัก

# # 5871456321 : MAJOR ELECTRICAL ENGINEERING

KEYWO Grid-friendly dispatch strategy, PV generation system,

RD: Battery energy storage, Power system

Sarute Srisontisuk : Grid-friendly Dispatch Strategy of PV Generation System with Battery Energy Storage. Advisor: Assoc. Prof. NAEBBOON HOONCHAREON, Ph.D.

High PV penetration reduces stability tolerance due to the lower of system inertia and system ramp capability. To handle higher PV penetration issues, the system operator and PV owners should consider the operation improvement. For the system operator, critical system ramp capability with respect to PV penetration ratio can be useful to determine the lower bound of system ramp capability for handling N-1 contingency and expected disturbances. In the case study, test results reveal that the system can operate securely with PV penetration ratio up to 40%, in which it will require system ramp capability in the range of 0.05-0.09 p.u./min. In such case, when magnitude ratio of expected disturbance of aggregated PV output power is kept below 0.3, it will not need to impose a PV ramp limit on an individual PV plant. For PV owners, the grid-friendly dispatch strategy can partly compensate decreased revenue from energy payment by additional revenue from load frequency regulation ancillary service. Furthermore, the proposed method avoids unnecessary PV energy curtailment by providing load frequency regulation and frequency support, and avoids battery energy storage degradation by using internal active power reserve for frequency support component, instead. Overall, in so doing, system frequency security can be improved by 16.6%, when PV performance achieves day-ahead scheduled power compliance index at 94.3 % and load frequency power compliance index at 73.88%, respectively.

Field of Study:	Electrical Engineering	Student's Signature
Academic Year:	2019	.....
		Advisor's Signature
		.....

## ACKNOWLEDGEMENTS

First and foremost, I would like to express my gratitude to Chulalongkorn University that granted “The 100th Anniversary Chulalongkorn University Fund for Doctoral Scholarship” and Dr. Naebboon Hoonchareon, my thesis supervisor, for his guidance and direction throughout my Ph.D. program. I would also like to acknowledge him for appointing me as a research assistant during my Ph.D. study. Without his continued support and guidance, I could not have completed this dissertation.

I would like to offer my sincerest thanks to my dissertation committee members: Professor David Banjerdpongchai, Ph.D., Associate Professor Surachai Chaitusaney, Ph.D., Associate Professor Kulyos Audomvongseree, Ph.D., Professor Issarachai Ngamroo, Ph.D. and Somphop Asadamongkol, Ph.D. for agreeing to serve in my committee and for their valuable guidance and input throughout my Ph.D. study.

I am deeply grateful to my colleagues for their help and advice in ways both small and large. There are several people whom I would like to single out for special thanks for their support and assistance which contributed a lot to the completion of this dissertation: Pisitpol Chirapongsananurak and Duangjai Khunsang.

Last but not least, it would have been impossible for me to pursue a Ph.D. without the support from my beloved family. I owe a debt of gratitude to my parents for their unconditional love and endless support, without which I would not have finished this dissertation.

Sarute Srisontisuk

# TABLE OF CONTENTS

	<b>Page</b>
ABSTRACT (THAI) .....	iii
ABSTRACT (ENGLISH).....	iv
ACKNOWLEDGEMENTS .....	v
TABLE OF CONTENTS.....	vi
LIST OF TABLES .....	xi
LIST OF FIGURES .....	xii
NOMENCLATURE .....	xiv
Chapter 1 Introduction.....	1
1.1 Background and Motivation.....	1
1.2 Objectives.....	8
1.3 Scope of Work.....	8
1.4 Methodology .....	10
1.5 Expected Contribution .....	12
1.6 Dissertation Outline .....	12
Chapter 2 Literature Review .....	14
2.1 PV Control and Dispatch Strategy.....	14
2.1.1 Active Power Reserve.....	14
2.1.2 Dispatch Strategy.....	15
2.1.2.1 Deterministic Dispatch Model .....	17
2.1.2.2 Stochastic Dispatch Model .....	18
2.1.2.2.1 Scenario-based Optimization Model.....	18
2.1.2.2.2 Chance-Constrained Optimization Model.....	20
2.2 BES Control and PV-supported Application .....	23
2.2.1 Application of Battery Energy Storage.....	23
2.2.2 Control of State of Charge .....	24

2.3 Grid supports using PV with BES .....	28
2.3.1 Frequency Regulation .....	28
2.3.1.1 Inertia Response Support .....	28
2.3.1.2 Primary Response Support .....	29
2.3.1.3 Load Frequency Regulation.....	32
2.3.2 Ramp Rate Limit .....	33
2.3.2.1 Ramp Control Method.....	33
2.3.2.2 Ramp Limit Requirement .....	37
Chapter 3 System Models and Computation.....	40
3.1 PV Generation Model .....	40
3.1.1 Steady State PV Generation Model .....	40
3.1.2 PV with BES Configuration.....	40
3.2 Battery Energy Storage Model .....	42
3.2.1 BES Operation.....	42
3.2.2 Steady State BES Model.....	44
3.3 Power System Frequency Model.....	45
3.4 Linear Programming Method .....	48
3.4.1 Problem Formulation .....	49
3.4.2 Solution method.....	51
Chapter 4 Power System Frequency in High PV Penetration Network .....	54
4.1 Impact of PV Penetration on Key System Parameters .....	54
4.2 Expected PV Disturbance .....	57
4.3 Frequency Response Analysis.....	58
4.3.1 Frequency Security Index .....	59
4.3.2 Methodology .....	59
4.4 Case Studies .....	61
4.4.1 Frequency Response Characteristics .....	63
4.4.1.1 Effect of PV Penetration Ratio (PVR).....	64
4.4.1.2 Effect of System Ramp Capability (RC).....	65



4.4.2 Nadir Frequency .....	66
4.4.2.1 Effect of PVR and MRED (at RC=0.1p.u./min).....	66
4.4.2.2 Effect of PVR and RC (at 0.1 MRED).....	68
4.4.2.3 Effect of PVR and RC (at 0.03 p.u. Gen-Trip) .....	69
4.4.3 Critical System Ramp Capability .....	70
4.4.4 Conclusion.....	72
Chapter 5 Grid-Friendly Dispatch Strategy .....	74
5.1 Proposed Fundamental Concept .....	74
5.2 Day-Ahead Schedule (DAS) .....	77
5.2.1 Objective Function.....	77
5.2.2 Constraints.....	78
5.2.2.1 BES Model.....	78
5.2.2.2 Ramp Limitation .....	79
5.2.2.3 Power Balance.....	80
5.3 Hour Ahead Operating Reserve Service (HAS).....	81
5.3.1 Rolling Horizon Strategy .....	82
5.3.2 Objective Function.....	82
5.3.3 Constraints.....	83
5.3.3.1 BES Model.....	83
5.3.3.2 Power Balance.....	83
5.4 Real-Time Resource Management (RRM) .....	84
5.4.1 Output Power at PCC.....	85
5.4.2 Real-time Available Operating Reserve .....	87
5.4.3 Real-time PV Power Command .....	88
5.4.3.1 DSC at Real-Time .....	88
5.4.3.2 LRC at Real-Time .....	89
5.4.3.3 BRC at Real-Time.....	90
5.4.3.4 FSC at Real-Time.....	90
5.4.4 Real-time BES Power Command .....	91

5.4.4.1 DSC at Real-Time .....	92
5.4.4.2 LRC at Real-Time .....	92
5.4.4.3 BRC at Real-Time.....	92
5.4.5 Composition of Actual Output Power at PCC.....	93
5.4.5.1 DSC at Real-Time .....	94
5.4.5.2 LRC at Real-Time .....	95
5.4.5.3 BRC at Real-Time.....	95
5.5 Performance Evaluation Index .....	96
5.5.1 Owner Benefit Index.....	96
5.5.1.1 Revenue .....	96
5.5.1.2 PV Utilization Factor.....	98
5.5.1.3 State of Health of Battery .....	98
5.5.2 Grid Benefit Index .....	100
5.5.2.1 Day-ahead Scheduled Power Compliance Index .....	100
5.5.2.2 Load Frequency Regulation Power Compliance Index.....	101
5.5.2.3 Frequency Deviation Index.....	101
Chapter 6 Test Results .....	103
6.1 Simulation .....	103
6.1.1 Test System .....	103
6.1.2 Operating Conditions.....	104
6.1.3 Simulated Test Results.....	107
6.1.3.1 Sufficient Reserve .....	107
6.1.3.2 Insufficient Reserve.....	109
6.1.4 Verification of Power Commands .....	110
6.1.4.1 DSC Component .....	110
6.1.4.2 LRC Component .....	111
6.1.4.3 BRC Component.....	114
6.1.4.4 FSC Component.....	115
6.2 System Frequency Performance Evaluation .....	116

6.2.1 System Frequency Improvement .....	116
6.2.1.1 On Clear-Sky Day .....	117
6.2.1.2 On Rainy-Sky Day .....	118
6.2.2 Sudden Unserve Mitigation.....	119
6.2.2.1 Adaptive BES Power Algorithm (ABA) .....	120
6.2.2.2 Test Results.....	121
6.3 Dispatch Strategy Performance Evaluation .....	124
6.3.1 Owner Benefit .....	126
6.3.2 Grid Benefit.....	127
6.3.3 Overall Comparison.....	128
Chapter 7 Conclusion .....	131
7.1 Conclusion.....	131
7.2 Recommended Future Works.....	132
Appendix A.....	133
Test System Information.....	134
Optimization Information .....	136
REFERENCES.....	137
VITA.....	146

## LIST OF TABLES

	<b>Page</b>
Table 1-1 Additional active power control of PVPP with reserve. ....	7
Table 2-1 Battery application for PV power system [55, 56]. ....	23
Table 2-2 Primary frequency control for conventional generation [29]. ....	30
Table 2-3 Primary frequency control for non-synchronous generator [29]. ....	31
Table 2-4 PV Ramp-rate limit at normal operation [27, 66, 75, 76]. ....	37
Table 2-5 Grid code for Ramp-rate capability [29, 66, 76, 78]. ....	38
Table 4-1 Default values of test system parameters [90]. ....	62
Table 6-1 Parameters of the random noise generator. ....	106
Table 6-2 Owner benefit indexes. ....	126
Table 6-3 DCI and LCI indexes. ....	127
Table 6-4 FDI of 1-year frequency at 0.4 PVL. ....	128
Table A-1 Battery energy storage (BES) parameters. ....	134
Table A-2 PV power plant (PVPP) parameters. ....	134
Table A-3 Default values of network parameters [63]. ....	135
Table A-4 Time step parameters. ....	135
Table A-5 Price coefficients [100]. ....	136

## LIST OF FIGURES

	<b>Page</b>
Figure 1-1 Global PV capacity statistic. [2].....	1
Figure 1-2 Duck curve of California from 2012 to 2020. [9] .....	2
Figure 1-3 Scope of work. ....	9
Figure 1-4 The overview of the methodology.....	11
Figure 2-1 Active power control for PVPP. [47].....	14
Figure 2-2 Time frame of power system operation. [48].....	16
Figure 2-3 SOC partition for regulation. ....	24
Figure 2-4 Feedback SOC control.....	26
Figure 2-5 SOC-f droop cooperate with P-f droop.....	27
Figure 2-6 P-f droop curve.....	29
Figure 2-7 Additional integral control for selected generating unit providing LFR. [63].....	32
Figure 2-8 Ramp regulation concept. ....	34
Figure 3-1 Central configuration of PV generator. [47] .....	41
Figure 3-2 AC-coupled configuration [80]. ....	41
Figure 3-3 DC-coupled configuration [80]. ....	42
Figure 3-4 Power system dynamical model for frequency response study.....	46
Figure 4-1 PV ramp down disturbance. ....	57
Figure 4-2 Frequency response study flow chart. ....	60
Figure 4-3 Tested operating condition with 0.4 PVR.....	62
Figure 4-4 Effect of PVR to frequency response.....	64
Figure 4-5 Effect of RC to frequency response (at PVR 30%).....	65
Figure 4-6 Effect of PVR and MRED (at RC = 0.1 p.u./min). ....	67
Figure 4-7 Effect of PVR and RC (at 0.1 MRED). ....	68
Figure 4-8 Effect of PVR and RC (at 0.03 p.u. Gen-Trip).....	69
Figure 4-9 Critical RC with respect to PVR.....	70

Figure 4-10 Effect of MRED on critical RC. ....	71
Figure 5-1 The overview signal flow between controller and PVPP.....	76
Figure 6-1 Test system diagram. ....	103
Figure 6-2 Noise generator blocks. ....	106
Figure 6-3 Synthesis frequency deviation.....	107
Figure 6-4 Power profile on day 3 (sufficient reserve).....	108
Figure 6-5 Power profile on day 2 (insufficient reserve).....	109
Figure 6-6 DSC profile on day 2.....	111
Figure 6-7 LRC profile on day 2.....	112
Figure 6-8 The combination of DSC and LRC profile on day 2.....	113
Figure 6-9 BES profile on day 2.....	114
Figure 6-10 FSC Profile on day 2.....	115
Figure 6-11 Ppcc Profile on day 2.....	116
Figure 6-12 7-Day Frequency profile at 0.4 PVL.....	117
Figure 6-13 Frequency profile on the clear-sky day.....	118
Figure 6-14 Frequency profile on the rainy-sky day. ....	119
Figure 6-15 Rainy-sky frequency profile of sudden unserve mitigation on day 6...	121
Figure 6-16 Rainy-sky BES profile of sudden unserve mitigation at day 6 .....	122
Figure 6-17 Rainy-sky power profile of sudden unserve mitigation on day 6 .....	123
Figure 6-18 Energy ratio comparison. ....	125
Figure 6-19 Radar graph for performance comparison .....	129

## NOMENCLATURE

$\alpha(t)$	Capacity ratio of the units on-AGC at time t
$\beta$	Primary response characteristic
$\beta_i$	Primary response gain of synchronous generator unit i, with respect to its power rating $S_i$
$\beta_0$	Primary response gain
$\beta_0(t)$	Primary response gain when no PV output power in the system at time t
$\gamma$	Binary variable for activating inertia or primary response command
$\Delta f, df$	Frequency deviation from $f_n$
$ \overline{\Delta f_1} _i$	Absolute one-minute average frequency deviation of minute i
$\Delta P_{i(p.u.)}$	Per unit emulated inertia response power
$\delta$	Binary variable to control charged and discharged power could not occur at the same time
$\varepsilon_f^k$	Forecast error at time k
$\eta_{bd}$	Discharged power efficiency
$\eta_{bc}$	Charged power efficiency
$\eta_{pv}$	Conversion efficiency from radiance to power
$\vartheta$	Maximum confidential interval of actual power deviation
$\mu$	Average value of data set
$\sigma$	Standard deviation of data set
$\Phi'_k$	Conditional probability distribution of $\varepsilon_f^k$

$\omega$	Electrical angular speeds
$\omega_s$	Synchronous angular speeds
A	Matrix of the coefficient of inequality constraints
$A_{eq}$	Matrix of the coefficient of equality constraints
$\bar{A}$	Extended matrix that includes inequality and equality constraints
ABA	Adaptive BES power algorithm
$A_{pv}$	Area of PV panel
b	Vector of right-hand side value of inequality constraints
$b_{eq}$	Vector of right-hand side value of equality constraints
$\bar{b}$	Corresponding vector of extended matrix ( $\bar{A}$ ).
BRC	BES restoration component
$Cap_{bat}$	Battery capacity
$Cap_{cov,max}$	Maximum install capacity of the conventional generator when no PV penetration
$Cap_{gen,off}(t)$	Per-unit off-line rotating capacity at time t
$Cap_{gen,on}(t)$	Per-unit on-line rotating capacity at time t
$Cap_{reg}$	Capacity of renewable generation
$Cap_{pv}$	PV capacity
$Cap_{pv,total}$	Total PV install capacity
$c_p$	Penalty cost coefficient(\$/MWh)
$c_{pv}$	Temperature coefficient
$cp_{ha}$	Hour ahead capacity price coefficient (\$/MW)
$c_r$	Ramp cost coefficient (\$/MW/h)
D	Damping coefficient



DAS	Day-ahead power schedule
da	Case that PVPP provides only DSC
dar	Case that PVPP provides DSC and LRC
darf	Case that PVPP provides DSC, LRC, and FSC
DCI	Day-ahead scheduled power compliance index
$df_{eso}$	Historical frequency deviation of ESO 2019
$d_{full}$	Full-cycle of dept of discharge
$df_{sim}$	Simulated frequency deviation
$d_{half}$	Half-cycle of dept of discharge
$d_{max}$	Maximum allowable deviation factor
DSC	Day-ahead schedule component
$E_b$	BES energy
$E_{b,ch}$	Charged Energy
EDS	Expected disturbance slope
$E_{b,min}$	Minimum of usage BES energy
$E_{b,max}$	Maximum of usage BES energy
$E_{bs}$	BES energy in the simulation model
$\tilde{E}_{b,secure}$	Estimated secure reserve energy
$E_{b,TP}$	Energy throughput of Peukert model
$E_{b,TP}^{life}$	Total energy throughput entire lifetime of the chosen battery
$E_{b,j}$	Extreme battery energy state j (local maximum or local minimum) before changing by charging or discharging
$ep_{da}$	Day-ahead contract energy price coefficient (\$/MWh)
$ep_{nf}$	Non-firm energy price coefficient (\$/MWh).
$E_{r,a}^*$	Actual load frequency regulation command energy

$eR$	External active power reserve
$E_{pv,mppt}$	Maximum PV energy
$E_{pcc,sch}$	Day-ahead schedule energy
$E_{pcc,r}$	Load frequency regulation energy
$E_{pcc,ip}$	Frequency support energy
$E_{pv,curt}$	Curtailement energy
$E_{b,ref}$	SOC set point
$f^*, f_n$	Nominal frequency
$f, f_e$	Power system frequency at steady-state operation
FDI	Frequency deviation index
$f_{hist}$	Historical system frequency
$f_{nadir}$	Nadir frequency
FSC	Frequency support component
$G_F(t)$	Set of off-line rotating synchronous generators at time $t$
$G_O(t)$	Set of on-line rotating synchronous generators at time $t$
GFDS	Grid-friendly dispatch strategy
$\bar{H}$	Average per-unit system inertia
$H$	System inertia constant
$H_i$	Per unit inertia constant of synchronous generator unit $i$ , with respect to its power rating $S_i$
$H_{max}$	Maximum per-unit system inertia
$H_0(t)$	System inertia when there is no PV generated power at time $t$
$H_{0,avg}$	Average per-unit system inertia when no variable renewable generations in the system
HAS	Hour-ahead operating reserve service

$H_{pv}$	Emulated inertia constant provided by PVPP
$I_d$	Identity matrix
$I_{pv}$	Solar radiance
$iR$	Internal active power reserve
$K_{agc,pv}$	Automatic generation control gain for PVPP
$K_b$	BES restoration gain
$K_{in}$	Proportional gain for emulated inertia response power
$k_p$	Peukert lifetime constant
$K_s$	Secondary response gain
$L$	Lagrangian
$lb$	Lower bounds of decision variables vector
LCI	Load frequency regulation power compliance index
LRC	Load frequency regulation component
mppt	Base case that PVPP operates in MPPT mode
$N$	Total number of synchronous generators in the system
$N_p$	Prediction interval
$P_{agc,pv}^*$	Automatic generation power command for PVPP
$P_b^*$	Battery power setpoint sent from the controller
$\tilde{P}_b^*$	Adapted BES power command
$P_{b,ch}^*$	Actual charged power command (negative value)
$P_b$	BES output power
$P_{bc}$	Charged power
$P_{b,ch}$	Actual BES charging power (negative value)
$P_{bc,limit}$	Charged power limit
$P_{bc,max}$	Maximum charged power

$P_{bd}$	Discharged power
$P_{bd,limit}$	Discharged power limit
$P_{bd,max}$	Maximum discharged power
$P_{b,max}$	Maximum power of BES
$P_{b,min}$	Minimum power of BES
$P_{b,n}$	Separated charged power (positive value)
$P_{b,p}$	Separated discharged power (positive value)
$P_{e(p.u.)}$	Per unit electrical power
$P_{eb,a}$	Actual power of BRC without borrowing power
$P_{eb,br}^*$	Borrowed solar power command for BRC
$P_{eb,br,a}$	Actual borrowed power for BRC
$P_{eb,ch}^*$	Restored BES command
$P_{eb,br,uns}$	Un-serve borrowed power of BES restoration
$P_i^*$	Inertia frequency support power command
$P_{ip}^*$	Inertia and primary response power command
$P_{ip,a}^*$	Actual inertia and primary response power command
$P_{ip,a}$	Actual power of FSC without borrowing power
$P_{loads}$	Aggregated load in the power system
$P_{m(p.u.)}$	Per unit mechanical power
$P_n$	Nominal power capacity
$P_{net}(t)$	Netload at time t
$P_{or,a}$	Actual operating reserve
$P_{or,eb}$	BES restoration reserve
$P_{or,ip}$	Inertia and primary response operating reserve
$P_{or,sch}^*$	Hour ahead schedule operating reserve command

$P_{or,sch}$	Hour ahead schedule operating reserve for optimization
$P_{or,sch}^{max}$	Maximum expected available operating reserve power
$\tilde{P}_{or,sch}^{max}$	Modified maximum expected available operating reserve power
$P_{or,sch,v}$	Available hour-ahead operating reserve that frequency regulation power can be supplied, following 100% of the LRC command
$P_p^*$	Primary frequency support power command
$P_{pv}$	Maximum power from the PV power plant
$P_{pv,set}$	PV power set up by inverter follow PV setting command
$P_{pvs}$	Aggregated PV power in the power system
$P_{pv,set}^*$	PV power setpoint sent from the controller
$P_r^*$	Load frequency regulation power requested from the control center
$P_{r,a}^*, P_{r,cmd}$	Actual load frequency regulation power command
$\tilde{P}_r^*$	The adjusted load frequency regulation power command
$P_r$	Power registered capacity
$P_{r,a}$	Actual power of LRC without borrowing power
$P_{r,br}^*$	Borrowed BES power command for LRC
$P_{r,br,a}$	Actual borrowed power for LRC
$P_{r,br,uns}$	Un-serve borrowed power of load frequency regulation
$P_{re}$	Remaining power after using by $P_{sch,br,a}$
$\tilde{P}_{reg}$	Renewable power forecast plus forecast error
$P_{reg}$	Renewable energy generation power
$P_{pcc}$	Power at the point of common coupling

$P_{sch,da}$	Day-ahead scheduling power for optimization
$P_{pcc,eb}$	Restored power at the point of common coupling
$P_{pcc,ip}$	Inertia and primary response power at the point of common coupling
$P_{PCC,max}$	Maximum PV Output
$P_{PCC,min}$	Minimum PV Output
$P_{pcc,r}$	Load frequency regulation power at the point of common coupling
$P_{pcc,sch}$	Scheduled power at the point of common coupling
$p_{sch}$	Scheduled power price(\$/MWh)
$P_{sch,a}^*$	Actual scheduled power command
$P_{sch,a}$	Actual power of DSC without borrowing power
$P_{sch,br}^*$	Borrowed BES power command for DSC
$P_{sch,br,a}$	Actual borrowed power for DSC
$P_{sch,br,uns}$	Un-serve borrowed power of day-ahead schedule
$P_{sch,da}^*$	Day-ahead scheduled power command
$P_{sf}$	Solar power forecast
$P_{sf,da}$	Day-ahead solar forecast power
$\tilde{P}_{sf,da}$	Modified solar forecast power
$P_{sf,ha}$	Hour-ahead solar forecast power
$p_{or}$	Operating reserve price (\$/MW)
$P_{spr}(t)$	Spinning reserve power at time t
PUF	PV Utilization Factor
PVL	PV penetration level
PVR	Higher PV penetration ratio

$q$	Slack variables vector that adapts upper bounds to equality constraints
$Q$	Diagonal matrices related to the vectors $q$
$R$	Droop constant
RBC	Real-time BES power command
$r_c$	Size of $xv$ and $qw$ which are zero vectors at a solution
RC	System ramp capability
$r_d$	Dual residual
$Rev_{da}$	Revenue coming from DSC
$Rev_{mppt}$	Revenue of PVPP that operates base on the MPPT strategy
$Rev_r$	Revenue coming from LRC
ROCOF	The rate of change of frequency
ROR	Real-time available operating reserve
$r_p$	Primal residual
RPC	Real-time PV power command
$R_{pv}$	Primary response gain provided by PVPP
$R_r$	Power ramp rate
RRM	Real-time resource management
$R_{sch}$	Day-ahead scheduled power ramp
$r_{da}$	Reduction factor of day-ahead solar power forecast
$r_{ha}$	Reduction factor of an hour ahead expected operating reserve
$r_{sd}$	Rate of self-discharge of BES
$r_{up}$	Upper bound residual
$r_{vx}$	Lower bound complementarity residual

$r_{wq}$	Upper bound complementarity residual
$s$	Index of scenario
$S$	Total number of all possible scenarios
$S_b$ , baseMVA	System base (MVA)
$S_i$	Power rating of synchronous generator unit $i$
SO	System operator
SOC	State of charge
$SOC_0$	Minimum state of charge
$SOC_d$	Low threshold of state of charge
$SOC_u$	Upper threshold of state of charge
SOH	State of health of battery
spr	Spinning reserve ratio with respect to the net load
$T_g$	Governor time constant
$Tol_p$	Tolerance of primal residual
$Tol_d$	Tolerance of dual residual
$T_{pv}$	PV cell temperature
$t_s$	Timestep
$T_s$	Low pass filter time constant of the noise signal
$T_{secure}$	Defined security duration
$T_t$	Turbine time constant
$t_w$	Time window for ramp rate calculation
ub	Upper bounds of decision variables vector
$v$	Lagrange multipliers related to lower bound
$V$	Diagonal matrices related to the vectors $v$
$w$	Lagrange multipliers related to upper bound
$x$	Decision variables



$X$	Vector of decision variables
$X$	Diagonal matrices related to the vectors $x$
$x_0$	Initial condition of decision variables vector
$x_{feas}$	Feasible set of solutions
$x_{rp}$	Decision variables of relaxed MILP problem



# Chapter 1

## Introduction

### 1.1 Background and Motivation

Photovoltaic power plants (PVPPs) will be more prevalent because of continued decreasing costs of the PV system [1] and global commitment to reduce CO<sub>2</sub> emission. The trend of solar power capacity is increasing, as shown in Figure 1-1.

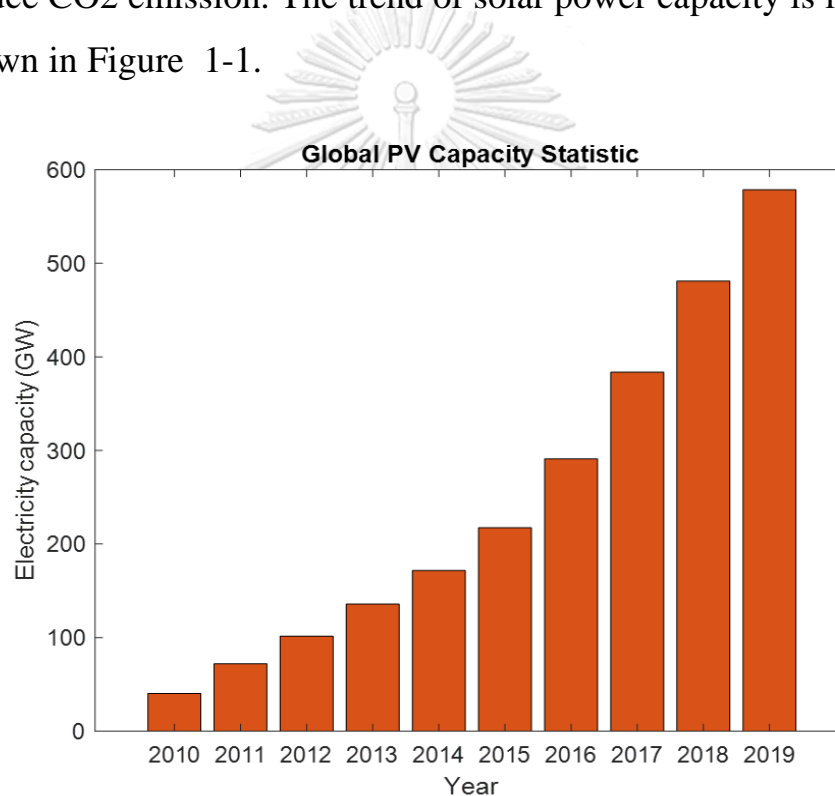


Figure 1-1 Global PV capacity statistic. [2]

The expected higher PV generation increases the problems of integrating a large amount of PV system. To handle this problem, it needs to improve operation from both the system operator and PVPP.

For the system operator side, the first part of this research is to clarify the problem of a large portion of PVPP on stability aspect related system

ramp capability for mainly suggesting critical ramp capability to the system operator. For the PVPP side, the second part of this research will receive the suggestion from the first part to design a grid-friendly dispatch strategy for PVPP with BES for frequency support. It is expected that the higher reliable PV power with stability support will increase the dependability of PV power plants and the amount of clean energy in the network following sustainable development goals [3].

A Higher PV penetration ratio (PVR) will degrade the system frequency response performance of a power system because some intrinsic inertia of synchronous generators is replaced by low/no-inertia of PV power plants [4, 5] [6], [7]. Besides, the reduction of on-line synchronous generators and the high rate reduction of PV power in a high PV penetration network (duck curve) [8] in the afternoon, as shown in Figure 1-2, can lead to another significant concern, that is insufficient of ramp capability.

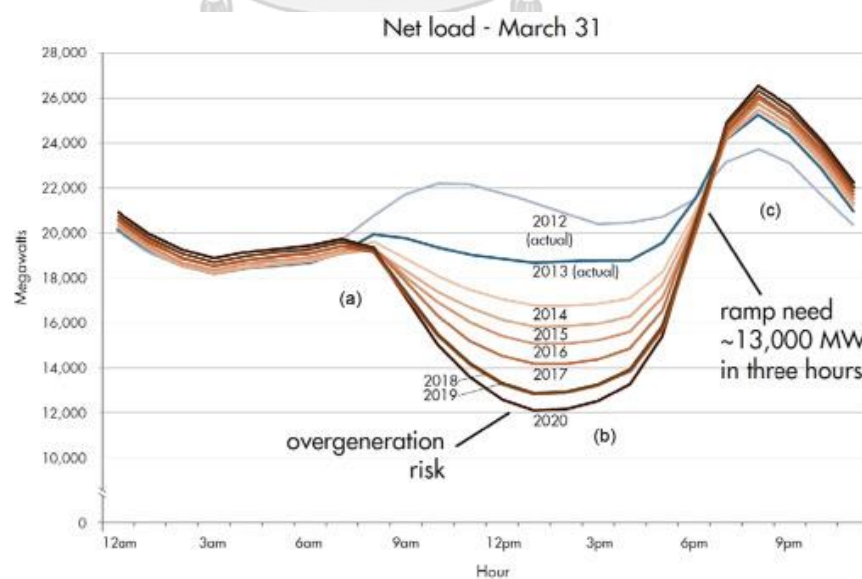


Figure 1-2 Duck curve of California from 2012 to 2020. [9]

The combination of lowering both system inertia and system ramp capability, plus significant intermittency of PV generated power, may easily cause system frequency to deviate beyond acceptable range with respect to generation protection settings. It hence could trigger cascading trips of the generators and lead to the system blackout, eventually.

There are quite a few methods to accommodate high PV penetration, which results in lower system inertia. Those methods can be deployed by both the system operator (SO) and the PV owners. In addition to system inertia and primary response improvement to cope with higher PVR [10], SO should prepare sufficient system headroom and ramp capability in dealing with the high ramp of the net load [11]. Meanwhile, PV owners can also be required to curtail PV power ramp rate to a specific ramp limit so that it can help mitigate the concern of sizable PV disturbance.

Previous research works have revealed influential factors on system frequency response, which are: 1) system inertia [10] that will be reduced due to replacement of rotational generation by inverter-based generation, 2) the amount of power imbalance caused by generation tripping [10], 3) the amount and response time of primary frequency response support [10, 12], 4) control strategy of a renewable power plant [13-15] and 5) headroom or spinning reserve which depends on the obtainable active governor and position of load control [16]. Relevant to the headroom, there has been so far no clear mechanism for estimating suitable headroom requirement on an instantaneous basis [16].

Additionally, ramp capability (RC) of a power system could become significantly lower as PVR increases, and therefore, should be another primary concern of the SO. Most of the previous literature examined ramp capability requirements with respect to quasi-steady state economic

operation and unit commitment problem formulation [11]. In such a case, system ramp capability can be modeled as a ramp rate limit [11, 17, 18]. Moreover, the ramp capability or ramp reserve requirement has been determined by some statistical measures pertinent to the uncertainty of the renewable generated power or the netload forecast information [18, 19]. To our best knowledge, examining ramp capability requirement with respect to the dynamical behavior of a power system with lowering inertia has not yet been reported.

Furthermore, the issue concerning PV intermittence needs being further investigated, especially in a microgrid with low inertia [20]. A steep and significant drop of aggregated PV power, combined with lower system ramp capability, may cause adverse impacts to the system frequency, leading to power system instability. Although the spatial effect of different PV power plants in the transmission system could result in smoothening PV fluctuation [21], a sharp drop of those PV outputs simultaneously could be plausible.

Thus, the first part of this research will investigate the minimum ramp capability requirement, or critical ramp capability, that a power system with lower inertia (high PV penetration) can endure significant disturbance without violating the frequency limit to ensure dynamic system security. In so doing, the effects of sizeable single generation trip (N-1), PV disturbance characteristic, and system ramp capability on system frequency response will be examined at various PV penetration levels. Then, the ramp capability requirement or critical ramp capability at each PVR will be identified with respect to the N-1 contingency security constraint. The condition that would require PV ramp curtailment will also be examined.

From the issues as mentioned above, not only SO should be aware of this expected problem, but PVPP also should be aware and participate in dealing with this problem too because the part of this problem coming from PVPP. The maximum power point tracking (MPPT) strategy, aim to maximize the revenue, is not valid anymore in a high PV penetration network. Therefore, it is necessary to reduce PV power uncertainty, fluctuation, and prevent stability problem related to higher PVPP penetration by improving PVPP operation for power reliability and system frequency support.

The grid integration code plays a vital role in improving the power from PV before injecting it into the network. The power limitation requirement was imposed on PVPP [22] to reduce the high variation of PV power. In reference [23, 24], ramp limiter is used to limit PV power ramp rate. In reference [24], the ramp limiter is coordinated with BES. [25] used a low pass filter or moving average method to determine the smoothed PV power. [26] added power fluctuation cost in the objective function of MPC. [27] provided dynamic ramp rate support with deloading reserve (internal active power reserve,  $iR$ ).

The primary response support requirement for PVPPs is specified in ENSOe, New Zealand, Spain, South Africa, and Puerto Rico [27-29]. The inertia requirement of ENSOe's grid code is not strict. It allows grid operators can freely specify inertia requirements [30]. In South Africa and Puerto Rico have a more strict rule. They require PV reserve by operating below MPP (maximum power point) to provide frequency and voltage support [22]. While Germany, Romania, and China do not require reserve [22]. However, in the near future, it is expected that other countries will establish a power reserve requirement for PVPP [22].

To improve PVPP operation, the key of an additional component to make PVPP possible to schedule PV power with higher accuracy is battery energy storage (BES) because it can absorb excess PV power instead of curtailment and inject stored power when insufficient of scheduled power. However, BES, in a single type of generation system as PVPP, is limit of capacity and could not be restored energy from other resources except uncertain solar power (in case of not allow borrowing power from the grid). Therefore, the energy management system is needed to utilize PVPP power with BES efficiently.

The dispatch strategy is essential to utilize the resource of PVPP with reserve efficiently. [31, 32] dispatch PV power with BES base on forecast power. [26] proposed a dispatch strategy with MPC to minimize operating costs of PVPP with BES. It could reduce PV uncertainty and overall system reserve. [33] solved the optimization problem using the solar power forecast as guideline information to create self-scheduling PV power with primary frequency response support (PFS) reserve.

Although, most RTOs do not trust renewable for participating in ancillary service because of its uncertainty [34]. CAISO found that PVPP can provide 90% accuracy of frequency regulation demand, which is almost double accuracy compare to conventional generator [34]. Besides, PVPP is an inverter-based generator that has fast response performance. Thus, PVPP has the potential to provide this service. While [35], [36], [37] and [38] provided inertia and primary response support with active power control or can be seen as an internal active power reserve (iR).

PVPP with reserve has more flexibility to provide more reliable power (schedulability) and ancillary service support (ramp, inertia, primary, secondary control), as shown in Table 1-1.

There are mixed-generation with reserve providing all additional service [39] mentioned in Table 1-1 in an isolated power system. However, only one renewable resource as PVPP with reserve, providing all mentioned control, has not been found on the grid-connected configuration. Besides, BES providing secondary control is found in reference [40], [41], and [42], which means PVPP with reserve has the potential to provide this service even though secondary control in PVPP has not been found in the literature.

Table 1-1 Additional active power control of PVPP with reserve.

Literature	Ramp Control (1)	Inertia Control (2)	Primary Control (3)	Secondary Control (4)	Schedulability (5)
<b>PVPP with BES</b>					
[23],[24],[25]	/	-	-	-	-
[26]	/	-	-	-	/
[31] [32]	-	-	-	-	/
[33]	/	-	/	-	/
[43]	/	-	/	-	-
<b>PVPP with internal Active Power Reserve (iR)</b>					
[27]	/	-	-	-	-
[44] ,[45]	-	-	/	-	-
[35],[36],[37],[38]	-	/	/	-	-

The cost of PVPP operation will increase [34] to make PVPP with BES more reliable for providing both scheduled power and frequency regulation because it is expected that PVPP should have its reserve[22].



Most of the works use only battery energy storage (BES) to provide frequency support [46]. However, the high duty cycle can reduce the BES's lifetime.

In this research, considering both owner and grid benefit, the grid-friendly dispatch strategy is proposed to efficiently utilization PVPP with both BES and internal active power reserve (iR) to provide multiple services (scheduled power, load frequency regulation, and frequency support). For grid benefit, PVPP will provide scheduled power and frequency support. BES is assigned to increase the reliability of PV power by correcting scheduled power. For owner benefit, PVPP will receive additional income by load frequency regulation service and assign frequency support to internal active power reserve (iR) of PVPP instead of BES to reduce BES degradation.

## 1.2 Objectives

1. Design grid-friendly dispatch strategy to efficiently utilize the resource of PV power plant (PVPP) with BES for reliable power and system frequency support.
2. Propose and demonstrate performance indexes of PV generation system which reflect balancing benefits to both PV owner and grid system operator

## 1.3 Scope of Work

The scope of work, as shown in Figure 1-3, the proposed dispatch strategy is designed for the PV power plant with BES for power reliability and system frequency support.

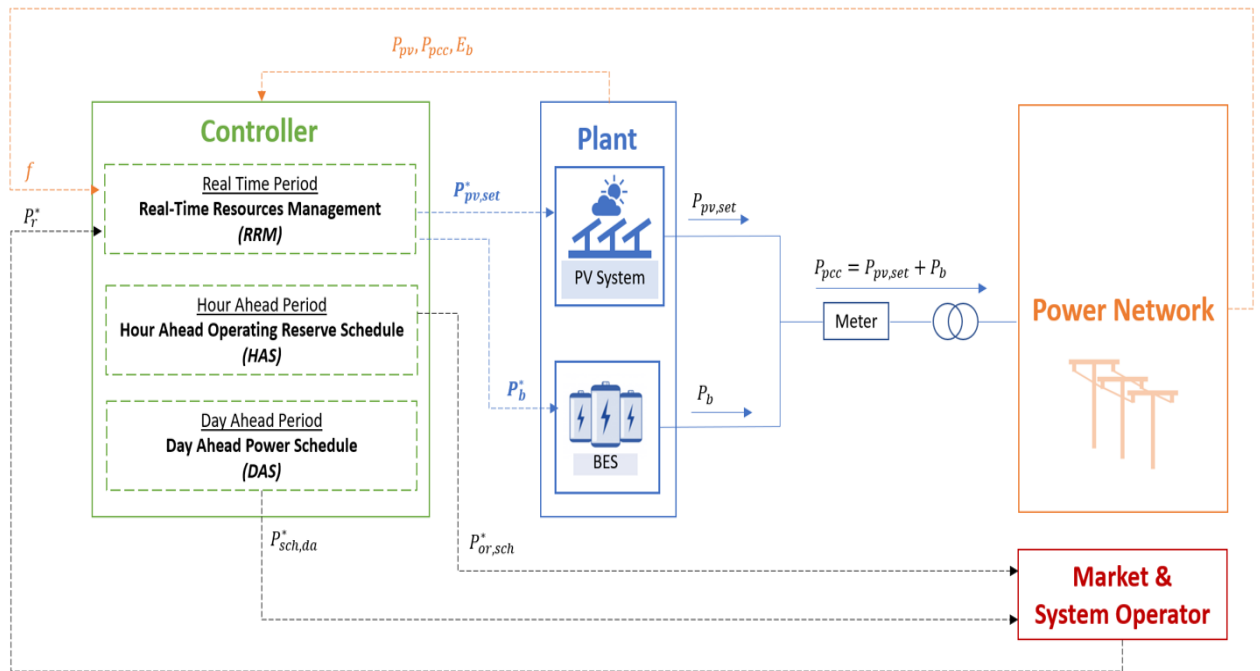


Figure 1-3 Scope of work.

where,  $P_{pv,set}^*$  is the PV power setpoint sent from the controller,

$P_b^*$  is the battery power setpoint sent from the controller,

$P_r^*$  is the load frequency regulation power requested from the control center.

$P_{pv,set}$  is PV power set up by inverter follow PV setting command,

$P_{pv}$  is the maximum power from PV power plant,

$P_b$  is the power from BES,

$P_{pcc}$  is the power at the point of common coupling.

$f$  is the power system frequency.

There are 3 main stages of the proposed grid-friendly dispatch strategy controller separated by the control period from the day ahead to real-time.

1. Day-ahead power schedule (DAS)
2. Hour-ahead operating reserve service (HAS)
3. Real-time resource management (RRM)

This controller monitors plant status ( $P_{pv}$ ,  $P_{pcc}$ ,  $E_b$ ) and local frequency status ( $f$ ), including load frequency regulation command from the system operator before computing the command sent to the PV system and BES. The power plant tries to inject power into the network following the command from the proposed controller.

## **1.4 Methodology**

The overview of the methodology would be shown in Figure 1-4; there are two main parts of the study. The first part is to study the system frequency response of a higher PV penetration network to understand the cause of problem-related to system ramp capability clearly. The results of the first part not only give the insight suggestion to system operator related to critical ramp capability but also give the suggested grid-friendly power control to PVPP. The second part receives the first part's suggestion to develop and evaluate the proposed algorithm by the test system. The result of part two is the grid-friendly dispatch strategy for PV owners.

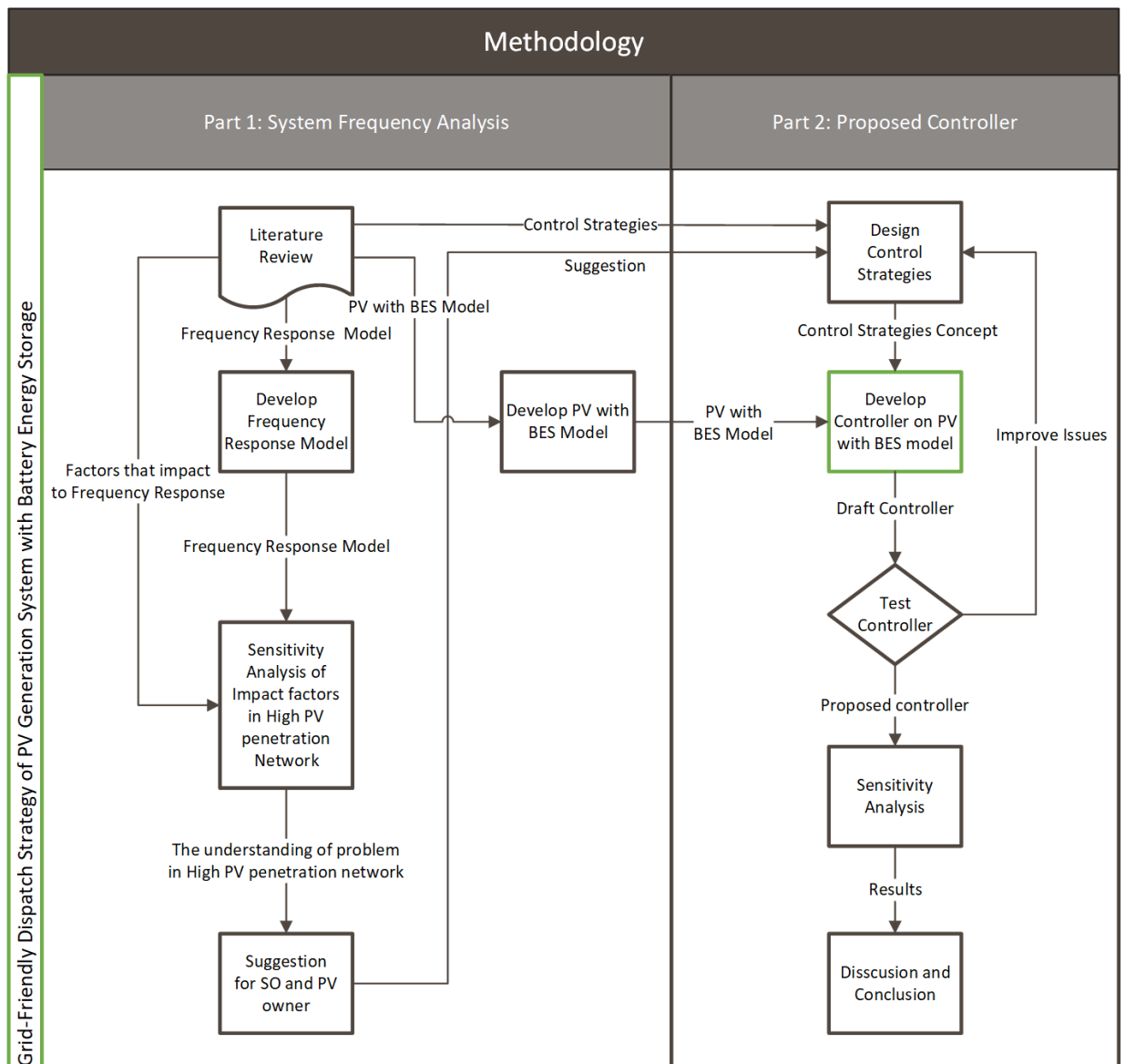


Figure 1-4 The overview of the methodology.

The following numbering can explain the step by step methodology:

1. Review literature:
  - a. Frequency response study in higher PV penetration context
  - b. System frequency response model with ramp capability or ramp limit

- c. PV and Inverter model, characteristic and control
  - d. BES model, application and control
  - e. Dispatch strategies of renewable energy with BES
  - f. Ramp requirement
  - g. Frequency support and control
    - i. load frequency regulation
    - ii. inertia and primary response support
2. Develop a model for frequency response analysis that reflects ramp capability.
  3. Simulate case studies to learn the frequency response impact related to key system parameters. (disturbances, PV penetration ratio, inertia, ramp capability).
  4. Develop a model and controller for PVPP with BES to increase reliability, reduce fluctuation, and provide frequency service.
  5. Evaluate and sensitivity analysis of the proposed controller.
  6. Conclusion and future work.

### **1.5 Expected Contribution**

1. The system frequency response is improved.
2. The reliability of PV power is improved.
3. The utilization of PV and BES resources is improved.
4. PV power fluctuation decrease.

### **1.6 Dissertation Outline**

This dissertation is organized as follows: Chapter 1 presents background and motivation, objective, the scope of work, and methodology. Chapter 2 and Chapter 3 presents the literature review, system models, and computation, respectively. Chapter 4 presents the

study of the impact of a high PV penetration ratio on system frequency related to key system parameters. The main part of this dissertation is in Chapter 5 and Chapter 6 that presents the proposed grid-friendly dispatch strategy, case studies for evaluating the proposed algorithm, both power and system frequency performance, simulation results, and discussion, followed by conclusions in Chapter 7.



## Chapter 2

# Literature Review

A higher level of PV penetration could increase clean resource in the power network. However, the intermittency nature, no inherent inertia, and high ramp of solar power could increase the balancing problem to SO. Although solving a balancing problem is the main duty of SO, the cause of the problem comes from PVPP. Therefore, PVPP should have some responsibility for friendly integration to the network. The methods to improve the integration of PV in terms of active power control will be described in the following sections.

### 2.1 PV Control and Dispatch Strategy

#### 2.1.1 Active Power Reserve

According to Puerto Rico, Romania, South Africa, and Germany grid codes, the active power control of large PVPP should consider power curtailment, ramp rate control, and active power reserve [47], as shown in Figure 2-1.

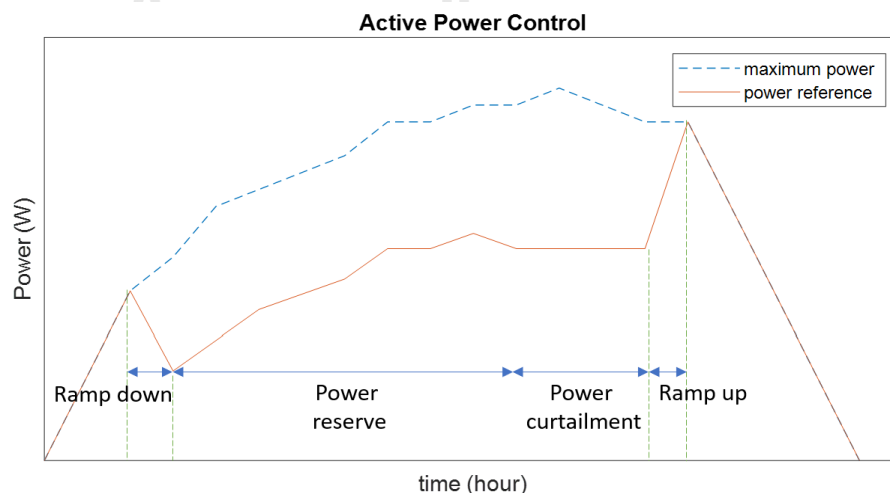


Figure 2-1 Active power control for PVPP. [47]

PVPP can operate in deloading mode instead of MPPT mode to provide an internal active power reserve (iR) [47]. In this mode, PVPP supplies reduced output power; the reduction of power from maximum power is a reserve that can be used co-response to the command.

### **2.1.2 Dispatch Strategy**

The uncertainty and fluctuated solar power are the negative impacts of integrating PVPP into the network. The coordination between PVPP and BES can offer more controllable power by the economic dispatch concept [48].

The economic dispatch (ED) problems are generally formulated and solved with optimization techniques. It requires mathematics objective function and model constraints of a chosen system. This allocation process base on solar power forecast will give generating set points to generation units in the system so that that system demand could be supplied economically [49].

There are two models for ED, deterministic and stochastic ED. Stochastic ED requires an uncertainty model (popular to dealing with uncertainty). In comparison, deterministic ED does not require an uncertainty model which are closeness to the current operation in industry practice [50] that requires a simple structure of optimization with good performance [50].



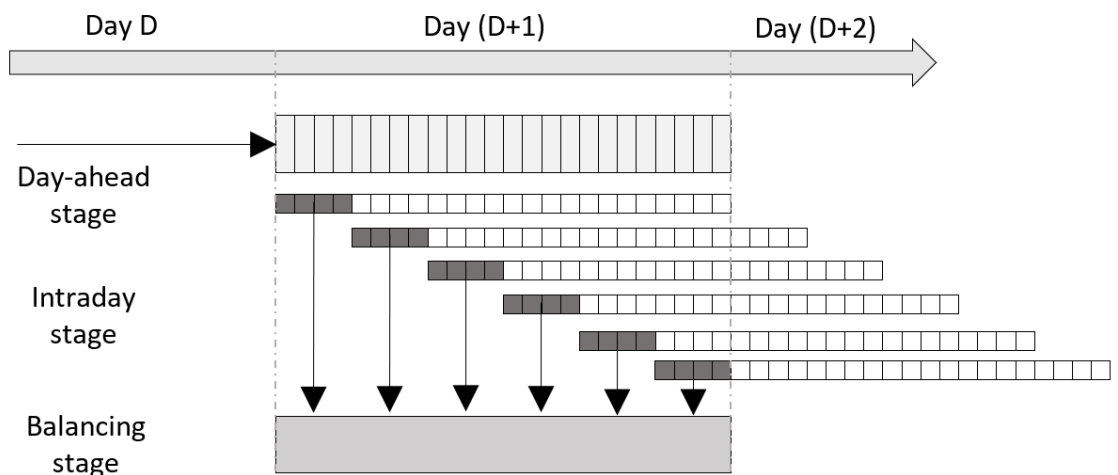


Figure 2-2 Time frame of power system operation. [48]

In power system operation, there are three stages (day-ahead, intraday, and real-time stage), as shown in Figure 2-2.

In the day-ahead stage, the generating unit should send an operation plan to cover 24 hours of the next day (D+1) [48]. The refined schedule power of 10-minute resolution will take place on the intraday stage, and each stage covers four hours [48]. The penalty will be charged when there is the deviation of scheduled power between intraday and day-ahead. At the real-time stage, the penalty will be applied to the power producer when there is a deviation between the scheduled power of intraday and average power output every 10 minutes.[48].

The formulation of the day-ahead and hour-ahead dispatch model is similar except for the updated data and some constraints. Thus, the day-ahead dispatch is only explained in the following section.

### 2.1.2.1 Deterministic Dispatch Model

In the day-ahead stage, the objective is to maximize the revenue subject to the constraints. In the case of PVPP with BES, the objective function can be formulated as an equation

2-1 [48].

$$\max \sum_{k \in t_i}^{t_f} p_{sch}(P_{reg}(k) + P_{bd}(k) - P_{bc}(k))t_s - c_p|P_{reg}(k) + P_{bd}(k) - P_{bc}(k) - P_{sch,da}|t_s \quad 2-1$$

where,  $P_{reg}$  is the renewable energy generation power.  $P_{sch,da}$  is the day ahead of scheduled power.  $P_{bc}$  is charge power to BES.  $P_{bd}$  is discharge power by BES.  $t_s$  is the time step.  $p_{sch}$  is scheduled power price(\$/MWh).  $c_p$  is penalty cost coefficient(\$/MWh).

The power of renewable energy ( $P_{reg}$ ) should not over the forecast power ( $P_f$ ) [48].

$$0 \leq P_{reg}(k) \leq P_f \quad 2-2$$

The schedule power fluctuation can be limited by the following constraint [48].

$$\begin{aligned} (1 - d_{max})P_{sch,da} &\leq P_{reg}(k) + P_{bd}(k) - P_{bc}(k) \\ &\leq (1 + d_{max})P_{sch,da} \end{aligned} \quad 2-3$$

where,  $d_{max}$  is the maximum allowable deviation factor.

The steady-state model of PVPP and BES are described in section 3.1.1 and 3.2.2, respectively.

### 2.1.2.2 Stochastic Dispatch Model

The day-ahead solar and wind power forecast still has a large error as 10-20%. [21, 51] . To incorporate the power forecasts error to the day-ahead schedule, the scenario-based and chance-constrained stochastic optimization models are suitable, as explained in the following section.

#### 2.1.2.2.1 Scenario-based Optimization Model

The uncertainty of solar power can be expressed by scenarios within the defined time horizon. Each power forecast profile in the possible set of forecast distribution represents one of the possible scenarios. The objective function of the scenario-based optimization model can be expressed in the following equation [48].

$$\max \sum_{s=1}^S w_s \sum_{k \in T_f} p_{sch} (P_{reg}(k) + P_{bd}(k) - P_{bc}(k)) t_s - c_p |P_{reg}(k) + P_{bd}(k) - P_{bc}(k) - P_{sch,da}| t_s \quad 2-4$$

where, S is the total number of all possible scenarios.  $w_s$  is the probability weight of scenario s.

Renewable power forecast can be modeled by different distributions [52]. Assuming the error of forecast distribution follows a normal distribution  $N(\mu, \sigma^2)$ , the weigh probability of scenario s ( $w_s$ ) of three scenarios [53] can be expressed by the following equation [48].

$$\left\{ \begin{array}{l} w_1 + w_2 + w_3 = 1 \\ w_1 x_1 + w_2 x_2 + w_3 x_3 = \int_{-\infty}^{\infty} f(x) x dx = \mu \\ w_1 x_1^2 + w_2 x_2^2 + w_3 x_3^2 = \int_{-\infty}^{\infty} f(x) x^2 dx = \mu^2 + \sigma^2 \end{array} \right. \quad 2-5$$

where,  $x_1, x_2$  and  $x_3$  are the scenarios of  $-3\sigma, 0$ , and  $3\sigma$ , respectively.  $w_1, w_2$  and  $w_3$  are the weighted probability of scenarios, respectively. Assuming  $\mu = 0$  and  $\sigma = 0.1P_f$ , solving the above equations get  $w_1 = w_2 = 0.056$  and  $w_3 = 0.888$ .

Considering the correlation between the consecutive time interval and number of scenarios (the numerical stability problem can occur when more than ten scenarios are taken into account, the sampling-based on forecast error distribution and autocorrelation of renewable power are applied on simulation-based methods [54]. Then, a suitable number of scenarios and corresponding weight are obtained by the clustering method or scenario reduction.

The deviation of power out of scenario  $s = 2$  ( $\mu = 0$ ) will be limited, as shown in the following equation [48].

$$\begin{aligned} (1 - d_{\max})P_{\text{sch,da}} &\leq P_{\text{reg,s}}(k) + P_{\text{bd}}(k) - P_{\text{bc}}(k) \\ &\leq (1 + d_{\max})P_{\text{sch,da}}, s = 2 \end{aligned} \quad 2-6$$

where,  $P_{\text{reg,s}}$  is the renewable power of scenario  $s$ .

For, the extreme scenarios  $s = 1, 3$ , the power deviation of power output is not limited by  $d_{\max}$ , but it requires sufficient reserve for PVPP

with BES to meet the extreme condition instead, as shown in the following equation [48].

$$P_{\text{reg},s}(k) + P_{\text{bd,max}} \geq P_{\text{sch,da}}, s = 1,3 \quad 2-7$$

#### 2.1.2.2.2 Chance-Constrained Optimization Model

The chance-constrained programming is presented to handle the uncertain of the parameter represented by random distributions. In many optimization problems, some constraints cannot always be accomplished, or the costs are very high. To relaxed this problem, the chosen constraints are converted to chance-constraints and a preset chance of meeting all or part of the inequality constraints lower than 1.

Chance-constrained optimization objective function can be formulated as the deterministic optimization model, as shown in equation

2-1 . The only difference is the replacement of chosen deterministic constraints to chance constraints with different confidential levels to reduce the actual power output fluctuation, as shown in the following equation [48].

$$\text{Prob}\{\tilde{P}_{\text{reg}}(k) + P_{\text{bd}}(k) - P_{\text{bc}}(k) \leq (1 + \vartheta)P_{\text{sch,da}}\} \geq \rho_{\alpha} \quad 2-8$$

$$\text{Prob}\{(1 - \vartheta)P_{\text{sch,da}} \leq \tilde{P}_{\text{reg}}(k) + P_{\text{bd}}(k) - P_{\text{bc}}(k)\} \geq \rho_{\beta} \quad 2-9$$

where,  $\text{Prob}\{\cdot\}$  is the probability of chance-constraints.  $\tilde{P}_{\text{reg}}$  is a renewable power forecast with the random variable of forecast error.  $\rho_{\alpha}, \rho_{\beta}$  are the probabilities of the power output that not violate the upper and lower limit, respectively.  $\vartheta$  is the maximum confidential interval of actual

power deviation. This  $\vartheta$  should be appropriately considered base on the value of  $\rho_\alpha$ , and  $\rho_\beta$ .

$\tilde{P}_{\text{reg}}(k)$  is the forecast power ( $P_f(k)$ ) plus the forecast error ( $\varepsilon_f^k$ ) at time  $k$ , as shown in the following equation [48].

$$\tilde{P}_{\text{reg}}(k) = P_f(k) + \varepsilon_f^k(\rho) \quad 2-10$$

The minimum of  $\tilde{P}_{\text{reg}}$  is zero, whereas the maximum of  $\tilde{P}_{\text{reg}}$  is the install capacity of renewable generation ( $\text{Cap}_{\text{reg}}$ ). Thus, the range of forecast error is between  $-P_f(k)$  to  $\text{Cap}_{\text{reg}} - P_f(k)$ . Based on normal distribution, the conditional probability distribution ( $\phi'_k$ ) of  $\varepsilon_f^k$  can be expressed in the following equation [48].

$$\phi'_k(\rho) = \frac{\phi_k(\rho) - \phi_k(-P_f(k))}{\phi_k(\text{Cap}_{\text{reg}} - P_f(k)) - \phi_k(-P_f(k))} \quad 2-11$$

where,  $\phi'_k(\rho) \sim N(0, (0.1P_f(k))^2)$ ,  $\rho$  is the probability of the power output that does not violate the upper and lower limit.

The inverse function of  $\phi'_k(\rho)$  is the following equation [48].

$$\phi_k'^{-1}(\rho) = \phi_k^{-1} \left[ \rho \phi_k(\text{Cap}_{\text{reg}} - P_f(k)) - (1 - \rho) \phi_k(-P_f(k)) \right] \quad 2-12$$

From equation 2-11 and 2-12, the constraints in equation 2-8 and 2-9 are equivalent to the following equation [48].

$$\begin{aligned}
(1 - \vartheta)P_{\text{sch,da}} + \Phi_k'^{-1}(\rho_\beta) &\leq P_{\text{reg}}(k) + P_{\text{bd}}(k) - P_{\text{bc}}(k) & 2-13 \\
&\leq (1 + \vartheta)P_{\text{sch,da}} - \Phi_k'^{-1}(\rho_\alpha)
\end{aligned}$$

The upper bound should be higher than the lower bound, as shown in the following equation [48].

$$\{(1 + \vartheta)P_{\text{sch,da}} - \Phi_k'^{-1}(\rho_\alpha)\} - \{(1 - \vartheta)P_{\text{sch,da}} + \Phi_k'^{-1}(\rho_\beta)\} \geq 0 \quad 2-14$$

Then, simplify equation 2-14 to be the following equation [48].

$$\Phi_k'^{-1}(\rho_\alpha) + \Phi_k'^{-1}(\rho_\beta) \leq 2\vartheta P_{\text{sch,da}} \quad 2-15$$

The simple alternative way to construct chance constraints can be expressed in the following equation [48].

$$\text{Prob}\{P_{\text{reg}}(k) \leq \tilde{P}_{\text{reg}}(k)\} \geq \rho'_\alpha \quad 2-16$$

$$\text{Prob}\{P_{\text{reg}}(k) \geq \tilde{P}_{\text{reg}}(k)\} \geq \rho'_\beta \quad 2-17$$

$$\rho'_\alpha + \rho'_\beta < 1 \quad 2-18$$

The constraint 2-17 and 2-18 can be converted to inverse function, as shown in the following equation [48].

$$F_{\rho'_\beta}^{-1}\{\tilde{P}_{\text{reg}}(k)\} \leq P_{\text{reg}}(k) \leq F_{1-\rho'_\alpha}^{-1}\{\tilde{P}_{\text{reg}}(k)\} \quad 2-19$$

where,  $F_{\rho_{\beta}}^{-1}\{\tilde{P}_{\text{reg}}(k)\}$  is the inverse function of renewable power distribution of quantile corresponding to  $\rho_{\beta}'$ .

## 2.2 BES Control and PV-supported Application

### 2.2.1 Application of Battery Energy Storage

BES can be installed in any part of the power system. It can improve generation flexibility in various applications and can be categorized by its application in Table 2-1 (C-rate is a ratio of charge-discharge power to energy capacity).

Table 2-1 Battery application for PV power system [55, 56].

<< High C-rate		Low C-rate >>
Regulation and Ancillary service		Energy management application
Seconds	Minute	Hours
<ul style="list-style-type: none"> <li>- Frequency support</li> <li>- Reactive power/Voltage support</li> <li>- Power quality</li> </ul>	<ul style="list-style-type: none"> <li>- Smoothing or ramp rate control</li> <li>- Balancing with spinning reserve</li> <li>- Frequency regulation</li> <li>- Voltage regulation</li> <li>- Emergency support</li> <li>- Black start</li> </ul>	<ul style="list-style-type: none"> <li>- Load leveling</li> <li>- Peak Shaving</li> <li>- Energy shifting</li> <li>- Economic dispatch</li> <li>- Unit commitment</li> <li>- Isolated operation</li> <li>- Renewables generation integration</li> </ul>

Without battery energy storage, GPVS cannot handle the case that requires additional power such as the correction of mismatch between scheduled PV power and actual PV power, down ramp regulation, and



under frequency events. In contrast, it can support the case of excess PV power by curtailment power, resulting in the loss of clean energy and revenue. Therefore, the battery energy storage is the critical components for dispatchable PV power and frequency support function because it can absorb excess PV power, instead of curtailment, and inject stored power to correct mismatch power and support frequency requirement.

### 2.2.2 Control of State of Charge

Even though the battery energy storage is fast enough to handle fast power changes, the energy capacity and life cycle are limits. Therefore, the energy management system is needed to efficiently utilize GPVS power to ensure BESS having an adequate reserve to handle power mismatch and expand battery lifetime.

There are two directions for regulation support. The first direction is upward regulation, where BESS operates as a power absorption unit when PV power exceeds the limit. The second direction is downward regulation, where BESS operates as a generating unit when PV power is below the limit.

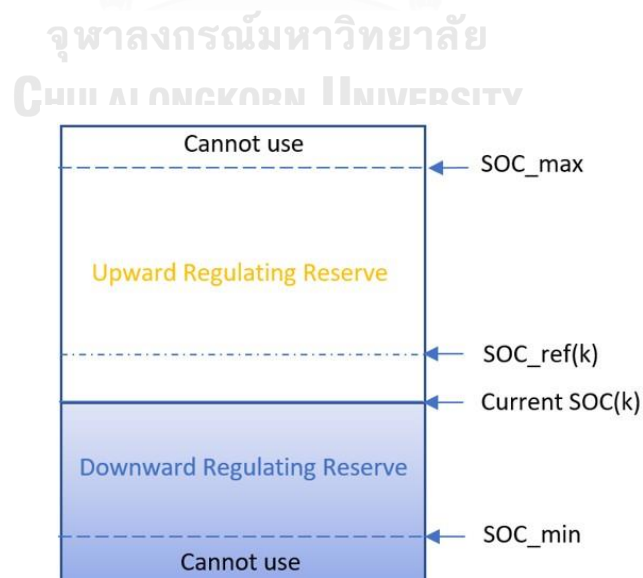


Figure 2-3 SOC partition for regulation.

In the case of no BESS management, when BESS is full during upward regulation of PV power, the excess power needs to be curtailed instead of charging power to BESS, which is a loss of clean energy. In contrast, BESS has not enough power to regulate a downward direction if BESS is empty. Thus, BESS should prepare both regulating upward and downward reserve, as shown in Figure 2-3.

For upward regulation, BESS should reserve space for charging. In contrast, BESS should maintain SOC at some level to handle the uncertainty of downward regulation. The SOC limitation range with considering the depth of discharge typically limits between 0.2-0.8, which has 60% in regulating range. While [43] controls SOC between 0.4-0.6, which has 20% in regulating range to expand BESS lifetime. Reference [25, 57] control SOC at convenient setting constant reference at 0.5 for reserving charge and discharge capacity. While [23] calculates SOC reference by taking the worst-case fluctuation model into account. Reference [58] applies droop for SOC control related to frequency. In reference [26, 59], prediction ability was implemented in the controller to improve performance. In conclusion, from the mentioned literature, there are three methods for SOC control in regulating application. 1. Feedback control, 2. SOC control by droop and 3. Predictive control.

### 1) Feedback Control

Feedback control uses set point error to tune current SOC to meet the reference point that is calculated from the chosen algorithm. In reference [59], the feedback SOC control was proposed; the diagram is shown in Figure 2-4. First control strategy, SOC set point ( $E_{b,ref}$ ) is constant at 50% while  $E_{b,ref}$  of second control strategy with proportional control is

based on maximum and minimum PV power output in a function of the worst fluctuation model [60].

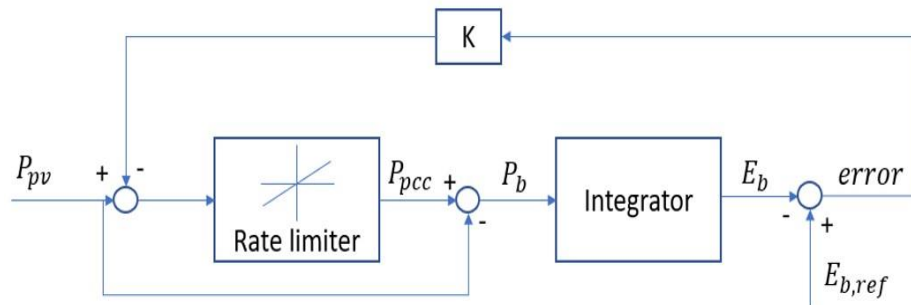


Figure 2-4 Feedback SOC control.

In reference [61], SOC management used the SOC feedback controller with a classic PI controller that tuning control parameters by gravitational search algorithm (GSA) and particle swarm optimization (PSO). In reference [62], the membership function of SOC for the fuzzy logic controller was set to command battery to charge and discharge when SOC is low and high, respectively.

## 2) SOC Control by Droop

Reference [58] uses SOC-f droop to control SOC to cooperate with P-f droop, as shown in Figure 2-5. During nominal frequency, the SOC controller keep SOC in the safe range between  $SOC_d$  to  $SOC_u$ . When the frequency is over the nominal frequency, PV power starts to decrease, and the excess power will store to BESS, then SOC will increase. While SOC will decrease and PV power will maintain at the maximum power point when operating frequency is under nominal frequency.

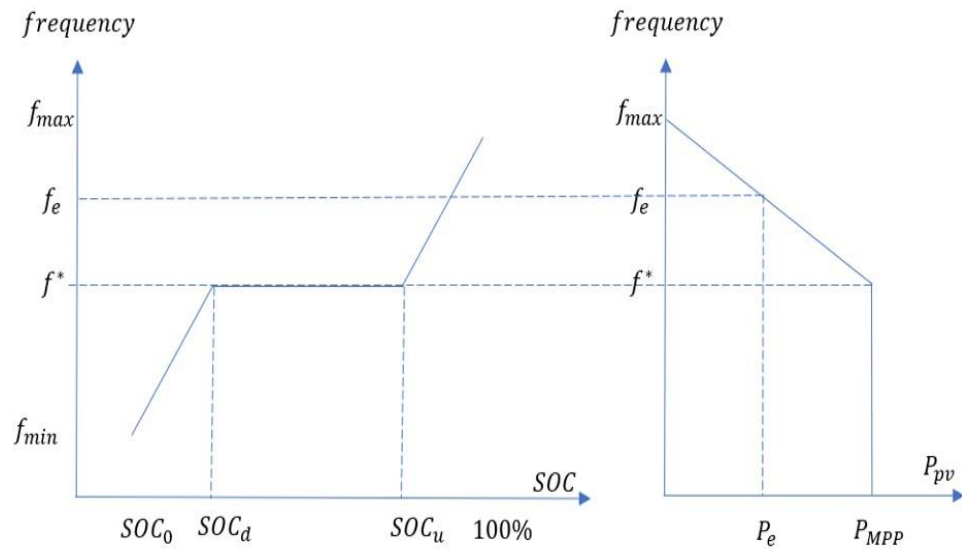


Figure 2-5 SOC-f droop cooperate with P-f droop.

where,  $SOC_0$  is minimum SOC,  $SOC_d$  is a low threshold.  $SOC_u$  is an upper threshold.  $f^*$  is nominal frequency.  $f_e$  and  $P_e$  is the frequency and power at steady-state operation.

### 3) Predictive Control

In reference [59], the saturation of ES can be anticipated by a predictive model in real-time energy management of GPVS with energy storage (ES). So, MPC with ES can manage the uncertainty of energy production for committing in the daily and intraday electricity markets to maximize revenue by reducing the economic penalty. Reference [26] proposed MPC for the grid-connected PV storage system to schedule storage for energy shifting and smoothed power over the control horizon by minimizing operating cost, the magnitude of power fluctuation in terms of cost, while receiving an online request or price signal from the system operator. The additional objective was added to expand battery lifetime by penalizing over-charge and over-discharge.

## 2.3 Grid supports using PV with BES

### 2.3.1 Frequency Regulation

#### 2.3.1.1 Inertia Response Support

Inertia response is the intrinsic behavior of released and stored kinetic energy of the rotating machine related to the power imbalance between demand and supply, as shown by swing equation 2-20 [63].

$$\frac{2H}{\omega_s} \frac{d\omega}{dt} = P_{m(p.u.)} - P_{e(p.u.)} \quad 2-20$$

where, H is per unit inertia.  $\omega$  and  $\omega_s$  are electrical and synchronous angular speeds, respectively.  $P_{m(p.u.)}$  and  $P_{e(p.u.)}$  are per unit mechanical and electrical power as an input of generator, respectively.

The inverter-based generation does not have this behavior, so that it does not automatically respond to the imbalance between demand and supply in the power system. However, the inertia response could be emulated via power electronic technology of inverter correspond with local measured frequency, as shown in equation 2-21. It could be seen as proportional control co-response with the rate of change of frequency.

$$\Delta P_{i(p.u.)} = -K_{in} \frac{df}{dt} \quad 2-21$$

where,  $\Delta P_{i(p.u.)}$  is per unit emulated inertia response power.  $K_{in}$  is the proportional gain for emulated inertia response power.

The inertia support is necessary for a small microgrid with a high inverter-based generation ratio. Thus it is expected that the transmission

system of high PV penetration level is also required the inertia emulation. It is expected that the inertia emulation feature will be in the future grid code. [64]. As specified in the EU-grid code, the value of the inertia requirement can independently specify by relevant TSO [28].

### 2.3.1.2 Primary Response Support

The regular operating frequency in many countries is 49.5-50.5 Hz [29]. When the frequency is out of range, conventional and renewable generation can provide a primary response control, as shown in Figure 2-6.

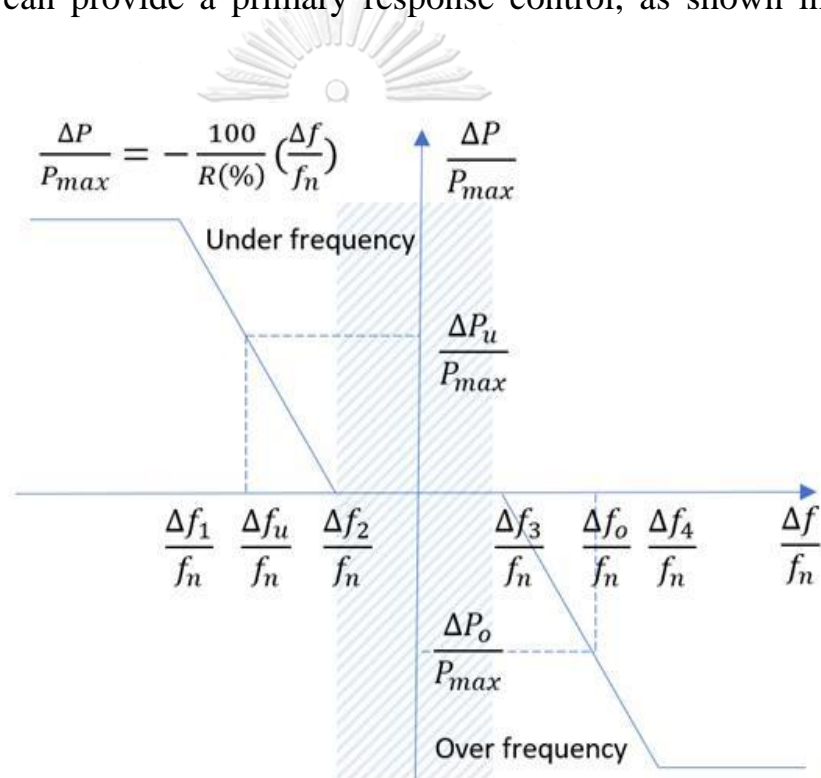


Figure 2-6 P-f droop curve.

Denote that  $f_n$  is nominal frequency,  $\Delta f$  is frequency deviation from  $f_n$ , and  $P_{max}$  is maximum power allocated for primary frequency support. The regulating power of the generator unit can be calculated by this curve. When the frequency deviation is  $\Delta f_o/f_n$  between  $\Delta f_3/f_n$  to  $\Delta f_4/f_n$  which is over frequency event, the generator unit should reduce power by

$\Delta P_o/P_{\max}$  correspond to  $\Delta f_o/f_n$ . In contrast, when the frequency deviation is  $\Delta f_u/f_n$  between  $\Delta f_1/f_n$  to  $\Delta f_2/f_n$  which is under frequency event, the generator unit should increase power to the setpoint  $\Delta P_u/P_{\max}$  correspond to  $\Delta f_u/f_n$ . The active power support range is between 1.5-10%, while the droop constant (R) varies between 2 to 12% [65]. The dead band of droop between  $\Delta f_2/f_n$  to  $\Delta f_3/f_n$  lies in the range 0-500 mHz [65], which is the difference between grid codes for preventing slightly response [29].

Some grid codes, as shown in

Table 2-2 requires a large inverter-based generator providing grid frequency support by Power-frequency (P-f) droop control when the frequency is out of the specified range [29].

Table 2-2 Primary frequency control for conventional generation [29].

Region	Droop Gain	Deadband	Response Time
Thai (IPP)[66]	4% for gas turbine	-	-
France SEI	3-8%	$\pm 15$ mHz	15 s
GB	3-5%	$\pm 15$ mHz	-
Northern Ireland	4%	-	-
Republic of Ireland	-	$\pm 15$ mHz	30 s
New Zealand	0-7%	-	-
Spain SEIE	2-5%	$\pm 30$ mHz	30 s

Previously, only conventional generators provide Power-frequency (P-f) droop control by the governor, which calculates regulating power output corresponds to rotor synchronous speed deviation. When the

inverter-based generators with no inertia become more abundant, they should provide P-f droop control for supporting grid frequency like conventional generators. The regulating power can be obtained from energy storage or curtailment or demand response [67]. Some countries' grid codes also require primary frequency control for non-synchronous generating units, while some countries do not require, which is shown in Table 2-3.

Table 2-3 Primary frequency control for non-synchronous generator [29].

Region	Droop Gain	Deadband	Response Time
Thai (IPP)[66]	-	-	-
France SEI	3-8%	$\pm 15$ mHz	15 s
Northern Ireland	4%	-	-
Republic of Ireland	-	$\pm 15$ mHz	30 s
New Zealand	0-7%	-	-
Spain SEIE	2-6.66%	$\pm 30$ mHz - $\pm 200$ mHz	15 s

The dead band is using for preventing too often frequent response on tiny frequency variation, which may lead an unstable control [67]. Besides, during frequency within the dead band, energy storage can regain energy from renewable energy resources to the setpoint level. The frequency regulation is the most expensive operational cost in the ancillary service market, which needs a fast response in the range of 2-15 seconds [68]. In reference [67], UK national grid creates a new service to enhanced frequency response (EFR) with fast response units such as



battery energy storage (BES). There are narrow and wide services with  $\pm 15\text{mHz}$  and  $\pm 50\text{mHz}$  dead-band, respectively.

Enhanced frequency response service is created by the national grid [69]. It is explicitly designed for fast response capability as a BES for delivering this service with the following requirement [69].

1. can provide service within 1 second
2. can provide both directions (export or import from the network)
3. can provide 100% capacity at least 15 minutes
4. can provide at least 95% availability to quality for full payment

### 2.3.1.3 Load Frequency Regulation

Inertia and primary response by generating unit can reduce frequency deviation due to load fluctuation. However, only primary control cannot return the steady-state frequency to the nominal value because the load changes all the time. The power system requires automatic generation control (AGC) or load frequency regulation (LFR) to adjust load reference setpoints of selected generating units to following total demand.

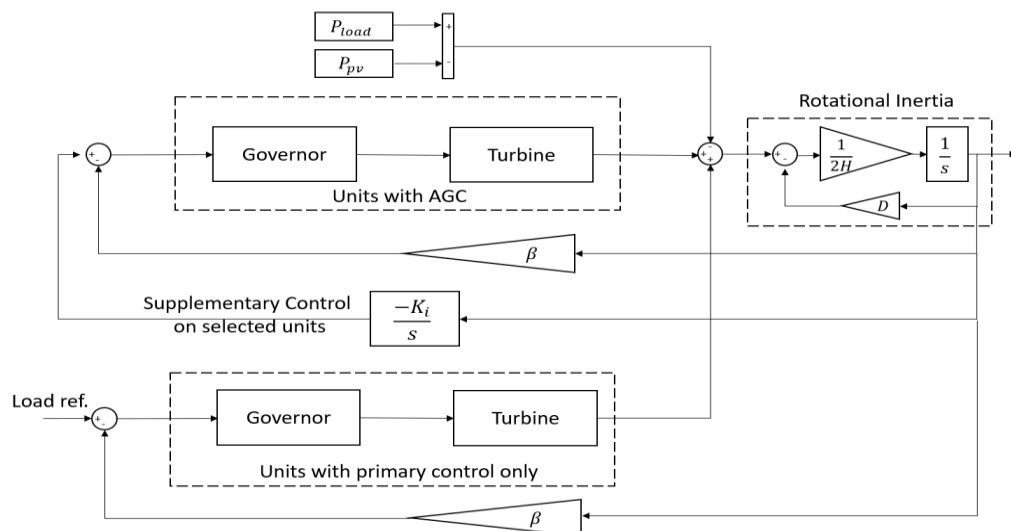


Figure 2-7 Additional integral control for selected generating unit providing LFR. [63]

The integral control will be added to generate a load reference setpoint and ensure zero error of frequency deviated from the nominal value in the steady-state, as shown in Figure 2-7.

### 2.3.2 Ramp Rate Limit

Generated power ramp rate ( $R_r$ ) can be calculated by equation 2-22.

$$R_r(k) = \frac{P(k) - P(k - 1)}{t_w} \quad 2-22$$

where,  $P$  is power and  $t_w$  is a time window for ramp rate calculation [70]. The events that the current power ramp rate is over the specified ramp rate limit (RRL) are called ramp events [70].

#### 2.3.2.1 Ramp Control Method

The basic concept of ramp rate control is to lower the power ramp rate. For the downward power ramp rate regulation, it needs supporting energy from energy storage (ES). While upward power ramp rate regulation does not need ES, it can curtail excess power. However, curtailment is a loss of clean energy. So, BES is the buffer component that necessary for both side regulation by absorb excess power in upward regulation and discharge power in downward regulation, which can be shown in Figure 2-8.

The smoothening strategies or ramp rate controls have been proposed in many studies. There are moving average smoothening (MA) method, exponential smoothening (ES) method, ramp rate limiter method, filtering method, fuzzy logic control, rule-based method, and model predictive control. All methods try to smooth power without considering the ramp

rate limit except the ramp rate limiter method. However, they can add a ramp rate limit to their strategy to compile with grid code requirements.

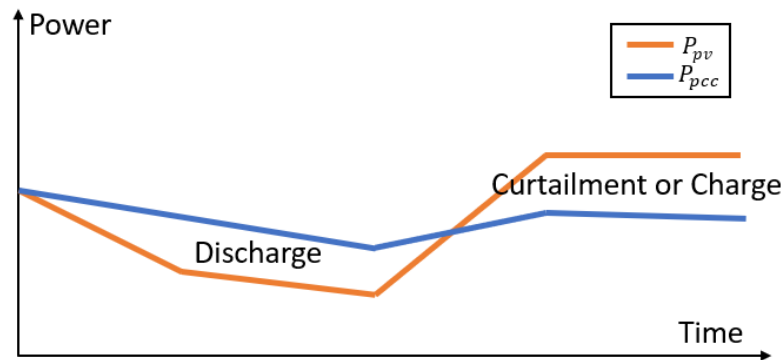


Figure 2-8 Ramp regulation concept.

where,  $P_{pv}$  is maximum PV power and  $P_{pcc}$  is power at the point of common coupling.

### 1) moving average smoothening (MA) method

Reference [71] and [72] used the moving average smoothening (MA) method, but [72] has two modes, first is MA and second is the following center of fluctuation (FCF) method that finds the average of max and min value during the interested period (10 minutes) to find a set point for significant PV fluctuation. MA with FCF has slightly better performance when compared to MA at the shorter average time.

Reference [31] proposed an hourly dispatchable rule base for BESS to set BESS power reference correspond with the power set point, determined by the next average hour solar power output while considering SOC and depth of discharge constraints. The power setpoint is the next average solar power output. This study used a third-order battery model that represents charge/discharge, self-discharge, and

overcharge properties. This method is also used in reference [62] that enhances battery management by SOC feedback control, which tuned control parameters by gravitational search algorithm (GSA) and particle swarm optimization (PSO).

## **2) exponential smoothing (ES) method**

Reference [73] used conventional exponential smoothing method (CES) of past data with fuel cell compared with the case of CES using solar power forecast (SF) data. The results showed that CES with SF has a slightly higher suppression performance than CES with past data. However, it requires more energy than another one as a result of lower fuel cell LOLP.

Reference [74] proposed an exponential smoothing method with modifications (CESM) comparing with the moving average method (MA) and the conventional exponential smoothing method (CES). The classic MA uses an average 41 data point of past data to set the smoothed power output in the current time step. In comparison, CES considers all data points and emphasizes more recent data points by giving continuously growing weights ( $\alpha=0.1$ ). Both MA and CES use much energy from storage and do not impose ramp rate requirements in the method, while the proposed CESM includes a 10% ramp rate limit in the CES method.

## **3) ramp rate limiter method**

In reference [23], the PV ramp rate has a downward and upward direction. In the upward direction, the power electronic function in the inverter can curtail over the limit power of PV power output directly without storage. In contrast, the downward direction needs external power from energy storage to regulate the net ramp rate within limit by ramp limiter ramp.

Reference [24] proposed new ramp rate control without memory effect, which can bias the smoothing reference PV output. It controls the ramp rate only when the PV ramp rate is out of constraints, which means the energy utilization can be improved. The ramp rate limit at each time is the difference, which depends on the PV ramp rate and SOC at that time. The desired ramp rate limit can be calculated by the proposed droop characteristic, which depends on the PV ramp rate at ramping events or SOC during out of ramping events.

#### **4) filtering method**

Reference [25] has two choices of control methods that consist of low pass filter and MA. The SOC was tracking by the proportional control to the set point of 0.6.

Reference [27] proposed a dynamic power ramp rate control (D-PRL) for large PV power plants and compared them with static power ramp rate control (S-PRC). S-PRC is a lower pass filter that does not consider the ramp rate limit, and the controller time constant is constant. While D-PRL time constant is dynamic and depends on power fluctuation and assigned ramp rate.

#### **5) model predictive control**

Reference [26] proposed MPC for a grid-connected PV storage system to schedule storage for energy shifting and smoothed power over the control horizon while receiving an online request or price signal from the system operator. Their objective function is to minimize operating costs, the magnitude of power fluctuation in terms of cost. The smoothness can measure by maximum range, the rate of change, and curvature. They also set an additional objective to expand battery lifetime by penalizing over-

charge and over-discharge. Their MPC time step and horizon is 4 minutes interval over 12 hours, which is a standard for DR and price signals.

### 2.3.2.2 Ramp Limit Requirement

With the rapid growth of renewable energy to the grid, the disturbance from the intermittency nature of renewable resources will become more concerned with a spinning reserve and stability issue. Thus, fluctuated power output will be limited by the ramp rate limit. PVPP requirements in some countries require a power ramp rate limit to reduce disturbance, which is governed by grid code [29] [27], as shown in Table 2-4.

Table 2-4 PV Ramp-rate limit at normal operation [27, 66, 75, 76].

Region	Ramp Up	Ramp down
PREPA (Puerto Rico)	10% $P_n$ /min	10% $P_n$ /min
Germany	10% $P_n$ /min	No req.
Australian	10% $P_n$ /min	10% $P_n$ /min (if the inverter has storage)
HECO (Hawaii)	1-2 MW/min	1-2 MW/min
HECO (Hawaii)	1-2 MW/s	1 MW/2s
ENTSO-E	-	-
THAI (PEA/EGAT)	-	-

From Table 2-4, PREPA, Germany, and Australian grid codes have the same 10% $P_n$ /min ramp rate limit while some grid codes such as ENTSO-E, PEA, and EGAT do not mention it. Germany grid code only set ramp rate limit for ramp-up rate. Thus, Intermittent generators in Germany do not require energy storage for controlling the required ramp rate, while renewable energy generation in PREPA, Australian, and

HECO may need energy storage to compensate for the power ramp rate within the ramp-down limit. Furthermore, In Hawaii island have a specific grid code to limit instantaneous ramp while many islands such as Azores, Canary, Pantelleria island does not mention about both typical and instantaneous ramp cases [77]. In another aspect of the ramp rate requirement, some grid codes do not set a ramp rate limit, but they set the minimum ramp rate capability requirement in both directions instead, as shown in Table 2-5.

Table 2-5 Grid code for Ramp-rate capability [29, 66, 76, 78].

Region	Ramp Up	Ramp down
EirGrid (CG, WF, DR)	1.5% $P_r$ /min	1.5% $P_r$ /min
Australian (CG)	3% $P_n$ /min	3% $P_n$ /min
Northern Ireland (CG)	3% $P_n$ /min	3% $P_n$ /min
Germany (CG)	1% $P_n$ /min	1% $P_n$ /min
Germany (IG)	-	10% $P_n$ /min
Thailand (PEA/EGAT) (IG)	-	10% $P_n$ /min

CG = conventional generators, IG = inverter based generators, WF=Wind farm DR= Demand respond unit,  $P_n$ =nominal power capacity,  $P_r$ = power registered capacity

From Table 2-5, Eirgrid is the most comprehensive grid code, which includes wind farms and demand response units that are connected to the network. The registered capacity is only used in this grid code while other grid codes use nominal power capacity as a unit. Grid code in Germany and Thailand is noticed that there is only a ramp down capability requirement for inverter-based generators, which implies that it does not

require energy storage. While the Danish grid code sets a ramp rate capability of the wind turbine to provide grid support in the broader range for 10-100%  $P_n$ /min when requested.





## Chapter 3

### System Models and Computation

#### 3.1 PV Generation Model

##### 3.1.1 Steady State PV Generation Model

Solar power is converted to electricity by a solar panel. Solar power directly depends on solar radiance, temperature, and size. For power system operation, solar power can be represented by the simplified model, as shown in equation 3-1[79].

$$P_{pv} = I_{pv}A_{pv}\eta(1 - cT_{pv}) \quad 3-1$$

where,  $P_{pv}$ ,  $I_{pv}$ ,  $A_{pv}$ ,  $\eta_{pv}$ ,  $T_{pv}$  and  $c_{pv}$  are solar power, solar radiance, the total area of PV panel, conversion efficiency from radiance to power, PV cell temperature, and temperature coefficient.

The major drawback of PV power is the uncertainty of solar power due to cloud cover. Thus, the reserve is necessary to increase the reliability of PV power.

##### 3.1.2 PV with BES Configuration

Large PVPP have hundreds of PV panel interconnected by three topologies as radial, ring, and star [47]. The most used topology is the radial configuration with a single inverter, as shown in Figure 3-1.

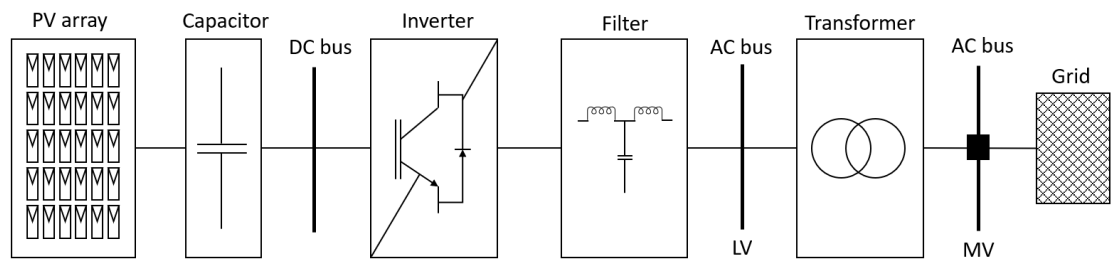


Figure 3-1 Central configuration of PV generator. [47]

The active power control for PVPP can incorporate with BES to improve reliability. There are two main configurations of utility-scale PV with BES [80].

- 1) **AC-Coupled System** is the configuration that both PV and BES have their inverter. The coupling between components is on the AC side of the inverter, as shown in Figure 3-2.

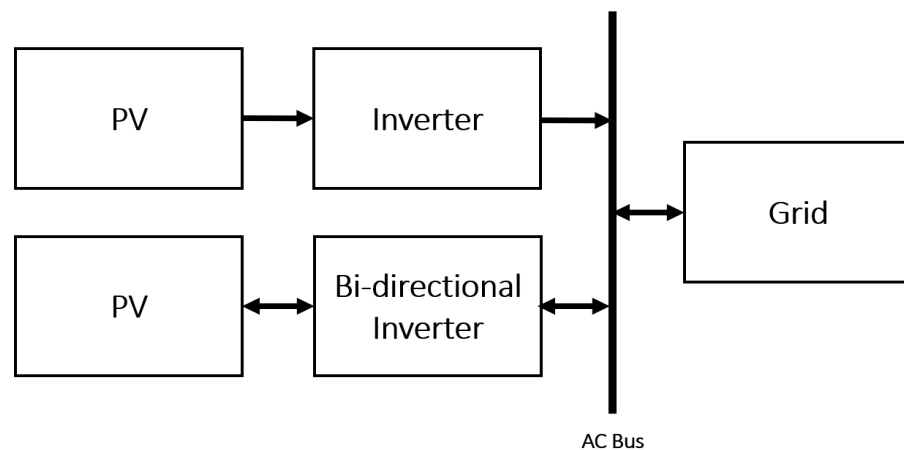


Figure 3-2 AC-coupled configuration [80].

From Figure 3-2, this configuration is easier to upgrade and install because the inverter is connected to each component separately. Up to

now, utility-scale systems have relied on AC-coupled configuration because the integrated hardware of DC-coupled systems is not affordable.

2) **DC-Coupled System** is the configuration that PV and BES share the same inverter on the DC side, as shown in Figure 3-3. This configuration is cheaper than the AC-coupled system.

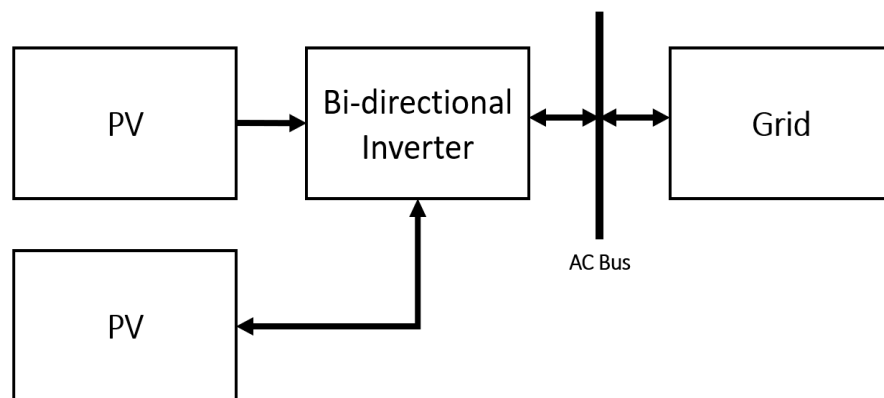


Figure 3-3 DC-coupled configuration [80].

From Figure 3-3, PV power can flow to the grid and BES by inverter. Because of only on the inverter, the combination power between PV and BES is limited.

## 3.2 Battery Energy Storage Model

### 3.2.1 BES Operation

Battery energy storage (BES) composes of battery packs, inverters, monitor/control systems, and protective devices. A battery converts chemical energy to electrical energy by the redox reaction of cathode and anode within the cell of the battery. There are two types of battery categorized by the flow of electrolyte (packaged and flow battery). The

electrolyte of a flow battery can circulate through cathode and anode while the packaged battery cannot.

Base on the power flow direction, the operation of BES can be categorized into three-mode (charge, discharge, and idle). The self-discharge can occur by the internal chemical reaction as a result of the slow loss of energy. In a lithium-ion battery, the internal impurity is the cause of self-discharge.

The essential parameters of Battery specification are state of charge (SOC), depth of discharge (DOD), C-rate, cycle life, and calendar life. SOC is the remaining battery capacity for discharge [81]. DOD is the percent of discharge energy when compared to battery capacity. C-rate is a ratio between charge-discharge current (A) and battery capacity (Ah) or the ratio between charge-discharge power (W) and battery capacity (Wh). Calendar life is a lifetime of the battery. The expected cycle life is estimated by the number of full charge-discharge cycles that it can handle before its capacity below specific performance criteria [82].

The battery is a chemical component that can degrade over time, depending on operation conditions. The factors that affect battery cycle life are time, operating temperature, SOC, DOD, and charge-discharge rate. The total degradation is the combination of calendar degradation and cycle degradation. Calendar degradation depends on SOC, temperature, and time [81]. While cycle degradation, when C-rate is higher than  $C/2$ , depends on DOD, C-rate, and cycle number[81].

To expand the battery lifetime, the operator should design appropriate battery operation conditions by reducing regarded degradation parameters. DOD, SOC C-rate, and cycle number (N) depend on usage, which can be limited by the range of use, but it is not efficient. Thus, to

efficiently reduce battery degradation, the BES control strategy is the critical part that leaves for the researcher to design.

### 3.2.2 Steady State BES Model

The updated BES energy with the self-discharge characteristic in each step [48] could be represented in equation 3-2.

$$E_b(k+1) = (1 - r_{sd})E_b(k) - t_s \frac{P_{bd}(k)}{\eta_{bd}} + t_s \eta_{bc} P_{bc}(k) \quad 3-2$$

where,  $P_{bd}$  and  $P_{bc}$  are discharged and charged power of BES, respectively.  $\eta_{bd}$  and  $\eta_{bc}$  are discharged and charged power efficiency, respectively.  $r_{sd}$  is the rate of self-discharge of BES.

The energy level of BES should be between maximum and minimum levels.

$$E_{b,\min} \leq E_b(k) \leq E_{b,\max} \quad 3-3$$

where,  $E_{b,\min}$  and  $E_{b,\max}$  are minimum and maximum of usage BES energy, respectively.

The charge and discharge power of BES should not over the minimum and maximum limit.

$$\begin{aligned} 0 &\leq P_{bd}(k) \leq \delta(k)P_{bd,\max} \\ 0 &\leq P_{bc}(k) \leq (1 - \delta(k))P_{bc,\max} \end{aligned} \quad 3-4$$

where,  $P_{bd,min}$  and  $P_{bd,max}$  are the minimum and maximum discharged power, respectively.  $P_{bc,min}$  and  $P_{bc,max}$  are minimum and maximum charged power, respectively.

$\delta$  is a binary variable to control charged and discharged power could not occur at the same time and is defined as the following equation.

$$\delta = \begin{cases} 0, & \text{charge} \\ 1, & \text{discharge} \end{cases} \quad 3-5$$

### 3.3 Power System Frequency Model

A complex model of a power system for frequency response study can be conveniently developed, for example, using MATLAB as in reference [4], or PSS/e<sup>R</sup> in reference [83]. Nonetheless, simplified models as being applied in reference [84] and [85] are also sufficiently applicable. In this study, the effects of system ramp capability and PV disturbance on system frequency characteristics are examined using the lumped frequency response model, consisting of system inertia, primary and secondary responses to frequency deviation, and ramp rate limit, as shown in Figure 3-4[10]. The key parameters include system inertia constant (H), primary response gain ( $\beta$ ), secondary response gain ( $K_s$ ) and system ramp capability (RC).

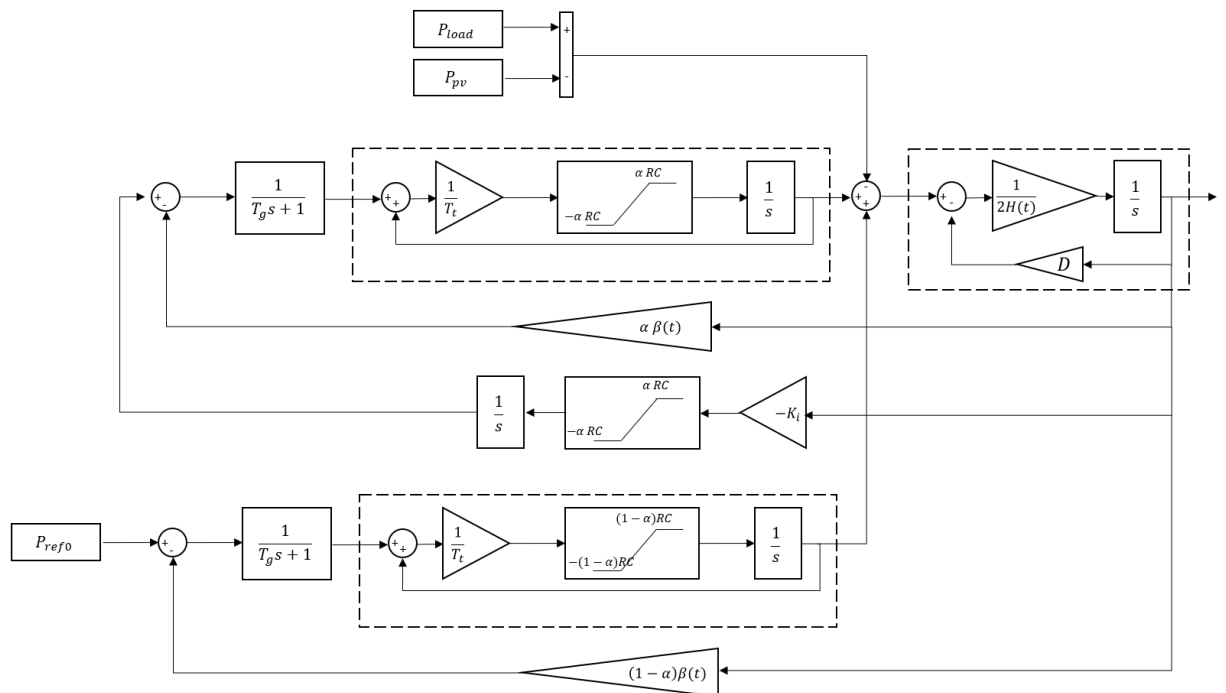


Figure 3-4 Power system dynamical model for frequency response study.

Files Rotating generation at each operating condition can be determined by net load (gross load minus non-rotating generation), plus spinning reserve. The per-unit inertia and the primary response of a power system at time  $t$  ( $H(t), \beta(t)$ ) corresponding to system base ( $S_b$ ) can be expressed in equations 3-6 and 3-7, respectively.

$$H(t) = \sum_{i \in G_o(t)} \frac{H_i S_i}{S_b} \quad 3-6$$

$$\beta(t) = \sum_{i \in G_o(t)} \frac{\beta_i S_i}{S_b} \quad 3-7$$

where,  $H_i, \beta_i$  are per unit inertia constant and primary response gain of synchronous generator unit  $i$ , with respect to its power rating  $S_i$ .  $G_O(t)$  is the set of on-line rotating synchronous generators at time  $t$ .

This model separates lumped synchronous generators into two groups; the units on-AGC provide both primary response and secondary response (through integral control of frequency deviation), where the units not on-AGC provide an only primary response. The total secondary response depends on the capacity of the first group and their total ramp capability. Here, the capacity ratio of the units on-AGC at time  $t$ , denoted  $\alpha(t)$ , is expressed in equation 3-8.

$$\alpha(t) = \frac{\sum_{i \in \text{on-AGC}(t)} S_i}{S_b} \quad 3-8$$

Without loss of generality, for the purpose of determining critical system ramp capability, it assumes here that there is enough magnitude of the spinning reserve to follow changes in load and PV disturbances. The system ramp capability limit is implemented by a saturation block for the generation rate constraint (GRC) within the lumped turbine models, as well as for the rate limit of load-frequency control response [86], as shown in Figure 3-4. As a result, the combined primary and secondary generation responses to system frequency deviation are affected by these ramp capability limitations. Overall, the system ramp capability (p.u./min) at time  $t$ , denoted  $RC(t)$ , can be expressed as in equation 3-9.

$$RC(t) = \frac{\sum_{i \in G_o(t)} R C_i S_i}{S_b} \quad 3-9$$



### 3.4 Linear Programming Method

The major components of the constrained optimization model are decision variables, objective function, and constraints.

1. *Decision variables* are the variables controlled by the decision-maker or the controller. For example, the decision variables  $x_j$  represent the number of kilograms of product  $j$  that the factory will produce during the defined period.

2. *The objective function* sets the criterion for evaluating the decision variables. For example, the objective function may quantify the cost or profit as a function of various products. It also gives the optimization direction for searching the optimal solution to the problems.

3. *Constraints* are a set of inequality and equality equations that construct a feasible set of decision variables—for example, the amount of limitation of raw material for producing the product.

There are both advantages and disadvantages of using optimization models. The main advantages are a quick, safe, and inexpensive method to find a possible solution. Others benefits are,

1. *Construct a systematic thought process.* The math modeling constructed by the optimization model is concise and organized because it is formulated after thinking through the problem. It is easier to identify a possible solution when defining clear decision variables, objectives, and constraints.

2. *Simplify the complex problem.* Many real-world problems are large and complex—for example, the determination of optimal routes of various product delivered from manufacture to geographically dispersed store. Optimization could make it easier to find the optimal solution.

3. *Facilitate sensitivity analysis.* Formulating problems with the mathematics model makes it easier to find the solution with a different scenario.

The disadvantage is that it is possible to mismodel large and complex problems. Thus, the optimal solution from the complex model may not be the optimal solution in a real problem. The decision-maker should be aware of this issue before making a decision.

### 3.4.1 Problem Formulation

A linear program is the constrained optimization model consists of objectives and constraints that satisfy there following requirements.

1. The decision variables must be continuous
2. The objection function must be a linear function
3. The constraint must be a linear function

The general form of the LP problem is shown in equation 3-10 [87].

$$\begin{array}{ll}
 \min z = & c_1x_1 + c_2x_2 + \dots + c_nx_n \\
 \text{subject to} & a_{11}x_1 + a_{12}x_2 + \dots + a_{1n}x_n \leq b_1 \\
 & a_{21}x_1 + a_{22}x_2 + \dots + a_{2n}x_n \leq b_2 \\
 & \vdots \\
 & a_{m1}x_1 + a_{m2}x_2 + \dots + a_{mn}x_n \leq b_m \\
 \\ 
 \text{subject to} & a_{11}^{eq}x_1 + a_{12}^{eq}x_2 + \dots + a_{1n}^{eq}x_n = b_1^{eq} \\
 & a_{21}^{eq}x_1 + a_{22}^{eq}x_2 + \dots + a_{2n}^{eq}x_n = b_2^{eq} \\
 & \vdots \\
 & a_{p1}^{eq}x_1 + a_{p2}^{eq}x_2 + \dots + a_{pn}^{eq}x_n = b_q^{eq}
 \end{array} \tag{3-10}$$

where, min is the abbreviation of minimizing.  $c_j$ ,  $a_{ij}$  and  $b_i$ , where  $i = 1, 2, \dots, m$  and  $j = 1, 2, \dots, n$ , are real number coefficient of the objective

function, inequality constraints, and input value, respectively.  $m$  and  $n$  are the total number of inequality equations and decision variables, respectively.

$a_{ij}^{eq}$  and  $b_i^{eq}$ , where  $i = 1, 2, \dots, p$  and  $j = 1, 2, \dots, n$ , are real number coefficient of the objective function, equality constraints, and input value, respectively.  $p$  and  $n$  are the total number of equality equations and decision variables, respectively.

$x_1, x_2, \dots, x_n$  are decision variables that minimize objective function subject to inequality and equality constraints.

Equation 3-11 [87] could be written using matrix notation, as shown in the following equation.

$$\begin{aligned} \min z &= c^T x \\ \text{subject to} \quad & Ax \leq b \\ & A_{eq} x \leq b_{eq} \end{aligned} \tag{3-11}$$

where,  $c, x \in R^n, b \in R^m, b_{eq} \in R^p$  and  $A \in R^{m \times n}, A_{eq} \in R^{p \times n}$ .  $z$  is the cost function.  $x$  is the vector of decision variables.  $A$  and  $A_{eq}$  are the matrix of the coefficient of inequality and equality constraints, respectively.  $b$  and  $b_{eq}$  are the vector of right-hand side value of inequality and equality constraints, respectively.  $c$  is the vector of coefficients of the objective function.

From the problem description, the linear programming model could be formulated by the following steps [87].

**1. Identify the decision variables.** Interpret the problem and precisely define decision variables with the appropriate unit.

**2. Identify the objective function** Determine the criterion as a function consisted of decision variables for evaluating alternative solutions.

**3. Identify the inequality and equality constraints** Transform the constraints description components to mathematics equation. If the decision variables have not been defined precisely, the formulation process would be iterated by redefining existing variables or adding new variables.

### 3.4.2 Solution method

The linear program problem can be solved by the systematical iterative method in the following steps [88].

1. Simplify and convert the problem to a standard form
2. Generate the starting point before the first iteration
3. Iterate predictor-corrector to solve the first-order necessary condition

The algorithm attempts to find a point that satisfies Karush-Kuhn-Tucker (KKT) condition in each iteration.

KKT method allows only equality constraints. Thus, the problem with constraints is required to transform to the problem with only equality constraints by adding slack variables with Lagrange multipliers, as shown in the equation below [88].

$$\begin{array}{ll}
 \min z & z = c^T x \\
 \text{subject to} & \bar{A}x = \bar{b} \\
 & x + q = u \\
 & x, q \geq 0
 \end{array}
 \tag{3-12}$$

where,  $\bar{A}$  is the extended matrix that includes inequality (A) and equality ( $A_{eq}$ ) constraints, as shown in the following equation [88].  $\bar{b}$  is the corresponding vector of the extended matrix ( $\bar{A}$ ).  $q$  is the slack variables vector that adapts upper bounds to equality constraints.

$$\bar{A}x = \begin{bmatrix} A_{eq} & 0 \\ A & I_d \end{bmatrix} \begin{bmatrix} x_0 \\ s \end{bmatrix} \quad 3-13$$

where,  $I_d$  is the identity matrix.  $x_0$  is the start value of vector  $x$ .

The Lagrangian (L) [88] is;

$$L = c^T x - y^T (\bar{A}x - \bar{b}) - v^T x - w^T (u - x - t) \quad 3-14$$

where,  $y$  is Lagrange multipliers related to linear equality constraints.  $v$  is Lagrange multipliers related to lower bound.  $w$  is Lagrange multipliers related to the upper bound.

From equation 3-14, the system of KKT conditions of the problem with constraints can be formulated as shown in the following equation [88].

$$c - \bar{A}^T y - v + w = 0 \quad 3-15$$

$$\bar{A}x = \bar{b}$$

$$x + q = u$$

$$v_i x_i = 0$$

$$w_i q_i = 0$$

$$(x, v, e, q) \geq 0$$

The Newton-Raphson step can be formulated, as shown in the following equation [88].

$$\begin{bmatrix} 0 & -\bar{A}^T & 0 & -I_d & I \\ \bar{A} & 0 & 0 & 0 & 0 \\ -I & 0 & -I & 0 & 0 \\ V & 0 & 0 & X & 0 \\ 0 & 0 & W & 0 & T \end{bmatrix} \begin{bmatrix} \Delta x \\ \Delta y \\ \Delta t \\ \Delta v \\ \Delta w \end{bmatrix} = - \begin{bmatrix} c - \bar{A}^T y - v + w \\ \bar{A}x - \bar{b} \\ u - x - q \\ VX \\ WQ \end{bmatrix} = - \begin{bmatrix} r_d \\ r_p \\ r_{ub} \\ r_{vx} \\ r_{wq} \end{bmatrix} \quad 3-16$$

where,  $X, V, W,$  and  $Q$  are diagonal matrices related to the vectors  $x, v, w,$  and  $q,$  respectively.  $r_d, r_p, r_{ub}, r_{vx}$  and  $r_{wq}$  are the dual, primal, upper bound, lower bound complementarity, and upper bound complementarity residual, respectively.

The predictor first forecasts a step from the Newton-Raphson formula and then calculates a corrector step before going to the next iteration. The iteration of predictor-corrector continues until it reaches the feasible solution that satisfies the constraints within the defined tolerances and defined relative step sizes.

The stopping criteria of this algorithm are the following conditions [88].

$$\|r_p\|_1 + \|r_{ub}\|_1 \leq \rho \text{Tol}_p \quad 3-17$$

$$\|r_d\|_\infty \leq \rho \text{Tol}_d$$

$$r_c \leq \text{Tol}_{fun}$$

where,

$$\rho = \max(1, \|\bar{A}\|, \|c\|, \|\bar{b}\|) \quad 3-18$$

$$r_c \leq \max_i (\min(|x_i v_i|, |x_i|, |v_i|), \min(|q_i w_i|, |t_i|, |w_i|))$$

where,  $\text{Tol}_p$  and  $\text{Tol}_d$  are the tolerance of primal and dual residual, respectively.  $r_c$  is the size of  $xv$  and  $qw,$  which are zero vectors at a solution.

## Chapter 4

# Power System Frequency in High PV Penetration Network

This chapter describes the study of system frequency response related to ramp capability in the network of the changeable characteristics depends on the PV penetration ratio.

### 4.1 Impact of PV Penetration on Key System Parameters

The critical system parameters related to system frequency response in high PV penetration networks are varied depending mainly on the on-line capacity of the rotating generation at that time. Typically, operating capacity at time  $t$  will be pre-determined by the unit commitment process [11, 17, 18]. For simplicity, the on-line capacity,  $Cap_{gen,on}(t)$ , can be written as:

$$Cap_{gen,on}(t) = P_{net}(t) + P_{spr}(t) \quad 4-1$$

where,  $P_{net}(t)$  is netload, and  $P_{spr}(t)$  spinning reserve power at time  $t$ . Assume that the spinning reserve ratio ( $spr$ ) with respect to the net load is constant. Then, we can write  $P_{spr}(t)$  as shown in equation 4-2.

$$P_{spr}(t) = spr \times P_{net}(t) \quad 4-2$$

With PV penetration, the on-line rotating capacity can be estimated by equation 4-3.

$$\begin{aligned}
\text{Cap}_{\text{gen,on}}(t) &= (1 + \text{spr})P_{\text{net}}(t) & 4-3 \\
&= (1 + \text{spr})(P_{\text{load}}(t) - P_{\text{pv}}(t)) \\
&= (1 + \text{spr})\left(1 - \frac{P_{\text{pv}}(t)}{P_{\text{load}}(t)}\right)P_{\text{load}}(t)
\end{aligned}$$

In general, PV penetration ratio (PVR) can be defined as:

$$\text{PVR}(t) = \frac{P_{\text{pv}}(t)}{P_{\text{load}}(t)} \quad 4-4$$

Let define  $H_{\text{max}}$  as the maximum per-unit system inertia, corresponding to the total number of synchronous generators in the system,  $N$ . Then, we can write

$$H_{\text{max}} = \frac{\sum_{i=1}^N H_i S_i}{S_b} \quad 4-5$$

At a time when the on-line rotating capacity has been reduced due to PV penetration at a certain level, the resulting system inertia also proportionately decreases, as explained in equation 4-6.

$$\begin{aligned}
H(t) &= \frac{\sum_{i=1}^N H_i S_i}{S_b} - \frac{\sum_{i \in G_F(t)} H_i S_i}{S_b} & 4-6 \\
&= (1 - \text{Cap}_{\text{gen,off}}(t))H_{\text{max}} \\
&= \text{Cap}_{\text{gen,on}}(t)H_{\text{max}}
\end{aligned}$$



where,  $G_F(t)$  is the set of off-line rotating synchronous generators,  $Cap_{gen,off}(t)$  is the per-unit off-line rotating capacity, and  $Cap_{gen,on}(t)$  the per-unit on-line rotating capacity, at time  $t$ , respectively.

Then, from equations 4-3, 4-4 and 4-6, the estimated system inertia as a function of PVR at time  $t$  can be written as:

$$\begin{aligned} H(t) &= (1 + spr)(1 - PVR(t))P_{load}(t)H_{max} \\ &= (1 - PVR(t))(1 + spr)P_{load}(t)H_{max} \\ &= (1 - PVR(t))H_0(t) \end{aligned} \quad 4-7$$

It is noted that  $H_0(t)$  is the system inertia when there is no PV generated power (e.g., during night time, or very cloudy period). When PVR gets higher, the system inertia will become lower, accordingly, provided the power system operates at nearly constant  $spr$ . The lower system inertia is the higher rate of change of frequency (ROCOF) and frequency deviation when power disturbance occurs.

The relation derived in equation 4-7 above is well consistent with what has been revealed in reference [84] on an average basis, as shown in equation 4-8, in which statistical approach was applied to simulated data of the power system with around 33-38% of renewable energy production, annually.

$$\bar{H} = (1 - PVR)H_{0,avg} \quad 4-8$$

where,  $\bar{H}$  is the average per-unit system inertia,  $H_{0,avg}$  the average per-unit system inertia when no variable renewable generations in the system.

Likewise, the system's primary response characteristic is also dependent on the on-line rotating capacity. In this study, we also assume the relation of such a key parameter, with respect to PVR, follows equation 4-9.

$$\beta(t) = (1 - \text{PVR}(t))\beta_0(t) \quad 4-9$$

where,  $\beta_0(t)$  is the primary response gain when no PV output power in the system.

In fact, the primary response characteristic of each individual unit can be different and entirely non-linear. Nonetheless, the aggregated impact of those distributed parameters on the system frequency is assumed to be linear in this case.

## 4.2 Expected PV Disturbance

The impact of expected PV disturbance on the system frequency response of a power system with lower inertia will be examined. Specifically, the rapid decrease of aggregated solar power will be modeled, as illustrated in Figure 4-1.

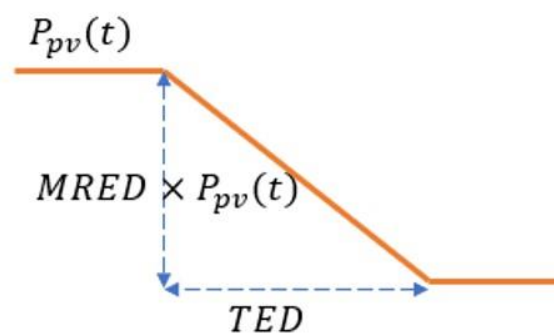


Figure 4-1 PV ramp down disturbance.

The rate of change of PV disturbance is related to PV output magnitude at that time. Thus, the expected disturbance slope (EDS) can be represented by equation 4-10.

$$\text{EDS}(t) = \frac{\text{MRED} \times P_{\text{pv}}(t)}{\text{TED}} \quad 4-10$$

where, EDS is expected disturbance slope, MRED is the magnitude ratio of expected disturbance with respect to  $P_{\text{pv}}(t)$ , its value between 0 to 1. TED is the time duration of the expected disturbance. In this study, it is necessary to emphasize that MRED can be interpreted as per unit PV ramp down of  $P_{\text{pv}}(t)$  per minute when TED is fixed as one minute. It is expected that the higher MRED requires a higher system ramp capability to catch up with higher PV ramp down.

In the case of the largest generator trip, we consider TED around zero or the corresponding EDS approaches infinity. Hence, the impact of N-1 contingency disturbance is expected to be more severe than that of PV disturbance at the same power disturbance magnitude. However, with more considerable PV penetration, the magnitude of PV power disturbance could become much higher, and therefore, the effect of such expected PV disturbance also needs to be investigated to ensure system security.

### 4.3 Frequency Response Analysis

Significant disturbance from a contingency event can cause a sizable imbalance between generation and load, leading to system frequency

deviating far away from the scheduled synchronous frequency. Synchronous generators must be operated around synchronous speed within the restricted allowable range to avoid wear and tear of the rotating part. If system frequency extends below its lower limit, under-frequency relay for generator protection will be active and send tripping commands to prevent damage on those generators. This action could exacerbate the stability of a power system. Meanwhile, the under-frequency load shedding relay (UFLS) will be activated [84] to help re-balance the generation and load accordingly.

#### **4.3.1 Frequency Security Index**

Generally, two frequency security indexes have been proposed for studying the impact of PV penetration on system frequency response performance; the first index is nadir frequency ( $f_{\text{nadir}}$ ) [89], which is defined as the minimum value of frequency response under significant disturbance, and second is the rate of change of frequency (ROCOF) [83]. It appears that nadir frequency is more sensitive to a large generator trip than is ROCOF [16]. Hence, in this study, we will analyze the frequency response of a high PV integrated power system using nadir frequency as a frequency security index.

#### **4.3.2 Methodology**

The main objective of this research is to determine the critical ramp capability requirement of a power system with relatively high PV penetration, satisfying N-1 security constraint. The proposed methodology contains two parts. The first part is to examine system frequency response at various combinations of PVR and disturbances, as shown in block (a) of Figure 4-2. Then, the second part is to find critical

system ramp capability at what could be considered as the worst-case operating scenario, as in block (b) of Figure 4-2.

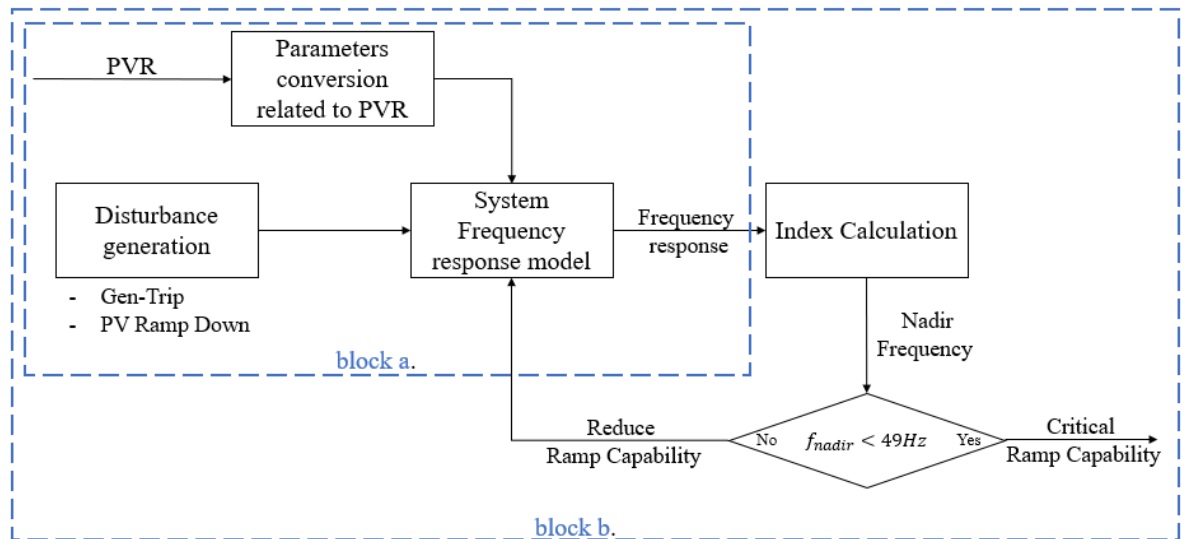


Figure 4-2 Frequency response study flow chart.

Two types of disturbances have been applied in the model. The N-1 security constraint is verified by the sudden trip of the largest rotating generating unit. PV disturbance is modeled as PV ramp down, as illustrated in Figure 4-1, where the magnitude of power disturbance is directly related to the specified PVR at that time. Key system dynamical parameters will be varied corresponding to such given PVR.

To determine critical system ramp capability for the given PVR, various expected disturbances will be applied to the simulated power system. The nadir frequency obtained from the ‘Index Calculation’ box is the minimum value of system frequency found among the cases being investigated from the block (a). Then, the system ramp capability, RC will be reduced, step-by-step, until such nadir frequency gets below 49 Hz, which is a typical value when the UFLS relay is being activated

[84]. The minimum system ramp capability that gives the nadir frequency nearest to and above the 49-Hz limit is the critical system ramp capability at such given PVR.

#### **4.4 Case Studies**

There are three main case studies. Firstly, the effects of PV penetration ratio (PVR) and of system ramp capability (RC) on system frequency response, under various expected disturbances, will be examined. Secondly, nadir frequency with respect to various combinations of PVR, MRED, and RC will be investigated. Lastly, critical system ramp capability with respect to PVR will be revealed, using the methodology explained in Figure 4-2.

The tested operating condition is set at around typical noontime when the total connected PV supposedly gives maximum output generation (the PV magnitude of disturbance could be highest) while the total demand is around 80% of peak demand, as depicted in Figure 4-3. For quantitative analysis, we assume total load consumption of 25,000 MW and spinning reserve at 20% (5,000 MW) at this operating time interval. Thus, the total on-line rotating generator, with no PV penetration, is 30,000 MW, which is also chosen as a system power base.

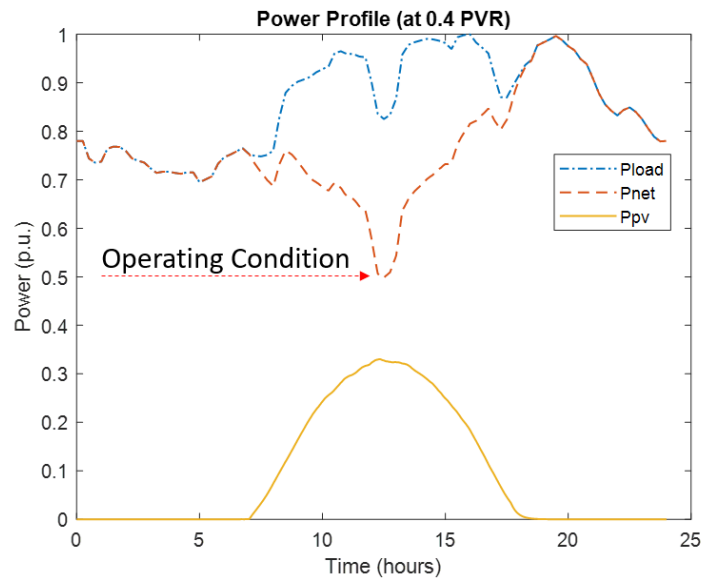


Figure 4-3 Tested operating condition with 0.4 PVR.

The default values of the parameters in the test system model are given in **Error! Reference source not found.** [90].

Table 4-1 Default values of test system parameters [90].

Symbol	Meaning	Values
$H_0$	per unit system inertia	5 s
D	damping coefficient	0.8
$T_g$	governor time constant	0.2 s
$T_t$	turbine time constant	0.5 s
$\beta_0$	primary response gain	1/0.05
$K_s$	secondary response gain	7
$\alpha$	on-AGC ratio	0.5
RC	system ramp capability	0.1 p.u./min [86]
Note: $S_b=30,000$ MVA, $P_{load}=25,000$ MW		

Time constants of the governor and turbine models for the two groups of lumped rotational generators are equal. Since we assume that UFLS

will be activated when system frequency goes below 49 Hz, the case of which it is below this limit will be considered unacceptable. This under-frequency limit line will also be drawn in the figures of the test results for the convenience of analysis.

In this study, the size of the largest rotating generation trip being applied is assumed to be 900 MW (0.03 p.u.). Referring to Fig. 3, in each case, the disturbance will be applied at time  $t = 10$  seconds, and the simulation will be carried on for 180 seconds, thereafter. During such a short period, it can be assumed that the system load remains constant [5].

In addition, PV disturbance is modeled as a ramp-down slope by varying MRED, while TED is fixed at 1 minute incoherent with the design of ramp rate requirement [19].

Various case studies on a lumped power system dynamic model with 5-sec equivalent system inertia at the base case are operating with a 20% spinning reserve and expecting PV generation varying from 0 – 70% PVR, have been conducted. It is anticipated that when PVR becomes higher, the system inertia and primary response characteristic will decrease proportionately. For clarity of understanding, firstly, the system frequency response is affected by higher PVR, and lower RC will be investigated in section 4.4.1. Then, the relation of nadir frequency and key dynamical factors (i.e., PVR, RC, and MRED) will be explored by 3D-illustration in section 4.4.2. Last, the critical ramp capability at each PVR will be examined in section 4.4.3.

#### **4.4.1 Frequency Response Characteristics**

The cases of system frequency responses under the largest generator trip are shown by G-label, and the cases under PV ramp down are shown by R-label. The results are plotted in the same figure to compare the



severity of impact on system frequency response between the G-cases and the R-cases.

#### 4.4.1.1 Effect of PV Penetration Ratio (PVR)

In this case study, the system is perturbed by the largest generator trip (0.03 p.u.) and by PV ramp down with MRED equal to 0.1, when PVR is at 50% and 70%, respectively. System ramp capability is fixed at 0.1 p.u./min.

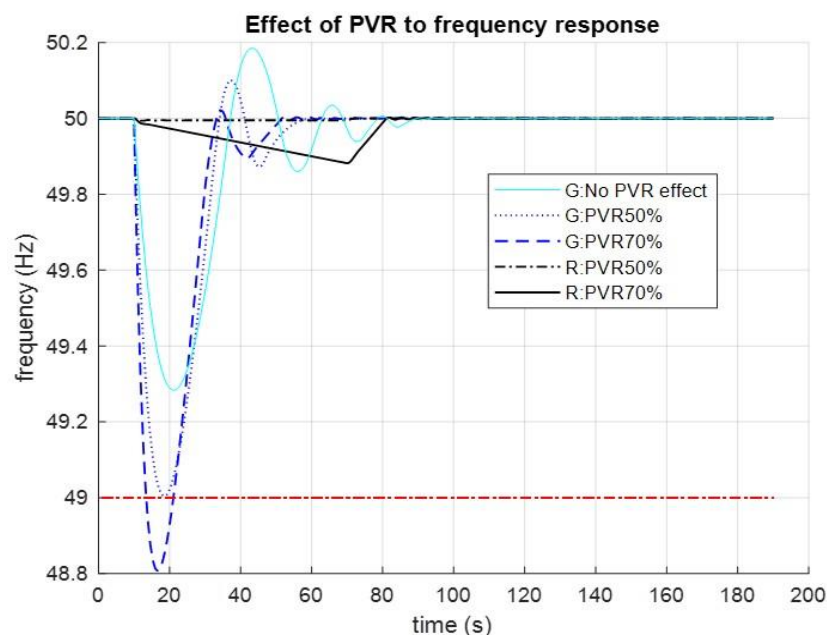


Figure 4-4 Effect of PVR to frequency response.

From Figure 4-4, the results show that the largest frequency drop and recovery time are worsened when PVR increases. This is because of the higher PVR, the lower system inertia, and the primary response to a frequency deviation.

For the range of PVR from 0 – 70 %, disturbance from the largest generator trip results in a far more severe impact than that from PV disturbance (being tested at 0.1 MRED). Furthermore, in G-case, the system cannot comply with N-1 contingency when PVR is above 50 %

because the nadir frequency will be lower than the 49-Hz limit (while nadir frequency in R-case is much higher and insignificant). Hence, the maximum allowable PVR could not be more than 50%, provided that system ramp capability remains constant regardless of PVR.

#### 4.4.1.2 Effect of System Ramp Capability (RC)

In this case study, the system will be perturbed by the largest generator trip (0.03 p.u.) and by PV ramp down with MRED equal to 0.1, where the value of RC is changed to 0.025 and 0.05 p.u./min, respectively, given PVR at 30%.

From Figure 4-5, the results show that the largest frequency drop and recovery time are worsened when RC decreases. This could imply that the aggregated responding generation ramps up hits the system ramp capability limit most of the time, due to the size and rate of change of the applied large disturbance. The effect of PVR even causes poorer frequency response performance.

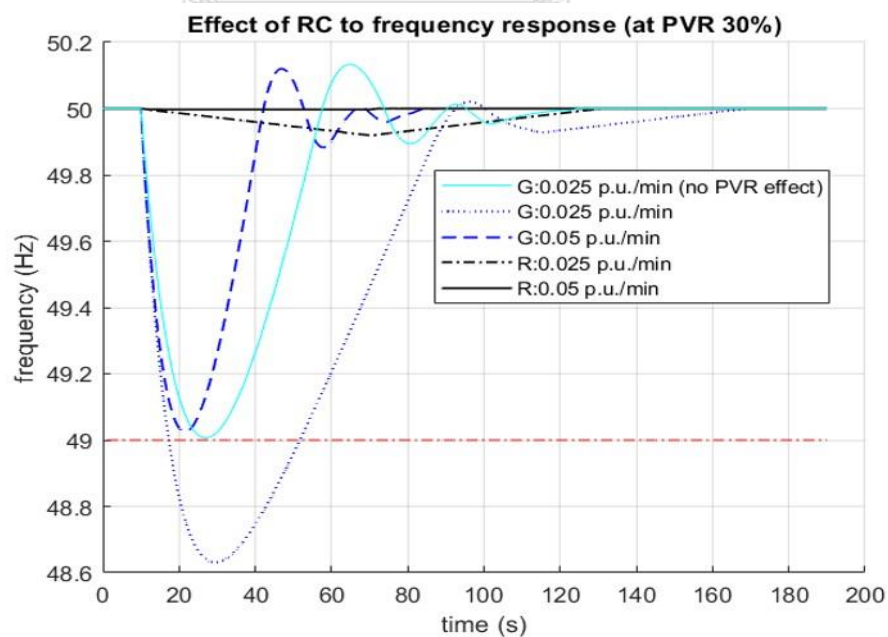


Figure 4-5 Effect of RC to frequency response (at PVR 30%).

At 30 % PVR, the system cannot comply with N-1 contingency when RC is less than 0.05 p.u./min because nadir frequency will be lower than the 49-Hz limit (while nadir frequency in R-case will be kept well within the limit even when RC is very low). Thus, in this case, RC of 0.025 p.u./min implies insufficient system ramp capability.

From Figure 4-4 and Figure 4-5, system frequency response with no PVR effect (cyan line) gives the best performance among the G-cases when system ramp capability is equal in all cases. Hence, maintaining system frequency support, through system inertia, primary and secondary responses, at the same level as when there is no PV penetration could significantly enhance system security, increase maximum allowable PVR, and require the least system ramp capability, concurrently.

#### **4.4.2 Nadir Frequency**

System operating condition changes with time, and that causes key variables that affect system frequency response being changed, accordingly. Here, we will use nadir frequency to assess the system security with respect to the expected ranges of PVR, MRED, and RC. Three-dimensional plots with cutting plane at 49 Hz are presented for the analyses to reveal secure operating zones and to identify critical system ramp capability.

##### **4.4.2.1 Effect of PVR and MRED (at RC=0.1p.u./min)**

It is expected that MRED of aggregated PV output power from several PV systems would be much lower than that of a single plant, due to the diversity effect. Thus, in this case study, MRED will be varied from 0.02 to 0.3, and PVR from 0.1 – 0.7. It is to be noted that the magnitude of PV disturbance at each specified MRED will be higher as PVR increases.

From Figure 4-6, with only disturbances from PV, the results show that nadir frequency is rather flat and well above 49 Hz for the operating condition with PVR up to 0.4 (40%). When PVR increases from 0.4 to 0.7, nadir frequency gradually gets lower with increasing slope when MRED is higher. Then, when PVR is above 0.7, nadir frequency steeply drops, especially for higher MRED. For example, at 0.7 PVR, the nadir frequency drops from 49.27 Hz to 45.47 Hz as MRED increases from 0.18 to 0.3.

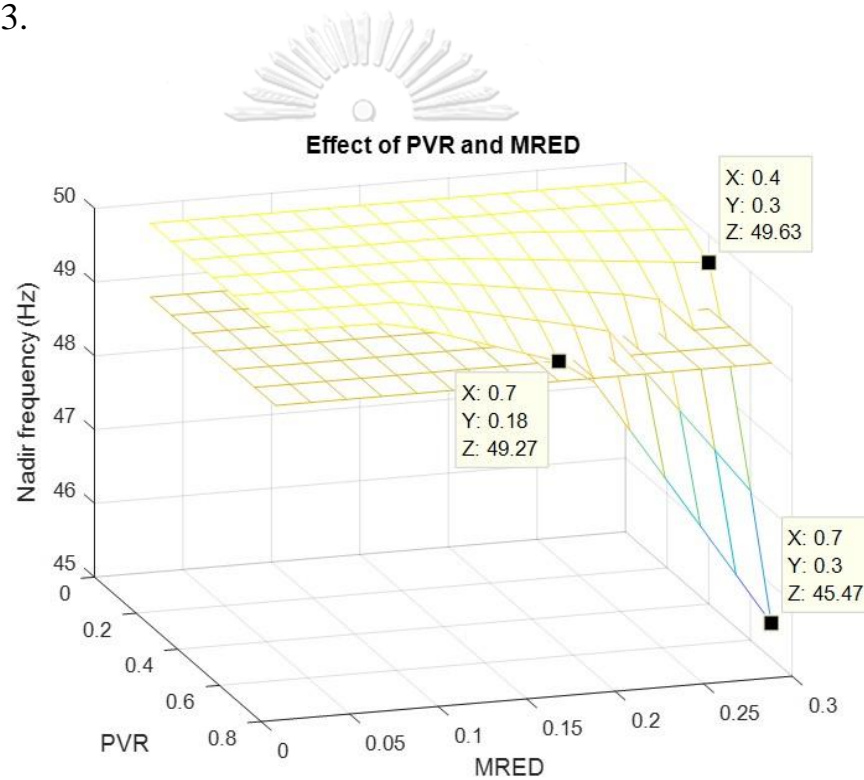


Figure 4-6 Effect of PVR and MRED (at RC = 0.1 p.u./min).

This suggests that when PVR is more than 0.4, curtailment of MRED should be considered.

#### 4.4.2.2 Effect of PVR and RC (at 0.1 MRED)

The ramp capability of conventional rotating generators is relatively slow and has limitations because of the intrinsic nature of those generators. In this case, we will examine the effect of system ramp capability by varying RC from 0.02 to 0.2 p.u./min, for the range of PVR from 0.1 – 0.7, and with only disturbances from PV. Although MRED is fixed at 0.1, the magnitude of PV disturbance becomes higher as PVR increases.

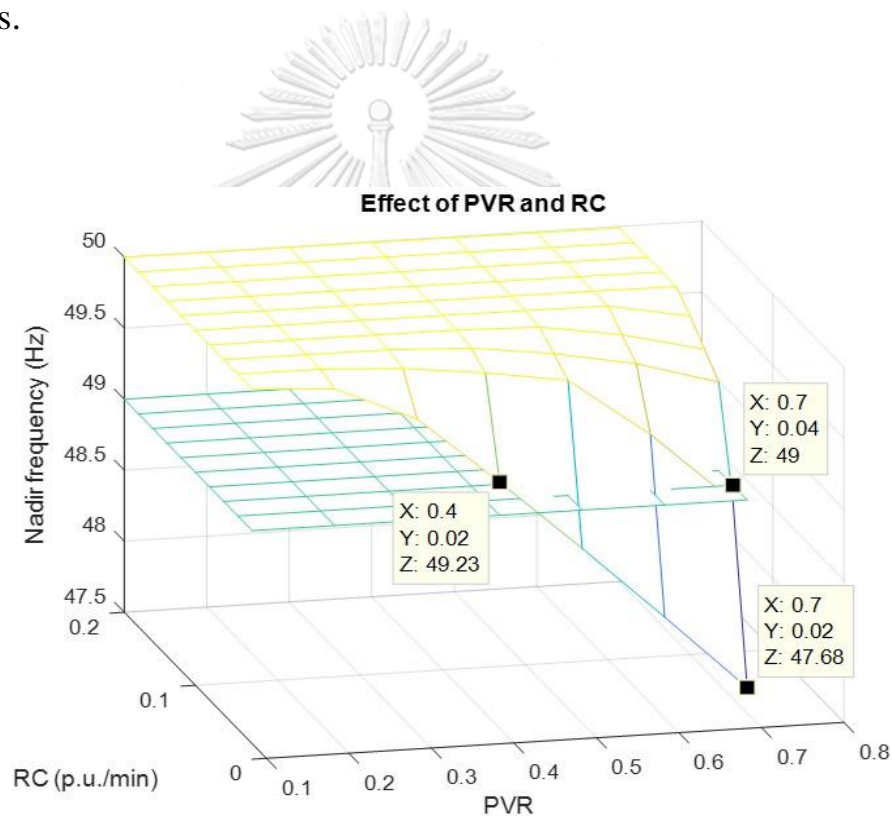


Figure 4-7 Effect of PVR and RC (at 0.1 MRED).

As seen in Figure 4-7, the results show that nadir frequency is rather flat and well above 49 Hz with PVR up to 0.4 (40 %). However, when PVR increases from 0.4 to 0.7, nadir frequency sharply drops with an increasing slope when RC is lower. For example, at 0.7 PVR, the nadir

frequency drops from 49 Hz to 47.68 Hz as RC reduces from 0.04 to 0.02 p.u./min. This suggests that sufficient RC is critical to ensure the power system security, especially when PVR is more than 0.4.

#### 4.4.2.3 Effect of PVR and RC (at 0.03 p.u. Gen-Trip)

In this case, nadir frequency will be examined when the system is subject to a generator trip of 0.03 p.u., for the operating ranges of RC from 0.02 to 0.2 p.u./min, and of PVR from 0.1 – 0.7, respectively.

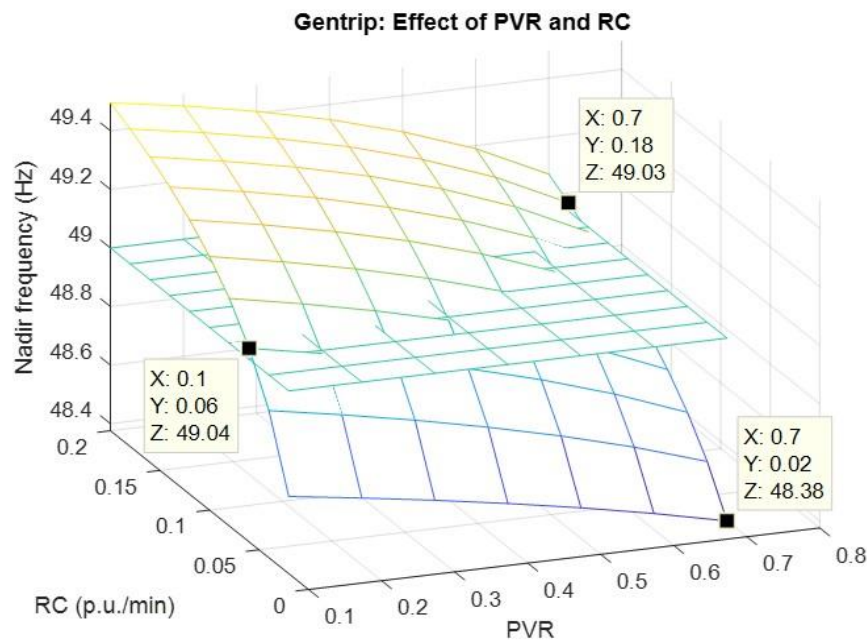


Figure 4-8 Effect of PVR and RC (at 0.03 p.u. Gen-Trip).

From Figure 4-8, it shows that the secure operating region is bounded by PVR from 0 - 0.7 and RC from 0.06 - 0.18 p.u./min. The system will require a minimum RC of 0.18 p.u./min to accommodate PVR of 0.7, while it will require minimum RC of 0.06 p.u./min for PVR of 0.1. Hence, this indicates that the system operator should prepare RC higher than certain critical values for the anticipated maximum PVR to comply with the N-1 contingency of the largest generator trip.

### 4.4.3 Critical System Ramp Capability

Critical system ramp capability is the minimum ramp capability requirement so that a power system can withstand the largest disturbance of N-1 contingency without violating the pre-determined frequency limit. This critical value will be beneficial for the system operator to ensure the security of a power system at the expected PVR. Here, critical system ramp capability will be obtained using the methodology, as presented in Fig. 3. The effect of system inertia improvement on reduced critical system ramp capability will also be revealed.

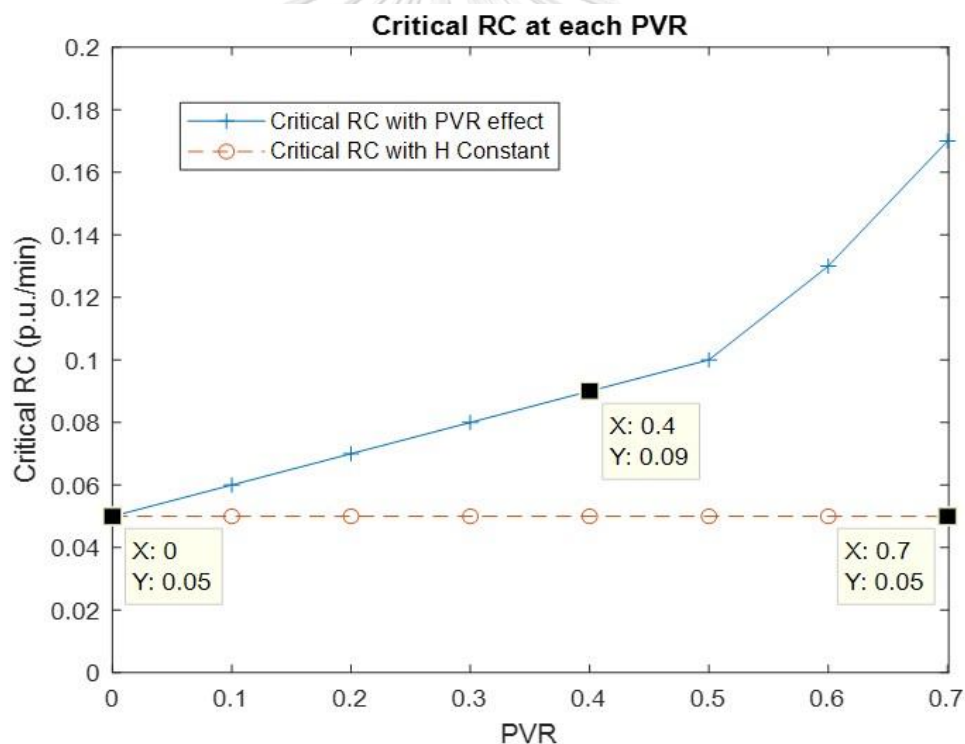


Figure 4-9 Critical RC with respect to PVR.

Figure 4-9 shows the critical value of system ramp capability (RC) with respect to PVR. It increases approximately with the parabola rate when PVR increases. However, if the total system inertia (H) can be

maintained constant at H0, independent of PVR, the critical value of RC does not need to be increased when PVR gets higher. Hence, this confirms that the system ramp capability requirement can be relaxed with additional (virtual) inertia to substitute for inertia loss due to the reduced number of on-line rotating generators.

The plot, as illustrated in Figure 4-9, can be deployed by the system operator for preparing system ramp capability to ensure power system security complying with N-1 contingency at each operating condition. For example, when expected PVR is equal to 0.4, the system ramp capability should be more than 0.09 p.u./min

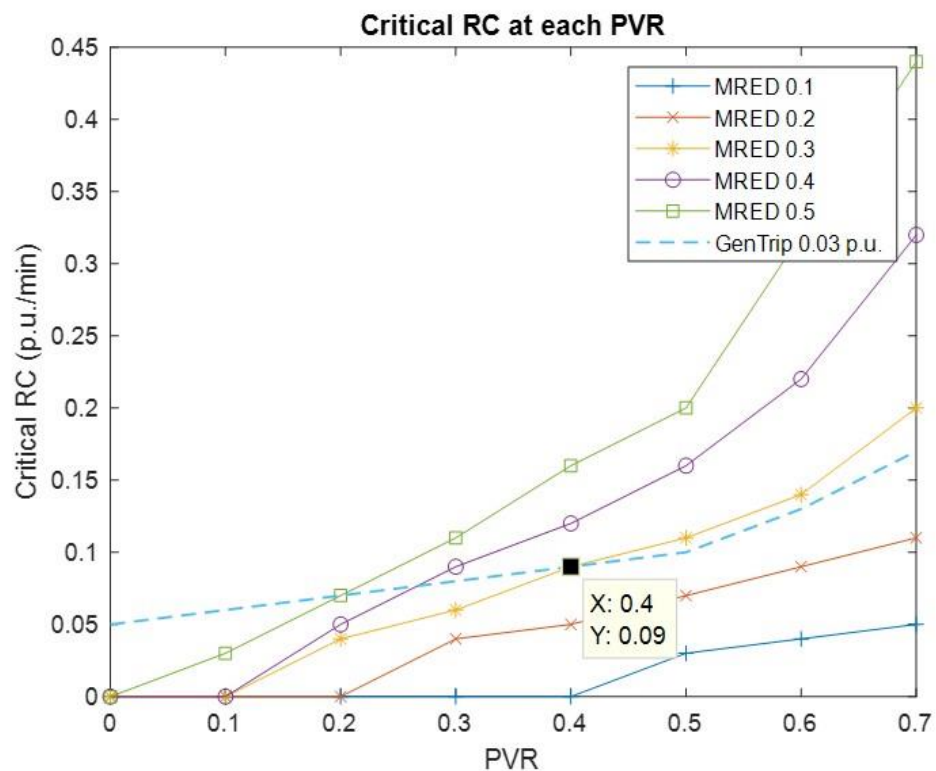


Figure 4-10 Effect of MRED on critical RC.

Figure 4-10 compares critical RC determined by PV disturbance with MRED being varied from 0.1 – 0.5 (MRED-line) to that determined by



the largest generator trip (GenTrip-line). For MRED well below 0.3, critical RC can be determined by the largest generator trip for the entire considered range of PVR. In addition, suppose that MRED is increased to 0.3, 0.4, and 0.5, critical RC determined by PV disturbance will still be lower than that determined by the largest generator trip when PVR less than 0.4, 0.26, and 0.2, respectively. Hence, assume that system ramp capability requirement is determined by the GenTrip-line, we suggest that the system operator should have a control measure to reassure MRED will be curtailed according to an expected PVR.

For example, the maximum allowable MRED should be 0.5 at PVR up to 0.2, and be reduced to 0.3 at PVR up to 0.4. In so doing, it will not need to impose PV ramp curtailment on an individual PV plant, also noting that MRED of aggregated PV power tends to be lower than that of a single PV plant [21]. Thus, the extra cost of control for PV output generation could be avoided.

#### **4.4.4 Conclusion**

System ramp capability is critical to accommodating large PV penetration while ensuring system security. Reviewed researches in this area[11, 16] showed that the system ramp capability requirement had not yet been addressed and examined based on the dynamic behavior of a power system. This study aims to determine the system ramp capability requirement in an anticipated high PV generation power network. Dynamical simulation method has been proposed to examine critical ramp capability for various combinations of PV penetration ratio (PVR) and its associated magnitude ratio of expected disturbance (MRED). This proposed method can also be conveniently applied to any complex dynamical model of a power system.

Various case studies on a lumped power system dynamic model with 5-sec equivalent system inertia at base case, operating with 20% spinning reserve, and expecting PV generation up to 70% PVR, have been conducted. Test results reveal that the system can operate securely with PVR up to 40%, in which it will require system ramp capability in the range of 0.05-0.09 p.u./min. In such a case, when MRED of aggregated PV output power is kept below 0.3, it will not need to impose a PV ramp limit on an individual PV plant, and thus the extra cost of control for PV output generation could be avoided.

From the test results, it can be concluded that to maintain system operation at the well-defined N-1 security level. The system operator should prepare ramp capability above the critical value for the anticipated level of PVR. Given such critical value, the aggregated PV's MRED should be curtailed below a certain level. Additionally, it is found that higher system inertia would significantly lessen system ramp capability requirement. In addition, if PVPP can provide additional service as inertia or primary response support, it is expected that system stability could be improved.

For policy implementation, this finding can be helpful to determine relevant requirements with respect to expected PVR, such as system ramp capability, additional virtual inertia, and ramp limit of an individual PV system, so that PV generation at the anticipated level can be integrated into the power network successfully while the security of the entire system not being compromised.

## Chapter 5

# Grid-Friendly Dispatch Strategy

In the past, with a small amount of PVPPs, the system operator saw solar power as a negative load because of its uncertainty. They do not require to provide any grid support, and their objective is to maximize its own benefit by producing power with maximum power point tracking (MPPT) strategy. However, at a high PV penetration network, PVPP needs to improve its operation to friendly integrate into the grid. From the conclusion of section 4.5, it is suggested that PVPP should provide reliable power and frequency support to maintain grid stability level.

### 5.1 Proposed Fundamental Concept

The challenge of operation improvement is the balance between operating costs and grid support from the solar resource. This research proposes a grid-friendly dispatch strategy (GFDS) while considering both the PV owner and grid benefit. To reduce BES degradation, low duty cycle application as correcting schedule reserve is assigned to BES. While high duty cycle application as frequency response service is assigned to an internal active power reserve (iR) instead.

The proposed grid-friendly dispatch strategy divides the PVPP power profile into 4 components to provide multiple functions ordering from high to low priority, as shown below.

1. Day-Ahead Schedule Component (DSC)

Scheduled power would reduce solar uncertainty and system reserve

2. Load Frequency Regulation Component (LRC)

This component can be an additional income for PVPP. Moreover, inverter-based PVPP is suitable to provide LRC because it has fast response capability with high accuracy [34].

### 3. BES Restoration Component (BRC)

BES needs to be restored from the solar resource for compensating insufficient scheduled power.

### 4. Frequency Support Component (FSC)

The excess scheduled power is not waste by turning it to FSC. It imitates a conventional generator, which is inertia and primary response support function [27].

The GFDS is the combination of DSC, LRC, BRC, and FSC. This strategy could be reduced SO concern in terms of reliability while providing additional support services. Both DSC and LRC are scheduled in the day ahead and hour ahead operation stage by solving the optimization problem in the day ahead period and hour ahead period, respectively.

The solar power forecast is necessary to estimate expected PV production in the next prediction horizon. Day-ahead solar forecasts have low accuracy compare to an hour ahead forecast and always have an error. Even though BES could compensate for this error, BES has limited resources. In this study, BES resource is coming from only one source, that is the solar resource. Thus, the lower DSC than a predicted day ahead solar power can reduce this component uncertainty. PVPP providing only DSC could lead to high curtailment, waste revenue, and waste green energy. This strategy made PVPP provide additional components as LRC to efficiently utilize the uncertainty resource by preparing operational reserve with an updated shorter period of solar power forecast (on an

hourly basis). In a real-time period, the excess power would be recharged to restore BES energy (BRC), and then the remaining is used as frequency support (FSC), as suggested by section 4.5, to reduce curtailment and system frequency deviation.

The overview signal flow between controller and PVPP can be described in Figure 5-1.

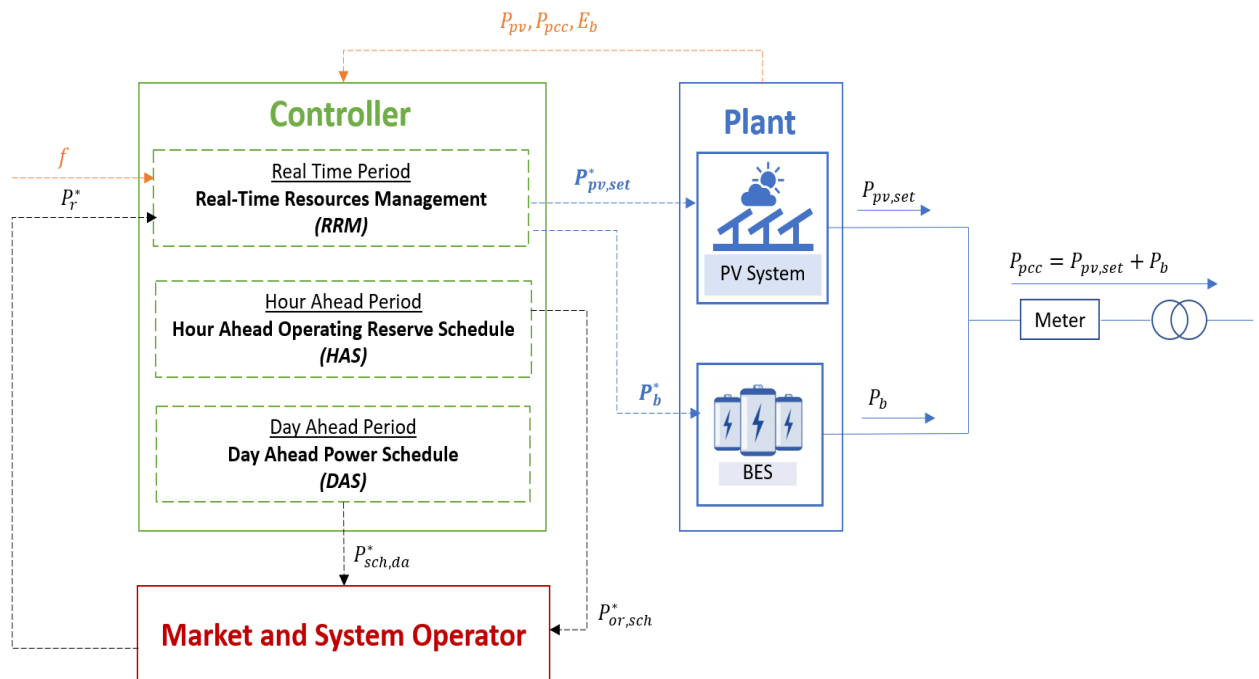


Figure 5-1 The overview signal flow between controller and PVPP.

From Figure 5-1, the controller has 3 time periods of operation, day ahead period, hour ahead period, and real-time period. It monitors MPPT PV power ( $P_{pv}$ ), power at the point power coupling ( $P_{pcc}$ ) and BES energy level ( $E_b$ ). The day-ahead period function is the day-ahead schedule (DAS) that give day ahead scheduling power set point ( $P_{sch,da}^*$ ) to the system operator for dispatch cooperation. Hour ahead period function is an hour ahead operating reserve service (HAS) that give hour-ahead schedule operating reserve ( $P_{or,sch}^*$ ) as a limitation for providing

LRC to the system operator. Real-time functions are real-time resources management (RRM), which trying to manage resources within the plant to correct scheduled components (DSC, LRC), restore BES (BRC) and provide frequency support (FSC). The controller combines all power components set points and then send the main setpoint ( $P_{pv,set}^*$ ,  $P_b^*$ ) to PV and BES inverter for adjusting PV and BES output ( $P_{pv,set}$ ,  $P_b$ ), respectively, following the command. The combination of PV and BES output is the power at the point of power coupling ( $P_{pcc}$ ) injected into the power system.

There are two models for economic dispatch (ED), deterministic and stochastic ED. Stochastic ED requires an uncertainty model (popular to dealing with uncertainty). In comparison, deterministic ED has not required an uncertainty model, which is closeness to the current operation in industry practice [50] that requires a simple structure of optimization with good performance [50]. Thus, the deterministic ED is chosen for determining DSC and LRC.

The following sections explain the day-ahead schedule (DAS), the hour-ahead schedule service (HAS), and real-time resources management (RRM) in detail.

## **5.2 Day-Ahead Schedule (DAS)**

Day-ahead schedule (DAS) formulates optimization problem incorporate grid code ramp limit to generate the day-ahead scheduled PV power set point ( $P_{sch,da}^*$ ) every 24-hour rolling horizon.

### **5.2.1 Objective Function**

The objective function aims to maximize plant profit as shown in equation 5-1, selling of day-ahead schedule power ( $P_{sch,da}$ ) is the revenue,

and the additional cost terms are BES operation cost and ramp cost. The higher ramp cost will reduce the profit, and produce a smoother profile of  $P_{sch,da}$ .

$$\max \sum_{k=T_i}^{k=T_f} (p_{sch} P_{sch,da}(k) t_s - c_r R_{sch}(k)) \quad 5-1$$

where,  $t_s$  is the time step.  $p_{sch}$  is scheduled power price (\$/MWh).  $c_r$  is the ramp cost coefficient (\$/MW/h), which is arbitrarily chosen depend on designed smoothness.  $R_{sch}$  is the day-ahead scheduled power ramp, which can be calculated by equation 5-4.

### 5.2.2 Constraints

PVPP with BES is connected to the network at the point of connection. PV power at maximum power point ( $P_{pv}$ ) and solar forecast power ( $P_{sf}$ ) are modeled as the input information. The constraints are comprised of BES, power balance, and PV ramp limitation, as described in the following section.

#### 5.2.2.1 BES Model

BES model is for updating BES energy ( $E_b$ ) at the next time step, as shown in equation 5-2.

$$E_b(k+1) = E_b(k) - t_s \frac{P_{bd}(k)}{\eta_{bd}} + t_s \eta_{bc} P_{bc}(k) \quad 5-2$$

where,  $P_{bd}$  is BES discharged power.  $P_{bc}$  is BES charged power.  $\eta_{bd}$  is BES discharged power efficiency.  $\eta_{bc}$  is BES charged power efficiency.

BES energy, discharged, and charged power should be within its limit, which could be represented in equation 5-3.

$$\begin{aligned} E_{b,\min} &\leq E_b(k) \leq E_{b,\max} \\ 0 &\leq P_{bd}(k) \leq P_{bd,\max} \\ 0 &\leq P_{bc}(k) \leq P_{bc,\max} \end{aligned} \quad 5-3$$

where,  $E_{b,\min}$  and  $E_{b,\max}$  are minimum and maximum of usage BES energy, respectively.  $P_{bd,\min}$  and  $P_{bd,\max}$  are the minimum and maximum discharged power, respectively.  $P_{bc,\min}$  and  $P_{bc,\max}$  are minimum and maximum charged power, respectively.

To simplify the solution method from MILP to LP, the binary variable ( $\delta$ ), as shown in equation 3-4 to prevent charged and discharged power occur at the same time, can be neglected because the loss of PV power always occurs during charge and discharge, thus BES with maximized revenue objective automatically does not charge and discharge at the same time.

#### 5.2.2.2 Ramp Limitation

Grid code ramp limitation can be implemented as ramp constraints. The excess scheduled power is assigned to LRC, which can be seen as ramp reserve. Typically, the ramp limit is applied to  $P_{pcc}$  to reduce disturbance to the network. However, in this research, the ramp limit can not implement to  $P_{pcc}$  because PVPP provides frequency support, which  $P_{pcc}$  profile can not be smooth because this fluctuation is beneficial to the grid. Thus, the ramp limit requirement will be imposed to  $P_{sch,da}$  instead.

The absolute day-ahead scheduled power ramp ( $R_{sch}$ ) can be calculated by equation 5-4.



$$R_{sch}(k) = \frac{|P_{sch,da}(k) - P_{sch,da}(k-1)|}{t_s} \quad 5-4$$

To make absolute equality constraint in equation 5-4 can be solved by linear programming, this equation will be transformed to inequality constraints, as shown in equation 5-5.

$$-R_{sch}(k) \leq \frac{P_{sch,da}(k) - P_{sch,da}(k-1)}{t_s} \leq R_{sch}(k) \quad 5-5$$

The day-ahead scheduled PV power should be less than the ramp limitation requirement ( $R_{limit}$ ), as shown in equation 5-6.

$$0 \leq R_{sch}(k) \leq R_{limit} \quad 5-6$$

To prevent stability problem from a large generator trip or sudden drop of PV power in high PV penetration system,  $R_{limit}$  can be set by using critical ramp capability in Figure 4-10 as a guide line.  $R_{limit}$  should be equal or lower than critical ramp capability at chosen PVR and expected disturbance.

### 5.2.2.3 Power Balance

DAS needs solar power prediction information to estimate the expected power. The day-ahead solar forecast power ( $P_{sf,da}$ ), as well as BES discharged power ( $P_{bd}$ ) can be seen as an expected input. The expected outputs which are day-ahead scheduled power ( $P_{sch,da}$ ) and charged power of BES ( $P_{bc}$ ) require power from expected inputs. The net

expected output should be less than the net expected input, as shown in equation 5-7.

$$P_{sch,da}(k) + P_{bc}(k) \leq \tilde{P}_{sf,da}(k) + P_{bd}(k) \quad 5-7$$

where,  $\tilde{P}_{sf,da}$  is the modified solar forecast power that depends on the reduction factor defined by the user.  $P_{sf,da}$  can be modified by multiplying the reduction factor of day-ahead solar power forecast ( $r_{da}$ ), as shown in equation 5-8.

$$\tilde{P}_{sf,da}(k) = r_{da} P_{sf,da}(k) \quad 5-8$$

The higher reduction factor can be seen as a higher expected internal active power reserve (iR). However, the revenue will decrease because of the lower DSC.

### 5.3 Hour Ahead Operating Reserve Service (HAS)

The expected excess power of the hour ahead solar power forecast, when compared to the day-ahead solar power forecast, can be seen as the expected operational reserve, which PVPP could provide.

However, PVPP should not provide the maximum value of expected excess energy because solar forecast always has uncertainty, and the BES reserve is limited. The optimization for scheduling will be established to generate hour-ahead scheduled power of operational reserve signal ( $P_{or,sch}^*$ ). This signal will be sent to SO every hour. It gives the operational reserve limit of load frequency regulation provided by PVPP.

### 5.3.1 Rolling Horizon Strategy

The solution will be generated in rolling horizon fashion that gives the optimal solution within the defined interval from the initial time step ( $t = k_i$ ) to final time step ( $t = k_f$ ) in the future. The rolling horizon strategy can reduce uncertainty by re-solved this problem when information update. To give a suitable set point, the updated solar forecast power every hour ( $P_{sf,ha}$ ) and updated BES energy ( $E_b(k_f)$ ) are required.

This optimization will be re-calculated every time step to correct the uncertainty. The prediction interval ( $N_p$ ) of the rolling horizon should be determined because a longer prediction interval has a higher error. In this research, the 2 step prediction interval is applied.

Note that; It can be assumed to use single  $P_{sf,ha}$  profile because the small prediction step interval leads each hour ahead solar forecast every time step is relatively similar.

### 5.3.2 Objective Function

The objective function is to maximize operating reserve revenue, as shown in equation 5-9.

$$\max \sum_{k=k_i}^{k=k_f} (p_{or} P_{or,sch}(k)) t_s \quad 5-9$$

where,  $p_{or}$  is an operating reserve price (\$/MW). The ramp cost is not considered because the load frequency regulation reserve needs high ramp capability performance.

### 5.3.3 Constraints

Ramp limitation constraints are not included in HAS because this model required high ramp capability performance. Other constraints are similar to DAS with some modifications, as shown in the following sections.

#### 5.3.3.1 BES Model

It is necessary to know the updated BES energy ( $E_b(k_i)$ ) because it gives the potential of uncertainty handling by BES. BES constraints are the same as DAS. However, BES energy at the final step ( $t = k_f$ ) should remain above the user's defined level (ex.  $0.5\text{Cap}_{\text{bat}}$ ), as shown in equation 5-10, to reserve BES for the next interval.

$$E_b(k_f) \leq 0.5\text{Cap}_{\text{bat}} \quad 5-10$$

#### 5.3.3.2 Power Balance

The differentiation between hour ahead solar power forecast and day-ahead scheduled power is the maximum expected available operating reserve power ( $P_{\text{or,sch}}^{\text{max}}$ ), as shown in equation 5-11.

$$P_{\text{or,sch}}^{\text{max}}(k) = \begin{cases} P_{\text{sf,ha}}(k) - P_{\text{sch,da}}(k), & P_{\text{sf,ha}}(k) \geq P_{\text{sch,da}}(k) \\ 0 & \text{Otherwise} \end{cases} \quad 5-11$$

where,  $P_{\text{bd}}$  is part of input and  $P_{\text{bc}}$  is part of the output. Summation of outputs ( $P_{\text{or,sch}}$  and  $P_{\text{bc}}$ ) should not be more than the summation of inputs ( $P_{\text{or,sch}}^{\text{max}}$  and  $P_{\text{bd}}$ ), as shown in equation 5-12.

$$P_{\text{or,sch}}(k) + P_{\text{bc}}(k) \leq \tilde{P}_{\text{or,sch}}^{\text{max}}(k) + P_{\text{bd}}(k) \quad 5-12$$

where,  $\tilde{P}_{or,sch}^{max}$  is the modified maximum expected available operating reserve power ( $P_{or,sch}^{max}$ ), as shown in equation 5-13 for reducing risk.

$$\tilde{P}_{or,sch}^{max}(k) = r_{ha} P_{or,sch}^{max}(k) \quad 5-13$$

where,  $r_{ha}$  is a reduction factor of an hour ahead expected operating reserve, which can be defined by the user. The higher reduction factor can be seen as higher internal active power (iR), but the revenue of this component will be reduced.

#### **5.4 Real-Time Resource Management (RRM)**

The  $P_{pv}$  power profile of GFDS is separated into 4 components (DSC, LRC, BRC, FSC). The internal and external active power reserve (iR and BES) help PVPP dispatch PV power by order of components priority. The first and second priorities are to compensate for the error of day-ahead scheduled PV power and the error of load frequency regulation by BES, respectively. The third priority is to maintain the state of charge (SOC) level for restoring BES. In this case, the SOC reference can be chosen as the maximum limit of SOC because BES does not need space from supporting function but only need to provide power to correct schedule error. The fourth priority is to providing frequency support by the remaining power instead of curtailment to manage the resource efficiently.

In concluding, four power components would be prioritized to use PVPP's reserve in the real-time period: 1. day-ahead schedule component (DSC), 2. load frequency regulation component (LRC), 3. energy

restoration component (BRC), and 4. frequency support component (FSC).

RRM is divided into three functions consist of real-time available operating reserve (ROR), real-time PV power command (RPC), and real-time BES power command (RBC) to provide the required aforementioned features. They will coordinate each other and send command setpoints to BES and PV inverter in real-time. ROR determines the actual iR of each power component and sends updated status to RPC for computing actual power setpoint without reserve of each component. RBC determine borrowed power from BES for DSC and LRC and borrowed power from  $P_{pv}$  for BRC. The power plant and controller were modeled by MATLAB/SIMULINK. Both plant models and algorithms will be described in the following section in detail.

Note:  $t$  represents the signal generated by the simulation in real-time at time  $t$ .

#### 5.4.1 Output Power at PCC

The power at the point of power coupling ( $P_{pcc}(t)$ ) is the combination of PV power output following the setpoint command ( $P_{pv,set}(t)$ ) and BES power output following setpoint command ( $P_b(t)$ ), as shown in equation 5-14.

$$P_{pcc}(t) = P_{pv,set}(t) + P_b(t) \quad 5-14$$

$P_{pv,set}(t)$  is the result of the PV inverter model after receiving the command  $P_{pv,set}^*(t)$ . Because this plant model is designed for power system application, it can be neglected inverter loss and be assumed that

PV inverter output can 100% follow the command from RRM, as shown in equation 5-15.

$$P_{pv,set}(t) = P_{pv,set}^*(t) \quad 5-15$$

BES energy in the simulation ( $E_{bs}(t)$ ) is modeled as an integrator to represent BES behavior. The stored energy is reduced and increased when discharging and charging, respectively, as shown in equation 5-16.

$$E_{bs}(t) = -\int P_b(t)dt \quad 5-16$$

$$E_{b,min} \leq E_{bs}(t) \leq E_{b,max}$$

where,  $E_{bs}$  and  $P_b$  are BES energy and power in the simulation, respectively, in real-time.

BES model receives the total borrow command  $P_b^*$  from the controller, the discharge sign is positive, and the charge sign is negative. The output BES power ( $P_b$ ) can not be over BES power limitation, as shown in equation 5-17.

$$P_b(t) = \begin{cases} \min(P_b^*(t), P_{bd,limit}), & \text{if } P_b^*(t) > 0 \\ \max(P_b^*(t), P_{bc,limit}), & \text{otherwise} \end{cases} \quad 5-17$$

However, BES energy is limit. If BES energy ( $E_{bs}$ ) reaches the minimum limit ( $E_{b,min}$ ), BES can not be discharged and discharged power limit ( $P_{bd,limit}$ ) will turn to zero, as shown in equation 5-18. On the other hand, if BES energy reaches the maximum limit ( $E_{b,max}$ ), BES can not be

charged and charged power limit ( $P_{bc,limit}$ ) will turn to zero, as shown in equation 5-19.

$$P_{bd,limit} = \begin{cases} P_{b,max}, & \text{if } E_{bs}(t) > E_{b,min} \\ 0, & \text{otherwise} \end{cases} \quad 5-18$$

$$P_{bc,limit} = \begin{cases} P_{b,min}, & \text{if } E_{bs}(t) < E_{b,max} \\ 0, & \text{otherwise} \end{cases} \quad 5-19$$

where,  $P_{b,max}$  and  $P_{b,min}$  are the maximum and minimum power of BES in the simulation, respectively.

#### 5.4.2 Real-time Available Operating Reserve

The operating reserve is determined in order of component priority. The internal active power reserve (iR) of day-ahead schedule power is determined first. The remaining power between  $P_{pv}$  minus by  $P_{sch,da}$  is the actual operating reserve ( $P_{or,a}$ ) that is determined by equation 5-20.

$$P_{or,a}(t) = \begin{cases} P_{pv}(t) - P_{sch,da}^*(t), & \text{if } P_{pv}(t) > P_{sch,da}^*(t) \\ 0, & \text{otherwise} \end{cases} \quad 5-20$$

This operating reserve ( $P_{or,a}$ ) will be used by actual load frequency regulation command ( $P_{r,a}^*$ ) sent from RPC. The remaining energy is for BES restoration reserve ( $P_{or,eb}$ ) and can be computed by equation 5-21.

$$P_{or,eb}(t) = \begin{cases} P_{or,a}(t) - P_{r,a}^*(t), & \text{if } P_{or,a}(t) > P_{r,a}^*(t) \\ 0, & \text{otherwise} \end{cases} \quad 5-21$$



$P_{or,eb}$  is used by BES charging power ( $P_{b,ch}$ ) to restore BES energy reaching the reference level. The remaining operating reserve ( $P_{or,ip}$ ), as shown in equation 5-22, will be returned to the grid for free by inertia and primary response power ( $P_{ip}$ ) as long as  $P_{or,ip}(t)$  is not deplete.

$$P_{or,ip}(t) = P_{or,eb}(t) - |P_{b,ch}(t)| \quad 5-22$$

### 5.4.3 Real-time PV Power Command

This function generates the setpoint command ( $P_{pv,set}^*(t)$ ) to PV inverter by the combination of each actual component power command, as shown in equation 5-23.

$$P_{pv,set}^*(t) = P_{sch,a}^*(t) + P_{r,a}^*(t) - P_{b,ch}^*(t) + P_{ip,a}^*(t) \quad 5-23$$

where,  $P_{sch,a}^*$  is the actual scheduled power command.  $P_{r,a}^*$  is the actual load frequency regulation command.  $P_{b,ch}^*$  is the actual charged power command (negative value).  $P_{ip,a}^*$  is the actual inertia and primary response power command.

The actual DSC, LRC, BRC, and FSC can be derived in the following section.

#### 5.4.3.1 DSC at Real-Time

$P_{sch,da}^*$  is determined base on the expected solar forecast from the previous day, which always has uncertainty. The lower value between  $P_{pv}(t)$  and  $P_{sch,da}^*(t)$  is the actual scheduled power command ( $P_{sch,a}^*$ ), as shown in equation 5-24.

$$P_{sch,a}^*(t) = \min(P_{pv}(t), P_{sch,da}^*(t)) \quad 5-24$$

### 5.4.3.2 LRC at Real-Time

Hour-ahead scheduled operating reserve command ( $P_{or,sch}^*$ ) is sent to SO to set the upper and lower limit for determining load frequency regulation command ( $P_r^*$ ), which can be calculated by equation 5-25.

$$P_r^*(t) = \begin{cases} \min(P_{agc,pv}^*(t), 0.5P_{or,sch}^*(t)), & \text{if } df(t) < 0 \\ \max(P_{agc,pv}^*(t), -0.5P_{or,sch}^*(t)), & \text{otherwise} \end{cases} \quad 5-25$$

$$P_{agc,pv}^*(t) = K_{agc,pv} \int df(t)dt \quad 5-26$$

where,  $P_{agc,pv}^*$  and  $K_{agc,pv}$  are automatic generation power command and control gain for PVPP, respectively.  $df$  is the system frequency deviation.

The actual load frequency regulation power ( $P_{r,a}$ ) in real-time operation can not swing into scheduled power at the point of common coupling ( $P_{pcc,sch}$ ) region. It swings on the operating baseline, which is equal to  $0.5P_{or,sch}^*$ . The adjusted load frequency regulation power command ( $\tilde{P}_r^*$ ) is shown in equation 5-27.

$$\tilde{P}_r^*(t) = P_r^*(t) + 0.5P_{or,sch}^*(t) \quad 5-27$$

$\tilde{P}_r^*$  is sent to RPC to determine actual load frequency regulation power command ( $P_{r,a}^*$ ) which can not over  $P_{or,a}$  as shown in equation 5-28.

$$P_{r,a}^*(t) = \min(\tilde{P}_r^*(t), P_{or,a}(t)) \quad 5-28$$

### 5.4.3.3 BRC at Real-Time

The actual charged power command ( $P_{b,ch}^*$ ) to restore BES energy is determined by equation 5-29.

$$P_{b,ch}(t) = \begin{cases} P_b(t), & \text{if } P_b(t) < 0 \\ 0, & \text{otherwise} \end{cases} \quad 5-29$$

$$P_{b,ch}^*(t) = P_{b,ch}(t)$$

where,  $P_b$  is the BES output power in the simulation.

### 5.4.3.4 FSC at Real-Time

Inertia frequency support power command ( $P_i^*$ ) is computed by equation 5-30.

$$P_i^*(t) = -H_{pv} \frac{df}{dt} \gamma \quad 5-30$$

where,  $H_{pv}$  is the emulated inertia constant provided by PVPP.  $\gamma$  is the binary variable for activating the command, which value is between 0 and 1, as shown in equation 5-31.

$$\gamma = \begin{cases} 0, & \text{if } P_{sch,da}^*(t) > 0 \\ 1, & \text{otherwise} \end{cases} \quad 5-31$$

The primary frequency support power command ( $P_p^*$ ) is computed by equation 5-32.

$$P_p^*(t) = -\frac{1}{R_{pv}} dfy \quad 5-32$$

where,  $R_{pv}$  is the primary response gain provided by PVPP. The combination  $P_i^*(t)$  and  $P_p^*(t)$  are limited by  $P_{or,ip}(t)$ .

The inertia and primary response power command ( $P_{ip}^*(t)$ ) is shown in equation 5-33.

$$P_{ip}^*(t) = \begin{cases} \min (P_i^*(t) + P_p^*(t), 0.5P_{or,ip}(t)), & \text{if } df(t) < 0 \\ \max (P_i^*(t) + P_p^*(t), -0.5P_{or,ip}(t)), & \text{otherwise} \end{cases} \quad 5-33$$

Actual inertia and primary response power ( $P_{ip,a}$ ) in real-time operation can not swing into the LRC region. It swings on the operating baseline, which is equal to  $0.5P_{or,ip}$ . The adjusted command is the actual inertia and primary response power command ( $P_{ip,a}^*$ ) can be shown in equation 5-34.

$$P_{ip,a}^*(t) = P_{ip}^*(t) + 0.5P_{or,ip}(t) \quad 5-34$$

#### 5.4.4 Real-time BES Power Command

This function generates the total borrowed command ( $P_b^*$ ) to BES, as shown in equation 5-35.

$$P_b^*(t) = P_{sch,br}^*(t) + P_{r,br}^*(t) - P_{eb,br}^*(t) \quad 5-35$$

where,  $P_{sch,br}^*$  and  $P_{r,br}^*$  are the borrowed BES power command for DSC and LRC, respectively.  $P_{eb,br}^*$  is borrowed solar power command for BRC.

Borrowed command of DSC, LRC, and BRC can be derived in the following section.

#### 5.4.4.1 DSC at Real-Time

When  $P_{pv}$  lower than  $P_{sch,da}^*$ , the controller calculates the borrowed command of day-ahead schedule power ( $P_{sch,br}^*$ ) from BES by the equation 5-36.

$$P_{sch,br}^*(t) = \begin{cases} P_{sch,da}^*(t) - P_{pv}(t), & \text{if } P_{pv}(t) < P_{sch,da}^*(t) \\ 0, & \text{otherwise} \end{cases} \quad 5-36$$

#### 5.4.4.2 LRC at Real-Time

When  $P_{r,a}^*(t)$  lower than  $P_r^*(t)$ , the controller calculates the borrow command of load frequency regulation ( $P_{r,br}^*(t)$ ) from BES by equation 5-37.

$$P_{r,br}^*(t) = \begin{cases} P_r^*(t) - P_{r,a}^*(t), & \text{if } P_{r,a}^*(t) < P_r^*(t) \\ 0, & \text{otherwise} \end{cases} \quad 5-37$$

#### 5.4.4.3 BRC at Real-Time

The restored BES command ( $P_{eb,ch}^*(t)$ ) is computed by equation 5-38.

$$P_{eb,ch}^*(t) = K_b(E_{b,ref} - E_b(t)) \quad 5-38$$

where,  $K_b$  is the BES restoration gain.

$P_{eb,ch}^*$  borrows energy from solar power, but  $iR$  is limited. The borrow command of BES energy restoration ( $P_{eb,br}^*$ ) should be not over the operating reserve  $P_{or,eb}$  as shown in equation 5-39.

$$P_{eb,br}^*(t) = \min(P_{eb,ch}^*(t), P_{or,eb}(t)) \quad 5-39$$

$P_{eb,br}^*$  is sent to the BES model, but BES energy is limited. Thus, the actual borrow power ( $P_{b,ch}$ ) can be less than  $P_{eb,br}^*$  which can be computed by equation 5-29.

#### 5.4.5 Composition of Actual Output Power at PCC

There are 4 power components of PVPP's power with GFDS at the point of common coupling ( $P_{pcc}$ ): 1. scheduled power ( $P_{pcc,sch}$ ) 2. load frequency regulation power ( $P_{pcc,r}$ ) 3. restored power ( $P_{pcc,eb}$ ) 4. inertia and primary response power ( $P_{pcc,ip}$ ). Component 1 and component 2 need to borrow energy from BES, and component 3 borrow energy from solar. Sometimes, the actual borrow power of each component is not equal to borrow command because the reserve is limit. The actual output of each component can be computed in equation 5-40-5-43.

$$P_{pcc,sch}(t) = P_{sch,a}(t) + P_{sch,br,a}(t) \quad 5-40$$

$$P_{pcc,r}(t) = P_{r,a}(t) + P_{r,br,a}(t) \quad 5-41$$

$$P_{pcc,eb}(t) = P_{eb,a}(t) + P_{eb,br,a}(t) \quad 5-42$$

$$P_{pcc,ip}(t) = P_{ip,a}(t) \quad 5-43$$

where,  $P_{sch,a}$ ,  $P_{r,a}$ ,  $P_{eb,a}$  and  $P_{ip}$  are the actual power of DSC, LRC, and BRC and FSC without borrowing power, respectively.  $P_{sch,br,a}$ ,  $P_{r,br,a}$ ,  $P_{eb,br,a}$  are the actual borrowed power for DSC, LRC, and BRC, respectively.

The actual borrowed power can be computed from the power command minus unserved power. Each component has the priority of borrowing reserve. Thus, the un-serve of borrowed power in each component can be calculated from the differentiation between  $P_b$  and borrowed power command of each component by order of priority (DSC, LRC, and BRC), respectively. The detail of the calculation is described in the following section.

Note: the BES output power ( $P_b$ ) has both positive and negative value. For the convenience of calculation, discharged and charged BES output power would be separated into two signals with a positive value, as shown in the following equation.

$$P_{b,p}(t) = \begin{cases} P_b(t), & \text{if } P_b(t) > 0 \\ 0, & \text{otherwise} \end{cases} \quad 5-44$$

$$P_{b,n}(t) = \begin{cases} |P_b(t)|, & \text{if } P_b(t) < 0 \\ 0, & \text{otherwise} \end{cases} \quad 5-45$$

where,  $P_{b,p}$  and  $P_{b,n}$  are the separated discharged and charged power (positive value).

#### 5.4.5.1 DSC at Real-Time

The unserved and actual borrowed power of day-ahead schedule command ( $P_{sch,br,uns}$ ,  $P_{sch,br,a}$ ) can be computed, as shown in equation 5-46 and 5-47.

$$P_{\text{sch,br,uns}}(t) = \begin{cases} P_{\text{sch,br}}^*(t) - P_{\text{b,p}}(t), & \text{if } P_{\text{sch,br}}^*(t) > P_{\text{b,p}}(t) \\ 0, & \text{otherwise} \end{cases} \quad 5-46$$

$$P_{\text{sch,br,a}}(t) = P_{\text{sch,br}}^*(t) - P_{\text{sch,br,uns}}(t) \quad 5-47$$

#### 5.4.5.2 LRC at Real-Time

$P_{\text{b,p}}$  is firstly used by  $P_{\text{sch,br,a}}$ . The remaining power can be calculated by equation 5-48.

$$P_{\text{re}}(t) = P_{\text{b,p}}(t) - P_{\text{sch,br,a}}(t) \quad 5-48$$

The unserved and actual borrowed power of load frequency regulation command ( $P_{\text{r,br,uns}}, P_{\text{r,br,a}}$ ) can be computed, as shown in equation 5-49 and 5-50.

$$P_{\text{r,br,uns}}(t) = \begin{cases} P_{\text{r,br}}^*(t) - P_{\text{re}}(t), & \text{if } P_{\text{r,br}}^*(t) > P_{\text{re}}(t) \\ 0, & \text{otherwise} \end{cases} \quad 5-49$$

$$P_{\text{r,br,a}}(t) = P_{\text{r,br}}^*(t) - P_{\text{r,br,uns}}(t); \quad 5-50$$

#### 5.4.5.3 BRC at Real-Time

The unserved and actual borrowed power of BES restoration command ( $P_{\text{eb,br,uns}}, P_{\text{eb,br,a}}$ ) can be computed, as shown in equation 5-51 and 5-52.

$$P_{\text{eb,br,uns}}(t) = \begin{cases} P_{\text{eb,br}}^*(t) - P_{\text{b,n}}(t), & \text{if } P_{\text{eb,br}}^*(t) > P_{\text{b,n}}(t) \\ 0, & \text{otherwise} \end{cases} \quad 5-51$$

$$P_{\text{eb,br,a}}(t) = P_{\text{eb,br}}^*(t) - P_{\text{eb,br,uns}}(t); \quad 5-52$$



## 5.5 Performance Evaluation Index

The contribution of grid-friendly dispatch strategy considers both sides, grid, and owner benefit.

The case studies are designed in the order of dispatch strategy development from base case (mppt) to proposed grid-friendly strategy (darf), as shown below.

1. mppt: PVPP provides maximum power (no control requirement).
2. da: PVPP with BES provides DSC with BRC
3. dar: PVPP with BES provides DSC and LRC with BRC
4. darf: PVPP with BES provide DSC, LRC, and FSC with BRC.

### 5.5.1 Owner Benefit Index

The benefit to the owner is evaluated by the revenue and resource utilization (solar and BES), as shown in the following section.

#### 5.5.1.1 Revenue

Revenue (Rev) with different strategies ( $Rev_{mppt}$ ,  $Rev_{da}$ ,  $Rev_{dar}$ ,  $Rev_{darf}$ ) are differently computed, as shown in equation 5-53 - 5-55.

$$Rev_{mppt} = ep_{nf}E_{pv,mppt} \quad 5-53$$

$$Rev_{da} = ep_{da}E_{pcc,sch} \quad 5-54$$

$$Rev_{darf} = Rev_{dar} = Rev_{da} + Rev_r \quad 5-55$$

where,  $Rev_{mppt}$  is the revenue of PVPP that operates base on the MPPT strategy.  $Rev_{da}$  is the revenue coming from DSC. The revenue of dar and darf case ( $Rev_{dar}, Rev_{darf}$ ) is equal because FSR is free frequency support. Thus, there is no revenue coming from this component.  $ep_{nf}$  is a non-firm energy price coefficient (\$/MWh).  $ep_{da}$  is the day-ahead contract energy price coefficient (\$/MWh).

Maximum PVPP energy without curtailment ( $E_{pv,mppt}$ ), total actual solar energy delivered to the grid at the point of common coupling ( $E_{pcc}$ ) during the interested period between initial time ( $t_1$ ) and final time ( $t_F$ ) can be calculated by the following equation.

$$E_{pv,mppt} = t_s \sum_{t=t_1}^{t=t_F} P_{pv}(t) \quad 5-56$$

$$E_{pcc} = t_s \sum_{t=t_1}^{t=t_F} P_{pcc}(t) \quad 5-57$$

$Rev_r$  is the revenue coming from LRC, as shown in equation 5-58. If actual load frequency regulation power ( $P_{r,a}$ ) cannot follow 100% of LRC command,  $P_{or,sch}$  for that hourly interval will turn to zero.

$$Rev_r = cp_{ha} \sum P_{or,sch,v} \quad 5-58$$

where,  $cp_{ha}$  is an hour ahead capacity price coefficient (\$/MW). The available hour-ahead operating reserve power ( $P_{or,sch,v}$ ) is the committed

hour-ahead operating reserve that frequency regulation power can be supplied, following 100% of the LRC command.

### 5.5.1.2 PV Utilization Factor

The power of PVPP might be curtailed to keep following the power command. PV utilization factor (PUF) evaluates the efficiency of solar resource utilization, as calculated in equation 5-59.

$$PUF = \left\{ 1 - \frac{E_{pv,curt}}{E_{pv,mppt}} \right\} \times 100 \quad 5-59$$

where,  $E_{pv,curt}$  is the curtailment of PV energy, which can be computed by the following equation.

$$E_{pv,curt} = (E_{pv,mppt} - E_{b,ch}) - E_{pcc} \quad 5-60$$

where, restore to BES ( $E_{b,ch}$ ) during the interested period between initial time ( $t_I$ ) and final time ( $t_F$ ) can be calculated by the following equation.

$$E_{b,ch} = t_s \sum_{t=t_I}^{t=t_F} |P_{b,ch}| (t) \quad 5-61$$

### 5.5.1.3 State of Health of Battery

The Peukert lifetime energy throughput (PLET) model [91] is used to estimate battery aging base on the depth of discharge (DOD) and the number of cycles.

PLET model proposed in reference [91] defines DOD as the inverse of SOC ( $100\% - \text{SOC}$ ). However, this definition cannot reflect all battery activity in terms of charge and discharge cycle in practice [92]. The definition counting cycle of dept of discharge base on the basis of rain flow counting algorithm [93] is chosen instead. It can be expressed by half cycle of dept of discharge ( $d_{\text{half},j}$ ) of cycle  $j$ , as shown in the following equation [94].

$$d_{\text{half},j} = \frac{|E_{b,j} - E_{b,j-1}|}{\text{Cap}_{\text{bat}}} \quad 5-62$$

where,  $E_{b,j}$  is extreme battery energy state  $j$  (local maximum or local minimum) before changing by charging or discharging.

The full cycle of dept ( $d_{\text{full},j}$ ) comprise of two of half-cycle of dept ( $d_{\text{half},j}$ ) with the assumption that the charge and discharge cycle is identical when evaluated on a daily basis [95]. Thus, the energy throughput of the Peukert model ( $E_{b,\text{TP}}$ ), calculated based on half-cycle dept of discharge ( $d_{\text{half},j}$ ) is estimated, as shown in the following equation [93].

$$E_{b,\text{TP}} = \sum_{j=1}^{N_c} d_{\text{full},j}^{k_p} = 0.5 \sum_{j=1}^{N_c} d_{\text{half},j}^{k_p} \quad 5-63$$

where,  $d_{\text{half},j}$  is the depth of discharge of cycle  $j$ .  $k_p$  is Peukert lifetime constant (typical range between 1.1-1.3).  $N_c$  is the total number cycle of the battery energy profile.

The state of health of battery (SOH) can be expressed by the following equation.

$$\text{SOH}(\%) = \left( 1 - \frac{E_{b,TP}}{E_{b,TP}^{\text{life}}} \right) \times 100 \quad 5-64$$

where,  $E_{b,TP}^{\text{life}}$  is the total energy throughput the entire lifetime of the chosen battery.

### 5.5.2 Grid Benefit Index

The benefit to the grid is evaluated by the amount of energy of each component sending to the grid and its quality, as shown in the following paragraph.

#### 5.5.2.1 Day-ahead Scheduled Power Compliance Index

The Day-ahead scheduled power compliance index (DCI) of PVPP can be calculated by equation 5-65. DCI indicates the dependability of day-ahead scheduled power. The higher value of DCI is more dependable because of the lower of unserved energy.

$$\text{DCI} = 1 - \frac{E_{\text{uns,sch}}}{E_{\text{sch,da}}} \times 100 \quad 5-65$$

$P_{pv}$  is uncertainty. Thus, there is a chance of PVPP cannot serve the day-ahead scheduled power to the grid. The unserved energy of day-ahead scheduled power ( $E_{\text{uns,sch}}$ ) and day-ahead scheduled energy ( $E_{\text{sch,da}}$ )

during the interested period between initial time ( $t_i$ ) and final time ( $t_f$ ) can be calculated, as shown in the following equation.

$$E_{\text{uns,sch}} = t_s \sum_{t=t_i}^{t=t_f} P_{\text{sch,br,uns}}(t) \quad 5-66$$

$$E_{\text{sch,da}} = t_s \sum_{t=t_i}^{t=t_f} P_{\text{sch,da}}(t) \quad 5-67$$

### 5.5.2.2 Load Frequency Regulation Power Compliance

#### Index

The load frequency regulation power compliance index (LCI) of PVPP can be calculated by equation 5-68. LCI indicates the dependability of load frequency regulation power. The higher value of LCI is more dependable because of the lower of unserved energy.

$$LCI = \frac{\sum P_{\text{or,sch,v}}}{\sum P_{\text{or,sch}}} \times 100 \quad 5-68$$

where,  $P_{\text{or,sch,v}}$  is the valid hour-ahead operating reserve power that can be supplied following 100% of the LRC command.

### 5.5.2.3 Frequency Deviation Index

The system frequency deviation typically swings around nominal frequency ( $f_n$ ) and should be minimized to secure system stability. To evaluate the frequency deviation performance with both positive and

negative value, the mean absolute one-minute average frequency deviation with respect to nominal frequency ( $f_n$ ), similarly used in CPS1 [96], can be used to express performance as a frequency deviation index (FDI), as shown in equation 5-69.

$$\text{FDI} = \frac{1}{N_f} \sum_{i=1}^{N_f} |\overline{\Delta f_1}|_i \quad 5-69$$

where,  $|\overline{\Delta f_1}|_i$  is the absolute one-minute average frequency deviation of minute  $i$ .  $N_f$  is the final minute of the frequency data set.

FDI can reflect on how friendly integrating large amounts of PVPP to the power network because it represents the summation of absolute one-minute average frequency deviation. The higher FDI means the low potential of the power system to inject and absorb power imbalance. In contrast, the lower FDI means the power system has more capability to reduce frequency deviation. If FDI is lower due to the proposed method, it can conclude that GFDS makes PVPP friendly integrated into the power system.

## Chapter 6

### Test Results

#### 6.1 Simulation

##### 6.1.1 Test System

The performance of the proposed strategy is evaluated by the simulation. The test system diagram, as shown in Figure 6-1, is modeled by MATLAB/SIMULINK. It consists of PVPP with BES, controller, and system operator. In the model, the controller receives system frequency ( $f$ ) and receive frequency regulation command ( $P_r^*$ ) from system operator to set up commands to generate expected power at the point of connection ( $P_{pcc}$ ). At the same time, it sends the schedule operating reserve ( $P_{or,sch}^*$ ) to the system operator for the next hour operation.

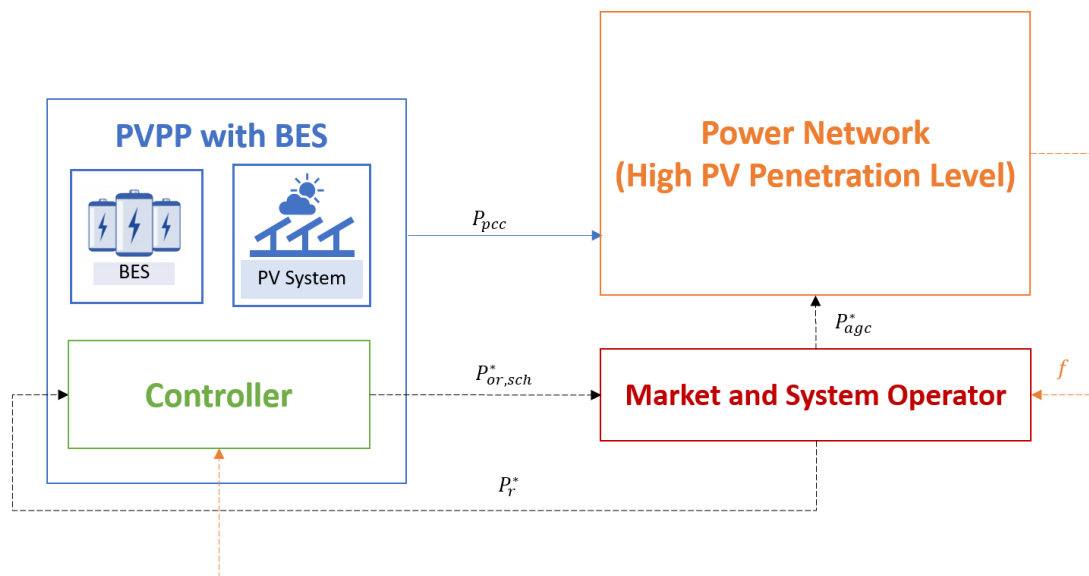


Figure 6-1 Test system diagram.



The test system model of PVPP and BES parameters are set as default and explained in Table A-1 and Table A-2, respectively. The price coefficients for optimization DAS and HAS, based on PJM market, are shown in Table A-5. BES control gain ( $K_b$ ) and SOC reference ( $E_{ref}$ ) are 1 and 80%, respectively. The reduction factor of day-ahead solar power forecast and hour-ahead expected operating reserve ( $r_{da}$ ,  $r_{ha}$ ) are 0.8 and 1, respectively. Prediction interval of HAS ( $N_p$ ) is for 2 hours.

To see the response of frequency related to injected PV power, therefore, the simulation needs a frequency response model as shown in Figure 3-4 using system parameters from the Table A-3. To represent the network characteristic of a high PV penetration, inertia and primary response gain of this model are changed related to the PV penetration level ( $PVR(t)$ ) as shown in equation 4-7 and 4-9 because PVPPs replace conventional generators.

### 6.1.2 Operating Conditions

The simulation model requires actual, day-ahead, and hour-ahead solar power profiles as inputs. Those profiles are obtained from the 1-year historical data of 70 MW Alabama's solar power plant entire year 2006 [97]. The data resolution of actual PV power ( $P_{pv}$ ), day-ahead forecast PV power ( $P_{sf,da}$ ) and hour ahead forecast PV power ( $P_{sf,ha}$ ) are 5, 60, and 60 minutes, respectively. The summary of simulation time step of input and output are shown in Table A-4.

The simulation situation is set at 40% of PV penetration level (PVL), which system has low inertia and receives power from PVPP with different strategies. For the worst-case experiment, by neglecting fluctuation power reduction due to disperse PVPPs, the aggregation of PVPPs with BES is modeled as a single PVPP with BES and scale power

up to the PVL setting. The model measures system frequency and sends power to the network, as shown in Figure 6-1; as a result, changing of system frequency.

PV penetration level (PVL) can be defined as:

$$\text{PVL} = \text{Cap}_{\text{PV,total}} / \text{baseMVA} \quad 6-1$$

where baseMVA is the system base (MVA), set equal to  $\text{Cap}_{\text{cov,max}}$ .  $\text{Cap}_{\text{PV,total}}$  and  $\text{Cap}_{\text{cov,max}}$  are total PV install capacity and maximum install capacity of the conventional generator when no PV penetration, respectively.

System frequency swings due to the unbalance between generation and netload. However, the resolution of the available net load profile is low at 5 minute-sampling rate of Thailand load profile in 2019 [98]. It can not represent the fluctuation of net load in the second sampling rate. Thus, the noise signal in second-resolution is generated as a synthesis net load fluctuation injected into the system model as a result in frequency fluctuation in the second sampling rate.

From observing sub-components of the reference frequency profile of nation grid ESO 2019 [99], there are 3 different cycle periods and magnitudes of sub-components, except the largest period that swings base on a 5-minute net load profile. The noise profile is generated by normally (Gaussian) distributed random function with zero means. These parameters of synthesis noise are designated by the sampling rate and variance of a random function, respectively. Before combining 3 noise signals to the load, each noise signal passes through a low pass filter to reduce the high-frequency component shown in Figure 6-2.

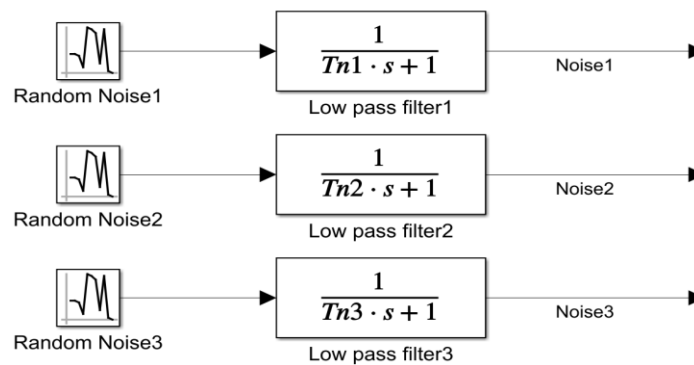


Figure 6-2 Noise generator blocks.

where,  $Ts_1$ ,  $Ts_2$ , and  $Ts_3$  are low pass filter time constant of noise signals 1, 2, and 3, respectively.

The parameters of the random noise generator can be shown in Table 6-1.

Table 6-1 Parameters of the random noise generator.

Signal Name	Mean	Variance	Noise Sampling (s)	Low pass Filter Time Constant (s)
Noise1	0	0.000002	1	10
Noise2	0	0.00001	10	20
Noise3	0	0.0003	100	180

The simulated frequency deviation  $df_{sim}$  compares with historical frequency deviation of ESO 2019 ( $df_{eso}$ ) are shown below.

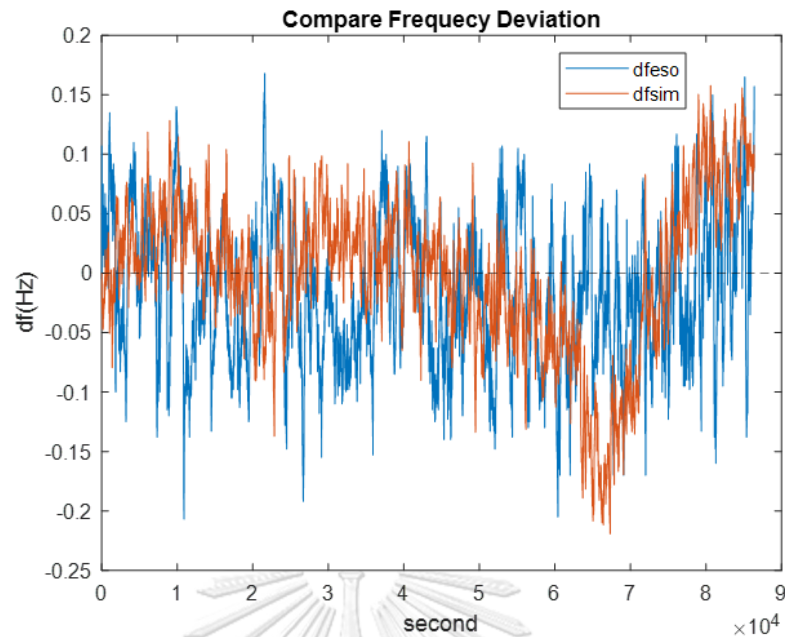


Figure 6-3 Synthesis frequency deviation.

From Figure 6-3, the largest cycle component of both frequency profile are different due to the difference in net load profile. However, the shorter period cycle of both frequency profile is similar. Thus, the synthesis frequency profile may represent a high-resolution characteristic of system frequency.

### 6.1.3 Simulated Test Results

The example overview profile of the selected day with sufficient and insufficient reserve is shown in the following section.

#### 6.1.3.1 Sufficient Reserve

The following figure shows the case of sufficient reserve on day 3.

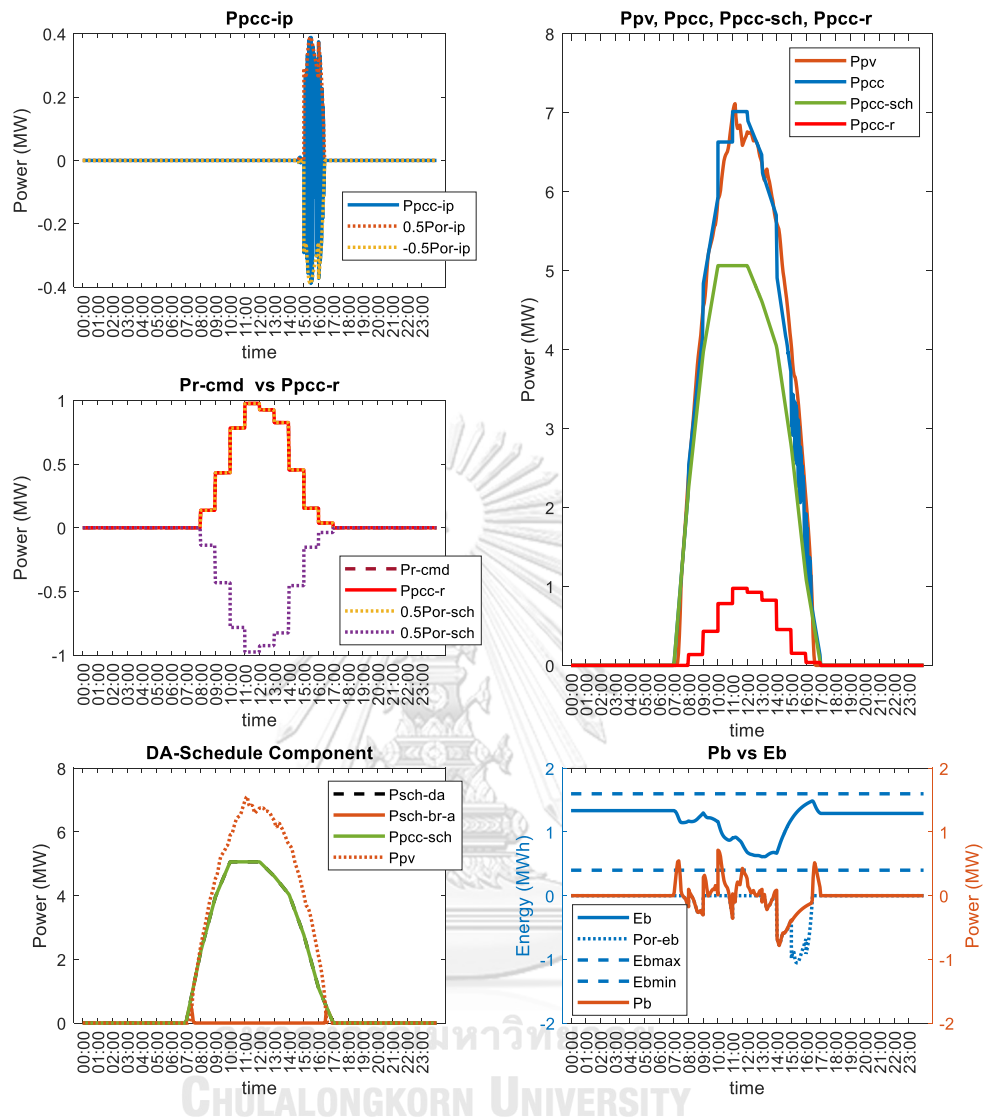


Figure 6-4 Power profile on day 3 (sufficient reserve).

From Figure 6-4, the proposed strategy can provide a reserve when  $P_{pv}$  is under components command because stored energy is enough for excess demand. For example,  $P_{pv}$  is under  $P_{sch,da}^*$  command at 7:00-7:30 and 16:30-17:00, and  $P_{pv}$  is under  $P_{sch,da}^*$  combined with  $P_{r,a}^*$  or  $P_{r,cmd}$  from 9:00-12:00. BES can compensate all this event.

### 6.1.3.2 Insufficient Reserve

The following figure shows the case of the insufficient reserve on day

2.

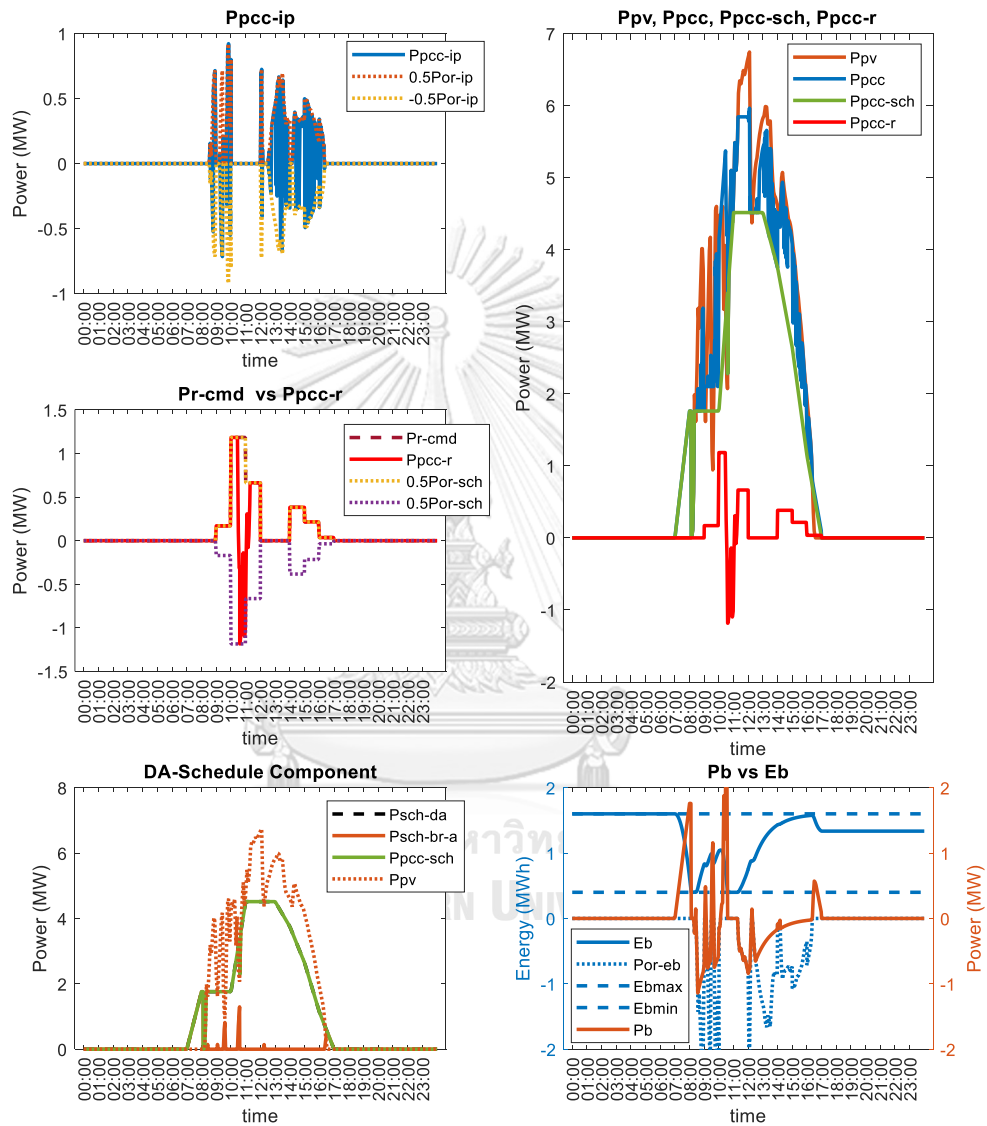


Figure 6-5 Power profile on day 2 (insufficient reserve).

From Figure 6-5, the proposed strategy can not provide a reserve when  $P_{pv}$  is under component command from 8:00-8:30 and 10:30

because large solar forecast error and the stored energy depleted. Another period with a small solar forecast error at 9:00 and 16:30-17:00, the proposed strategy can compensate for this error and can follow  $P_{sch,da}^*$  command.

For LRC, the unserved power event occurs during 10:00-11:00 because stored energy depleted as a result in minus  $P_{pcc,r}$ .

### 6.1.4 Verification of Power Commands

This section presents the figure of each component to verify the implemented algorithm by the simulation. If it works correctly, each component will not operate over the limit. When BES has enough energy to support insufficient power, each power component and the actual borrow power should follow the command. On the other hand, if BES energy is depleted, it should not follow the command.

The verification of power command in each component is passed, described in detail in the following section. The insufficient reserve day is chosen on day 2.

#### 6.1.4.1 DSC Component

The result of DAS is the first component as DSC or  $P_{pcc,sch}$  (green line). From Figure 6-6,  $P_{pcc,sch}$  can almost follow 1-day profile of  $P_{sch,da}^*$  (black dash line).  $P_{sch,br,a}$  (orange color) can correctly respond to insufficient of  $P_{pv}$ , except when the BES energy (blue line) is exhausted from 8:00-8:30, as shown in Figure 6-6.

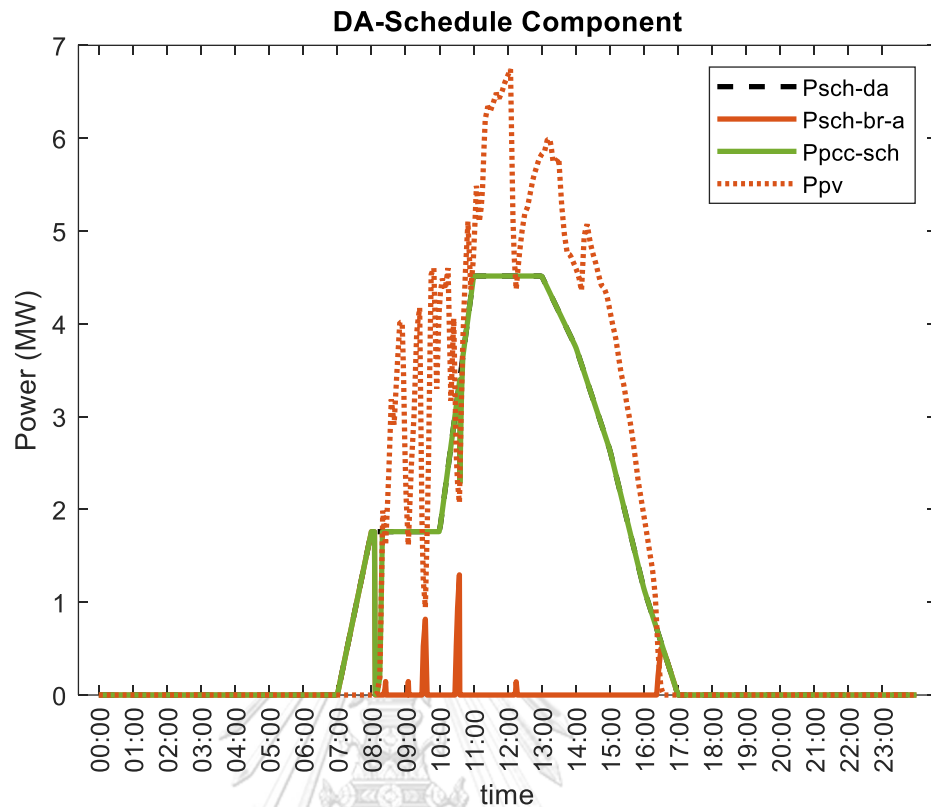


Figure 6-6 DSC profile on day 2.

#### 6.1.4.2 LRC Component

The result of HAS is the second component as LRC or  $P_{pcc,r}$  (red line). From Figure 6-7, when BES energy is not depleted, it can follow the 1-day profile of  $P_{r,a}^*$  or  $P_{r,cmd}$  (brown dash line), and is not over-scheduled operational reserve limit ( $0.5P_{or,sch}^*/-0.5P_{or,sch}^*$ ) (dot line).



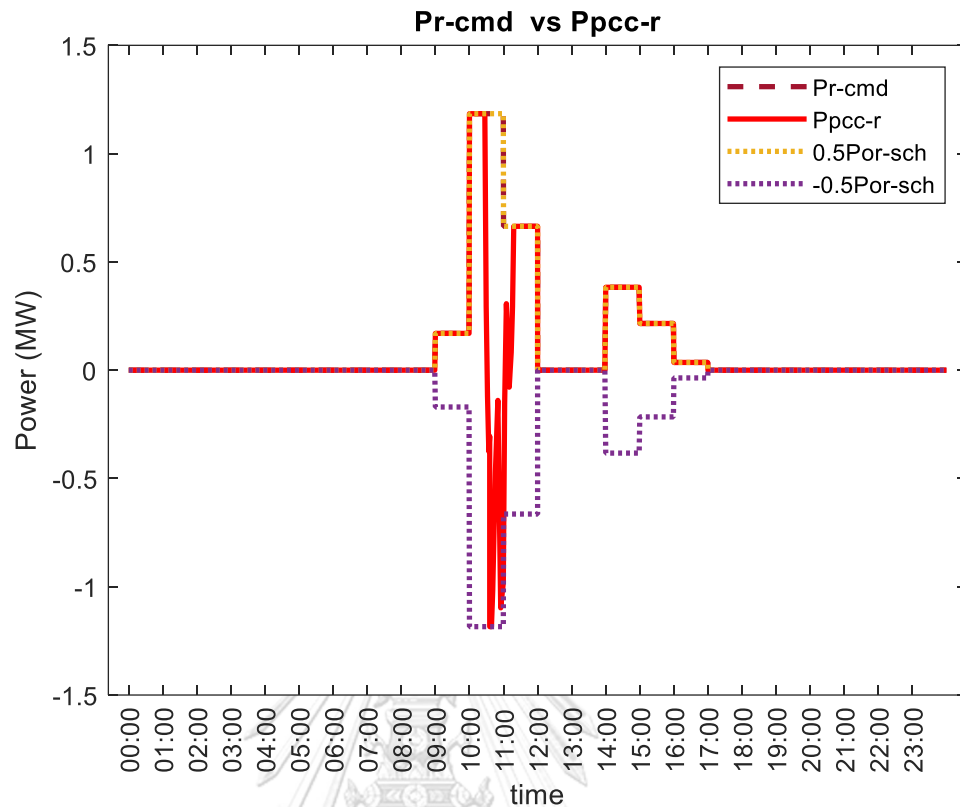


Figure 6-7 LRC profile on day 2.

Even though  $P_{r,a}^*$  or  $P_{r,cmd}$  is all positive,  $P_{pcc,r}$  can not follow the command and appears negative from 10:30 to 11:00 because large solar forecast error and BES energy are not enough to compensate this uncertainty. During this event, PVPP can not provide both  $P_{pcc,r}$  and  $0.5P_{or,sch}^*$ .

When  $P_{pcc,sch}$  combines with  $P_{pcc,r}$ ,  $P_{pcc,r}$  can be noticed on top of  $P_{pcc,sch}$  as shown as the white-blue line in Figure 6-8.

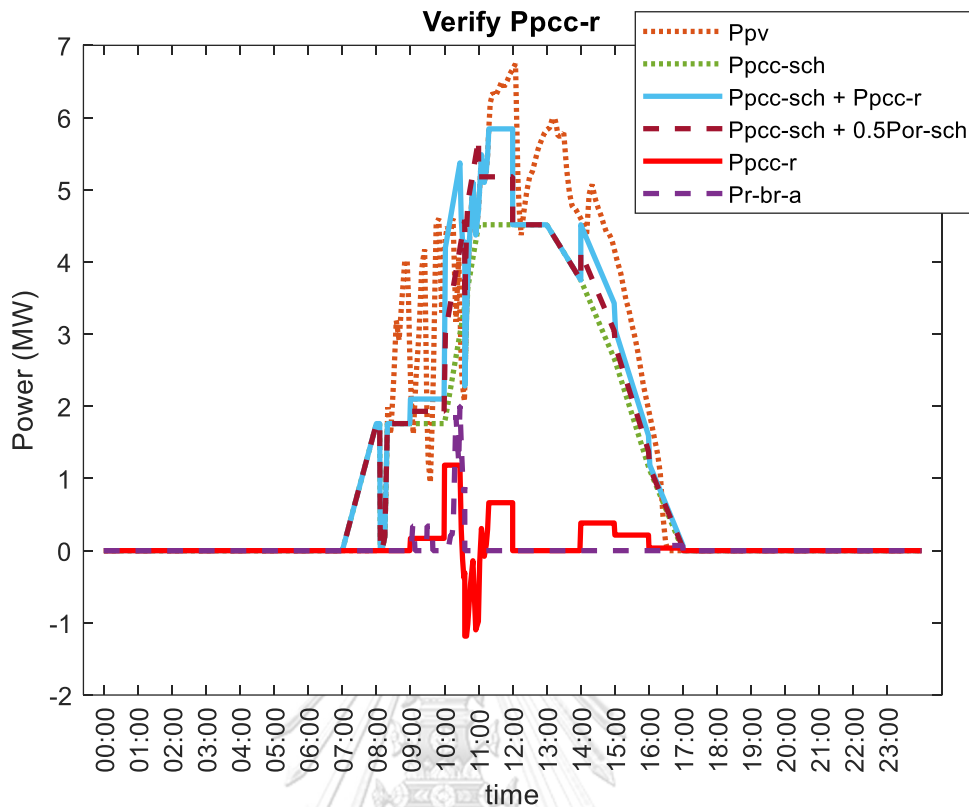


Figure 6-8 The combination of DSC and LRC profile on day 2.

$P_{pcc,r}$  (red line) can be a positive and negative value, thus midpoint of  $P_{or,sch}^*$  is typically injected and combined with  $P_{pcc,sch}$  as an operating baseline as shown as brown dash line ( $P_{pcc,sch} + 0.5P_{or,sch}^*$ ) that  $P_{pcc,r}$  can swing around. When comparing the white-blue line to the brown-dash line, it can be seen as  $P_{pcc,r}$  swings around the operating baseline ( $0.5P_{or,sch}^*$ ) above  $P_{pcc,sch}$  correspond with the magnitude of  $P_{pcc,r}$  (red line).

The insufficient of  $P_{pv}$  for  $P_{pcc,r}$  and  $0.5P_{or,sch}^*$  during 9:00-10:30 can be compensated with BES by  $P_{r,br,a}$ . However, BES energy depleted during 10:30-11:00 as a result in negative  $P_{pcc,r}$ .

### 6.1.4.3 BRC Component

The third component is BRC or  $P_b$  as shown in Figure 6-9.

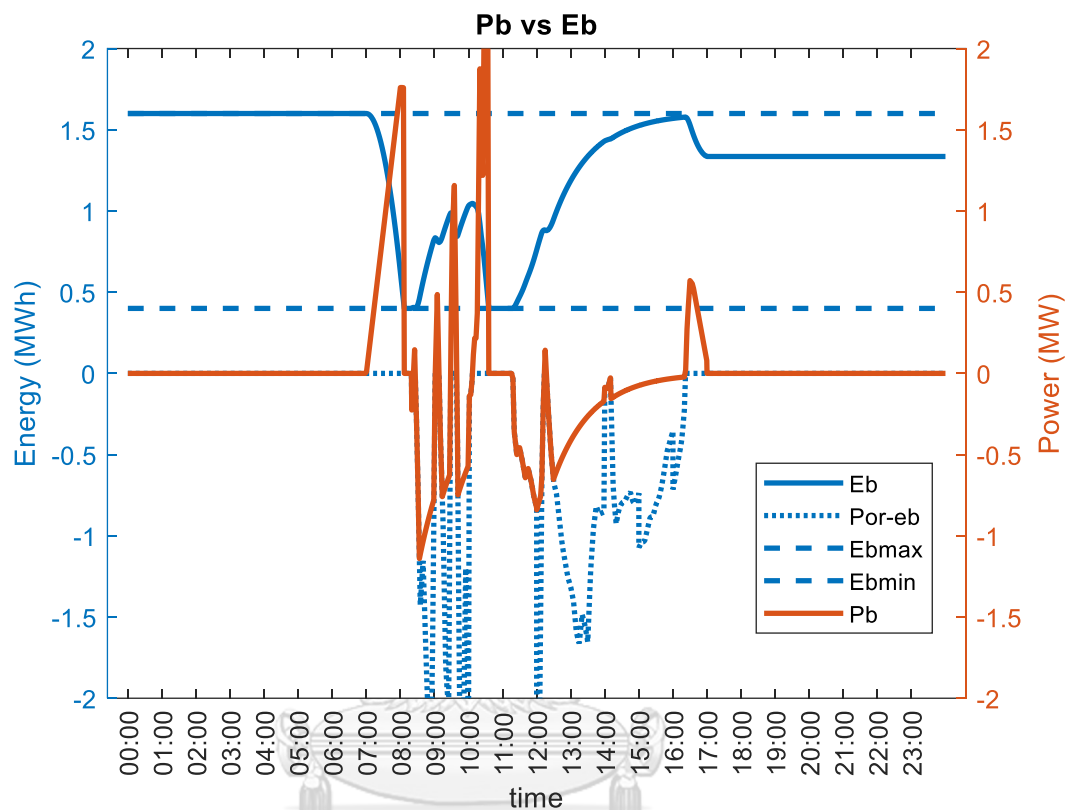


Figure 6-9 BES profile on day 2.

When  $E_b$  below  $E_{b,ref}$  ( $= E_{b,max}$ ) and there are still have the remaining  $P_{or,eb}$  (blue dot line) BES can be charged. This figure shows that charging power is not over the limit ( $P_{or,eb}$ ).  $E_b$  profile trend shows that BES operates correctly, correspond the need for DSC and LRC, and charged control gain  $K_b = 1$ .

#### 6.1.4.4 FSC Component

The Fourth component is FSC or  $P_{pcc,ip}$  as shown in Figure 6-10., This component operates correctly by not letting  $P_{pcc,ip}$  over the remaining power  $P_{or,ip}$  (dot line).

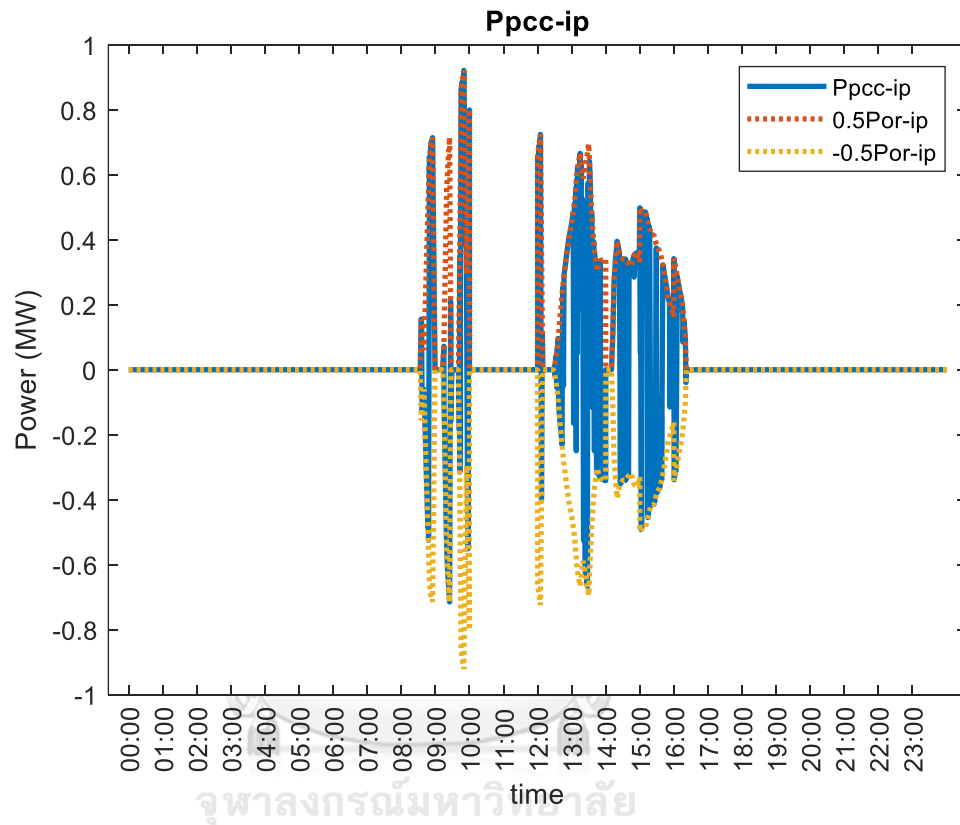


Figure 6-10 FSC Profile on day 2.

When four components (DSC, LRC, BRC, FSC) are combined as  $P_{pcc}$  (blue line) It can be shown in Figure 6-11. It can be noticed that  $P_{pcc}$  belows  $P_{pv}$ , if there is a need for BES restoration. If there is not enough power to restored BES or BES is full,  $P_{pcc}$  can be equal to  $P_{pv}$  when  $P_{pcc,ip}$  is positive.

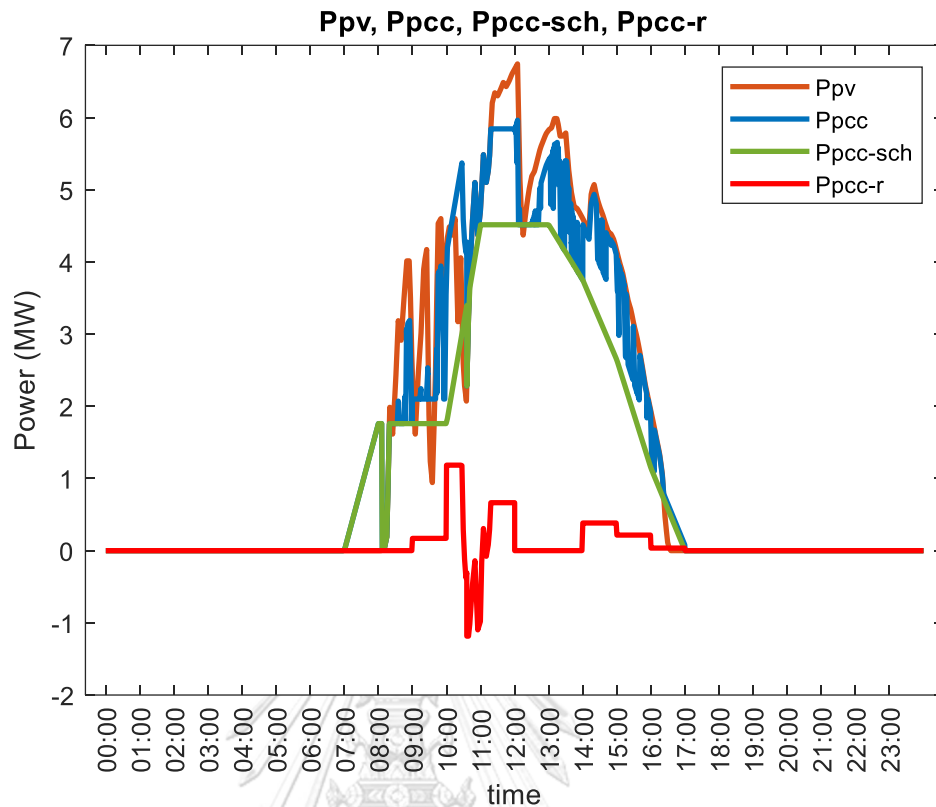


Figure 6-11  $P_{pcc}$  Profile on day 2.

## 6.2 System Frequency Performance Evaluation

This study aims to investigate the impact of PV power injects on the network with different strategies on frequency deviation in a high PV penetration network.

### 6.2.1 System Frequency Improvement

The study simulates the model explained in section 6.1 for 1 year. The PV power with difference strategies inject power to the system model at a high PV penetration level (0.4 PVL), the system frequency deviation of each case is observed.

The example of system frequency corresponds with 4 strategies for 7 days is shown in Figure 6-12.

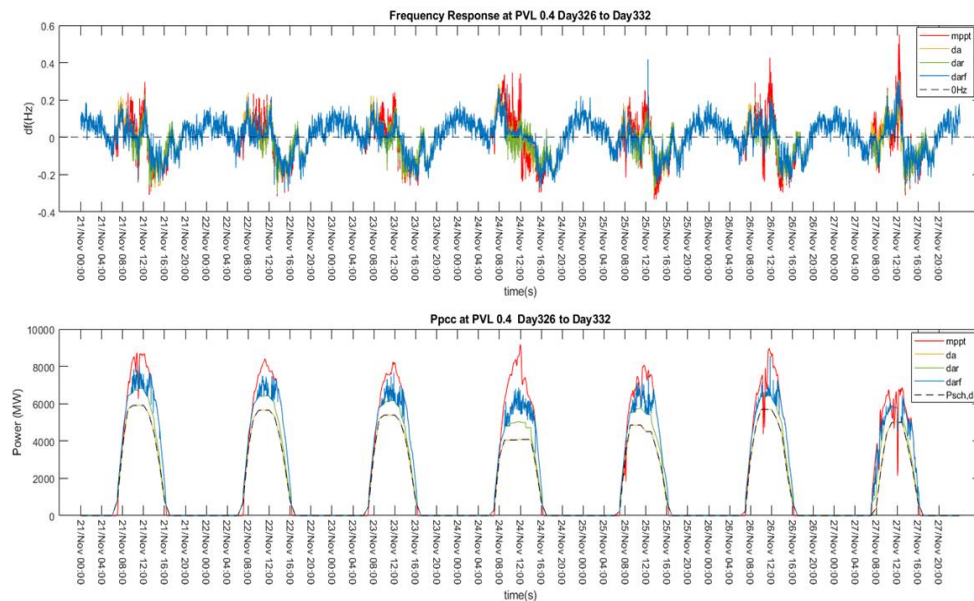


Figure 6-12 7-Day Frequency profile at 0.4 PVL.

Frequency of mppt swings larger than other cases during the day. The power of da and dar is lower than mppt but smoother. In contrast, the power of darf has high fluctuation due to provide FSC.

This following section compares the frequency deviation profile between the example frequency profile at 0.4 PVL of clear-sky day in Figure 6-13 and rainy-sky day in Figure 6-14.

### 6.2.1.1 On Clear-Sky Day

The prediction of solar power is accurate on a clear-sky day. Scheduled components (DSC and LRC) can be served to the grid as a plan. The system frequency performance of all strategies swings in the normal range ( $\pm 0.5\text{Hz}$ ), as shown in Figure 6-13.

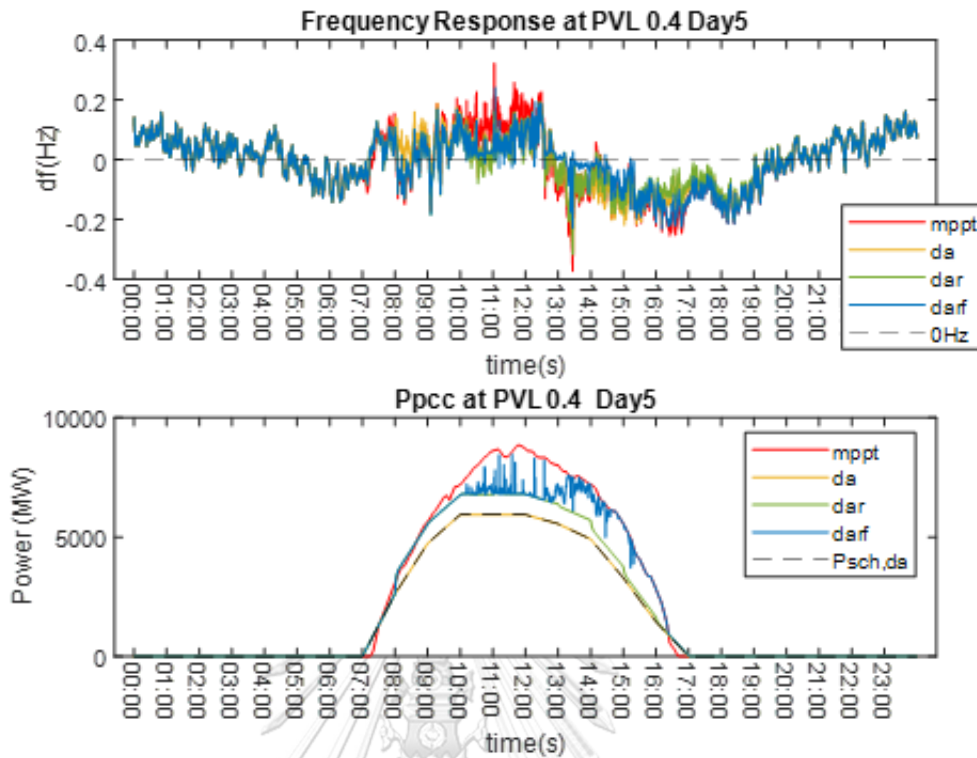


Figure 6-13 Frequency profile on the clear-sky day.

### 6.2.1.2 On Rainy-Sky Day

On rainy-sky day, the day-ahead solar power forecast can be inaccurate, as shown in Figure 6-14 and can lead large unserved power in da, dar, and darf. The system loses a large generation, and system frequency severely drops around 3.5Hz. Even though it can be recovered in this simulation, this event in real-world applications can not be accepted. To compromise this issue, it is suggested that the system operator should allow PVPP reschedule near real-time to avoid large unserved power or improve PVPP operation to mitigate sudden unserved power.

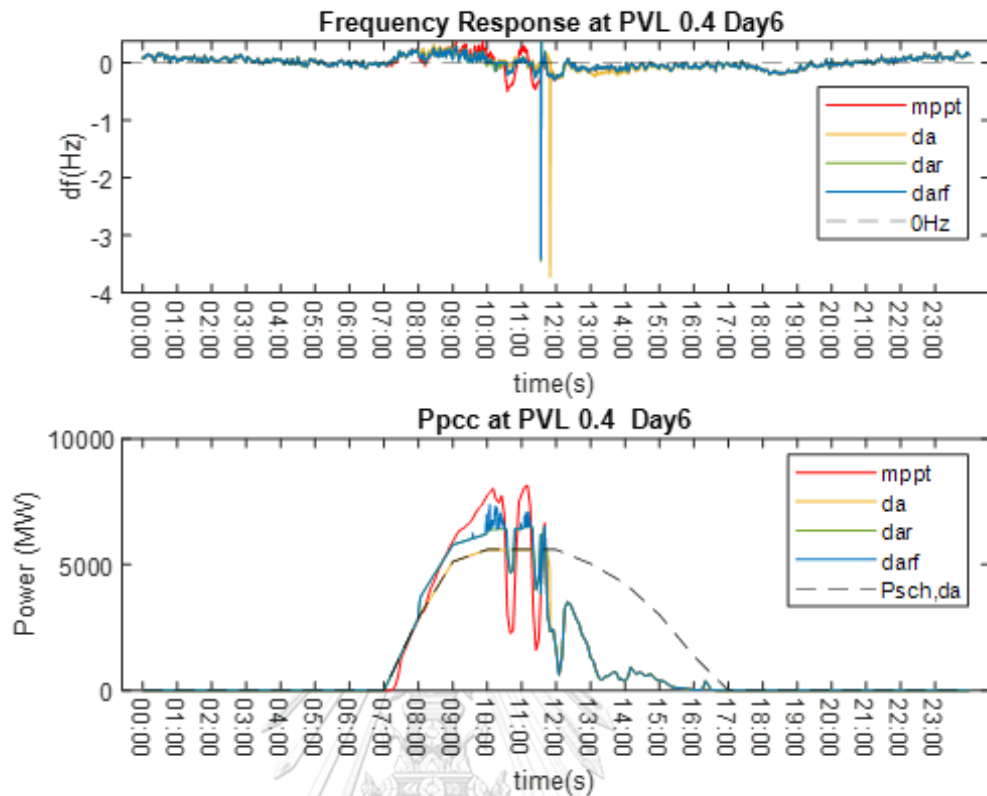


Figure 6-14 Frequency profile on the rainy-sky day.

### 6.2.2 Sudden Unserve Mitigation

The sudden unserved event occurs because PVPP tries to inject power to catch up with the scheduled power without considering the remaining reserve. The large schedule error both DSC and LRC correspond with an insufficient reserve can lead severe under generation on the power system, as shown in Figure 6-14.

The scheduled power relies on solar power forecast information that can not give the clue of an unexpected large error event. To deal with uncertainty, the dispatch strategy should be improved to secure the reserve for preventing large sudden insufficient energy by adding the adaptive BES power algorithm, as described in the following section.



### 6.2.2.1 Adaptive BES Power Algorithm (ABA)

The sudden large unserved power from PVPP can lead to a large disturbance to the network. To prevent sudden depletion of BES energy, the remaining BES energy every moment should be secured to handle the continuous constant discharge for a specific duration. The estimated secure reserve energy ( $\tilde{E}_{b,secure}$ ) can be calculated by equation 6-2.

$$\tilde{E}_{b,secure}(t) = P_b^*(t) \times T_{secure} \quad 6-2$$

where,  $P_b^*$  is the BES power command.  $T_{secure}$  is the defined secure duration that BES can continuously constant discharge equal to  $P_{b,cmd}$ .  $\tilde{E}_{b,secure}$  is estimated secure reserve energy and changed all the time depend on  $P_{bd,cmd}$ .

If the remaining BES energy at present ( $E_b(t)$ ) is less than the estimated secure reserve energy ( $\tilde{E}_{b,secure}$ ), the discharge power command ( $P_b^*(t)$ ) is adapted to a suitable level, as shown in equation 6-3.

$$\tilde{P}_b^*(t) = \frac{E_b(t)}{T_{secure}}, \text{ if } E_b(t) \leq \tilde{E}_{b,secure} \quad 6-3$$

where,  $\tilde{P}_b^*$  is adapted BES power command corresponds with the current remaining BES energy ( $E_b(t)$ ) and defined security duration ( $T_{secure}$ ). If continuous constant discharge power duration is not more than  $T_{secure}$ . This algorithm can guarantee sufficient support energy within this defined period.

### 6.2.2.2 Test Results

The study carries on the same model described in section 6.1 by adding an adaptive BES power algorithm (ABA) to each dispatch strategy controller.  $T_{\text{secure}}$  is set at 1 hour. The example result of the impact of ABA on the frequency profile on the rainy-sky day is shown below.

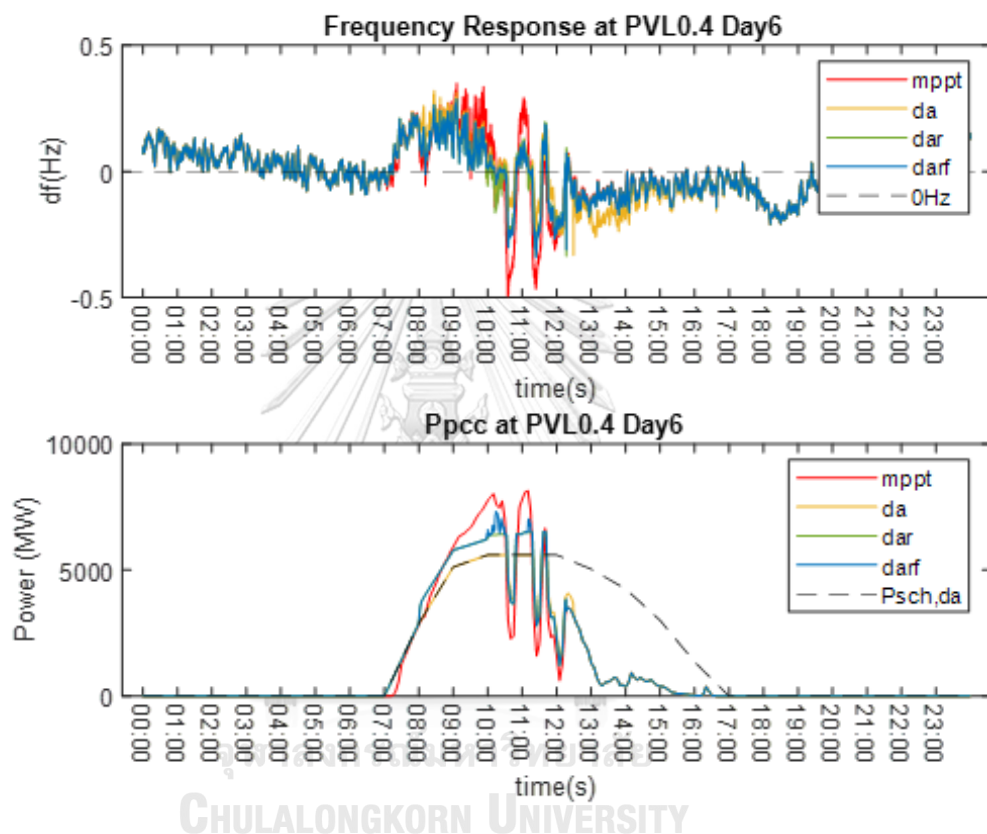


Figure 6-15 Rainy-sky frequency profile of sudden unserve mitigation on day 6

From Figure 6-15, it can be seen that there is no spike of frequency deviation due to unserved power, as shown in Figure 6-14 before adding ABA. Although the adaptive BES algorithm (ABA) can reduce sudden unserved power, the PVPP power of each case still can not catch up scheduled power.

From Figure 6-16, it can be seen that the discharge power value is not over the BES energy value when setting  $T_{\text{secure}}$  at 1 hour. This can guarantee the reserve at that moment for continuous constant discharge power into the grid for 1 hour.

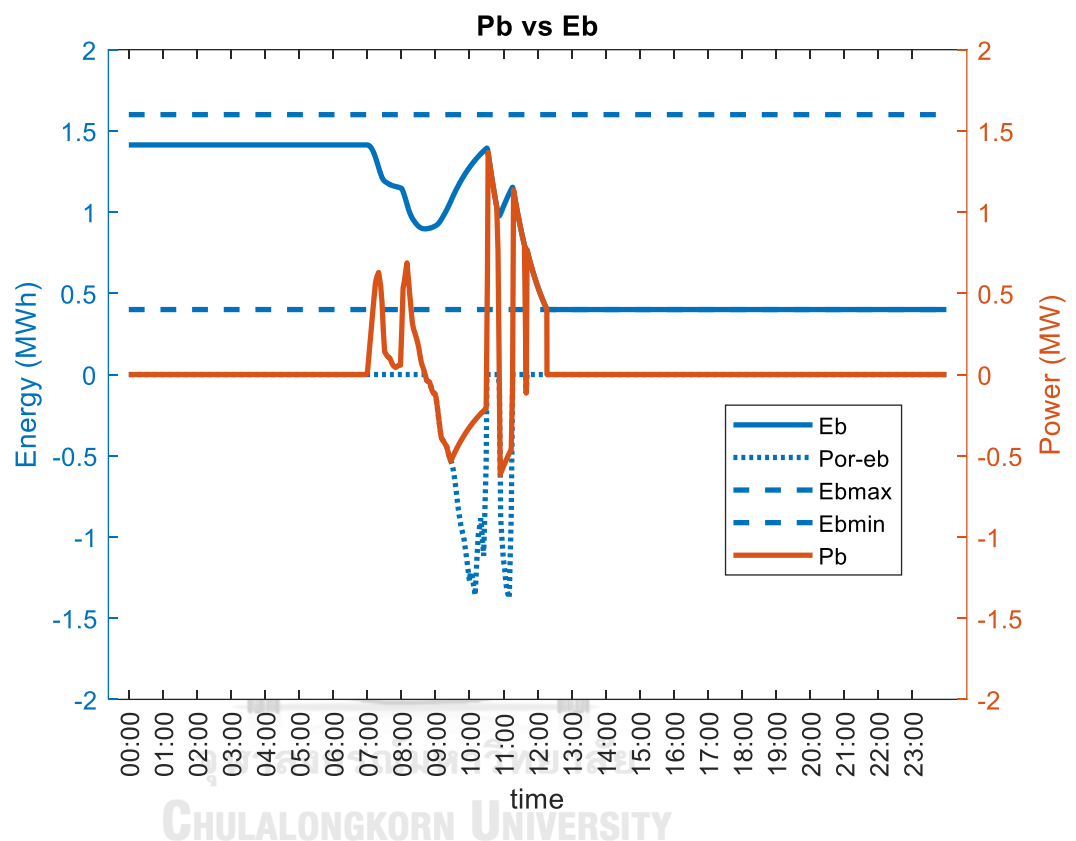


Figure 6-16 Rainy-sky BES profile of sudden unserve mitigation at day 6

From Figure 6-17, it shows each component power of daft. Only in the morning, BES has enough energy to compensate insufficient for scheduled power. The LRC is a negative value the entire day; however, the PVPP provides negative LRC excess the command because of unserved power. Even though the unserved power of LRC does not lead spike of frequency deviation, it still increases the burden to other

generators to compensate for excess negative LRC coming from PVPP. BRC or BES power swings correspond with the insufficient and excess PV power. When excess PV power occurs, it is charged into BES before assigning the remaining power to FSC.

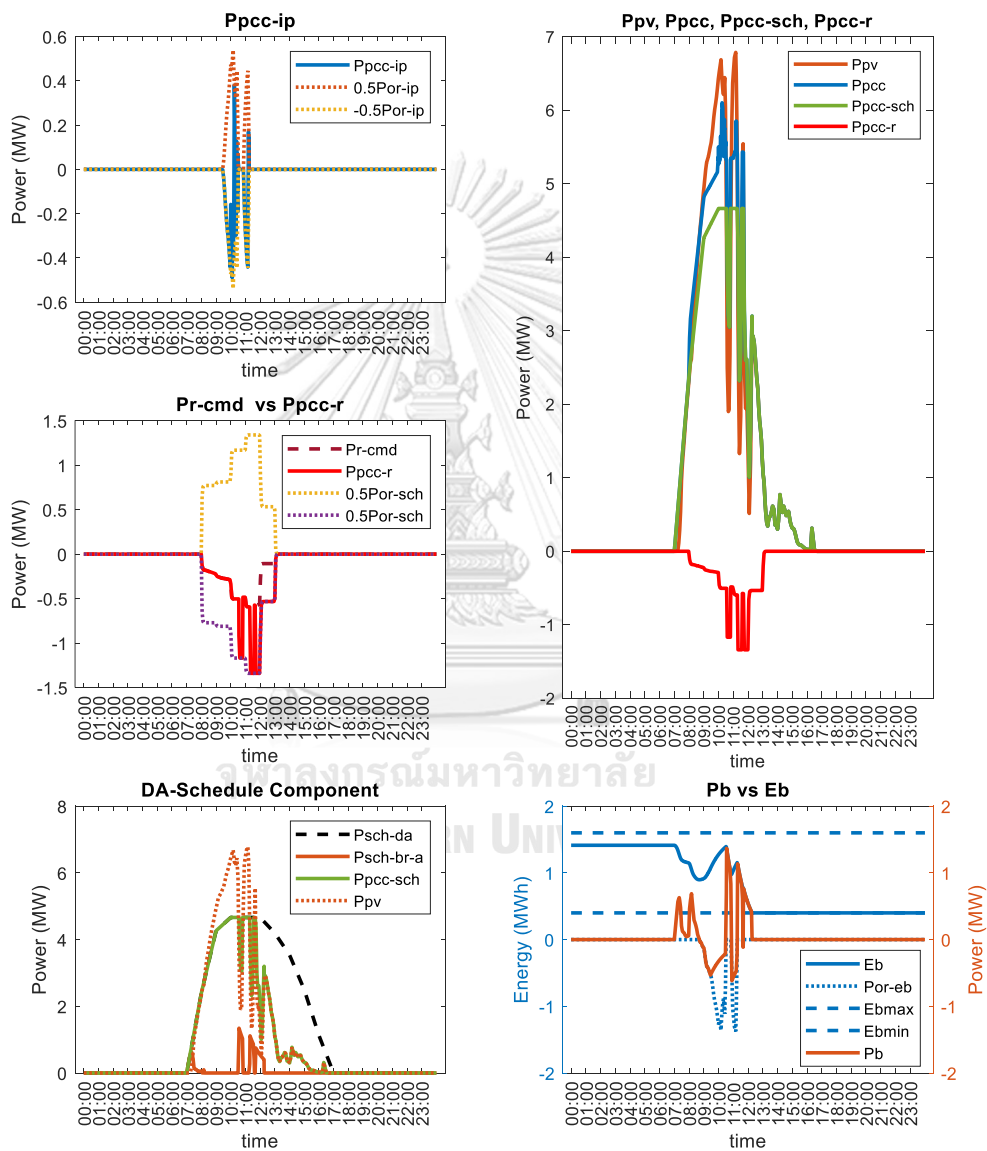


Figure 6-17 Rainy-sky power profile of sudden unserve mitigation on day 6

Note that, LRC value entire year before adding ABA is positive during schedule operating reserve duration because of often sudden unserved power leads frequency under generation event. After adding ABA, the LRC value entire year during schedule operating reserve duration turn to negative because there is a great reduction of sudden unserved power and only has the effect of the rise of PV generation that leads over generation event.

### 6.3 Dispatch Strategy Performance Evaluation

The order of case studies represents the development of dispatch strategies from the base case (mppt) to the proposed grid-friendly strategy (darf), as shown below.

1. mppt: PVPP provides maximum power (no control requirement).
2. da: PVPP with BES provides DSC with BRC
3. dar: PVPP with BES provides DSC and LRC with BRC
4. darf: PVPP with BES provide DSC, LRC, and FSC with BRC.

The mppt represents a non-considering grid impact dispatch strategy at a low PV penetration ratio network. The da represents a low-impact dispatch strategy that can schedule the smoother day-ahead PV power. The dar represents PVPP that can provide scheduled ancillary service to the grid as load frequency regulation. The darf represents the proposed grid-friendly dispatch strategy (GFDS), which develops from dar to return curtailment to the grid wisely as inertia and primary response support.

The energy component ratio in each case can be shown in Figure 6-18. Note that the operating baseline power ( $0.5P_{or,sch}^*$  and  $0.5P_{or,ip}$ ) are

excluded from  $P_{pcc,r}$  and  $P_{pcc,ip}$ , respectively to include the benefit of downward regulation energy instead of computing  $E_{pcc,r}$  and  $E_{pcc,ip}$ .

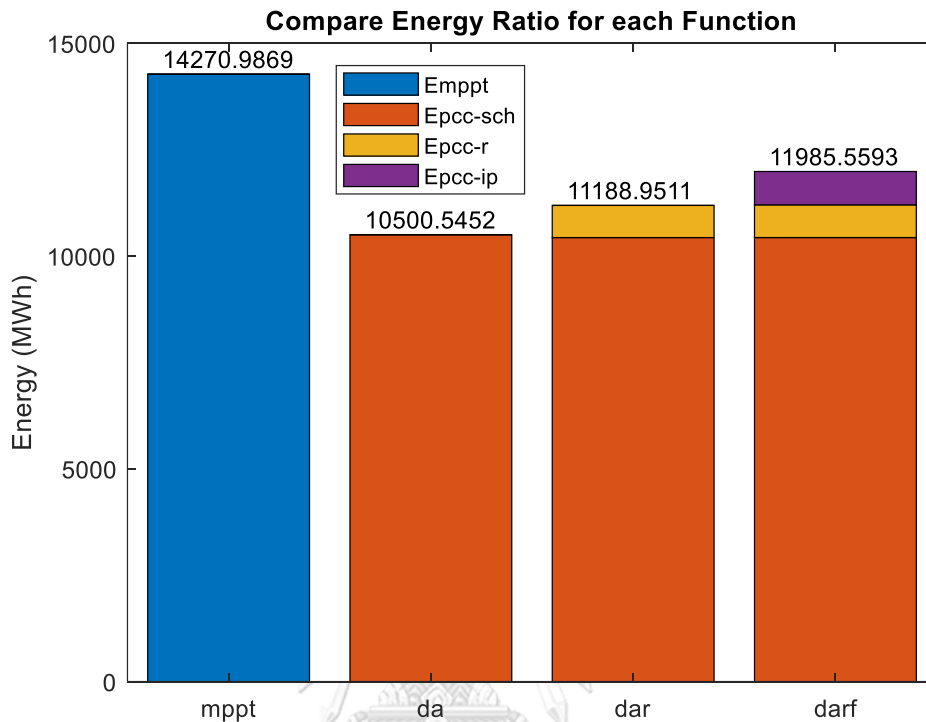


Figure 6-18 Energy ratio comparison.

Form Figure 6-18, mppt shows 100% of the solar resource. While da only provides DSC that leads to high curtailment. dar and darf utilize excess power of da for grid benefit and get revenue back by selling  $E_{pcc,r}$ .  $E_{pcc,ip}$  is not reliable; thus, it returns to the grid for free if excess energy is remaining after providing other components. The curtailment can be reduced from da if PVPP provides additional components. The lowest curtailment or maximum PV utilization is darf that using a grid-friendly dispatch strategy (GFDS).

### 6.3.1 Owner Benefit

The owner benefit of each case is shown in Table 6-2.

Table 6-2 Owner benefit indexes.

Evaluation Index	mppt	da	dar	darf
Rev (\$)	388599	285929	353430	353491
PUF (%)	100	74.10	74.30	93.69
SOH (%)	100	83.79	78.08	78.94

It can expect that mppt receives the highest Rev and PUF because there is no additional service and no need to curtail power. The Rev of darf and dar are second rank and both comparatively equal because darf gives FSC for free. The ratio of Rev between darf and mppt is 90.96%, which means the revenue of darf is reduced by only 9.04%. At the same time, the lowest revenue case is da with the reduction of revenue for 26.42% from mppt because da provides only one power component.

The rank of PUF is sorted from low to high by the following order, da, dar,darf, and mppt. PUF of darf is developed from da and can reach 93.69% from 74.10%. In other words, the waste of PV utilization of darf compared to da is reduced by 19.59%. In this study, dar has lower PUF than the expectation because of the negative LRC due to the over frequency event coming from injecting a large amount of PV power to the network. However, the revenue of dar is high as darf because it receives income from an operational reserve.

SOH indicates the remaining BES lifetime and reflects the usage cycle of BES. The higher value of SOH means the higher remaining lifetime due to lower cycle BES usage. Even though there is no BES in mppt,

SOH of mppt is set to be 100% compared to other cases because it has no BES cycle usage of BES in mppt. The SOH of dar and darf are comparatively equal but less than da because BES cycle usage of dar and darf are higher to compensate additional load frequency regulation component.

If using BES at the same size (2 MWh) provides only FSC (inertia and primary response) instead of iR, the SOH in this case is 53.52% lower than 78.94% of darf. Thus, this method can prevent the BES degradation by 25.42%.

### 6.3.2 Grid Benefit

The system operator can lose its benefit if PVPP cannot provide power to follow the committed power. Even though da, dar, and darf can provide more reliable power than mppt, they still have uncertainty and may not reach the commitment power. The compliance index of providing DSC and LRC can be shown in Table 6-3.

Table 6-3 DCI and LCI indexes.

Evaluation Index	mppt	da	dar	darf
DCI (%)	-	94.91	94.30	94.30
LCI (%)	-	-	73.81	73.88

DCI of da, dar, and darf is comparatively equal that means providing DSC, LRC, and FSR are not impact to DCI. While, LCI with 1  $r_{ha}$  is round 73.81% while DCI with 0.8  $r_{da}$  is around 94.30%. It means that a higher reduction factor (low iR) reduces the power compliance index. The compliance standard for PVPP might be defined by SO as a



connection code. If the compliance standard of LCI is over 95%, the reduction factor should be adjusted until LCI can follow the standard.

FDI indicates the mean absolute one-minute average frequency deviation with respect to nominal frequency ( $f_n$ ). The lower FDI is the better frequency performance for the network. The result of 1 year FDI is shown in Table 6-4.

Table 6-4 FDI of 1-year frequency at 0.4 PVL.

Evaluation Index	mppt	da	dar	darf
FDI (mHz)	84.85	73.69	73.53	70.76

From Table 6-4, it can be seen that the FDI of da and dar can reduce FDI from mppt around 13.3% because the scheduled PV power can reduce uncertainty and fluctuation. Even though PVPP participates in providing LRC to the network, there is no significant improvement of FDI by additional LRC because the total frequency regulation value of the network is still the same value. Even though the FDI of da and dar is comparatively equal, dar can gain more revenue from selling LRC.

FDI of darf has the best FDI performance because it can reduce the most amount of FDI among all cases compare to mppt around 16.6%. It can be suggested that PVPP should provide both DSC and FSC when integrating into the network.

### 6.3.3 Overall Comparison

The higher value of each index shows a better performance in each aspect, except FDI. In order to comparison in the same aspect (higher value is better) of other indexes, system frequency security improvement index (FSI) is used instead of FDI, as shown in the following equation.

$$FSI = \frac{FDI_{\max} - FDI}{FDI_{\max}} \times 100 \quad 6-4$$

where,  $FDI_{\max}$  and  $FDI_{\min}$  are the maximum and minimum FDI value of all cases.

A radar graph is chosen to compare the performance between strategies with many indexes, as shown below.

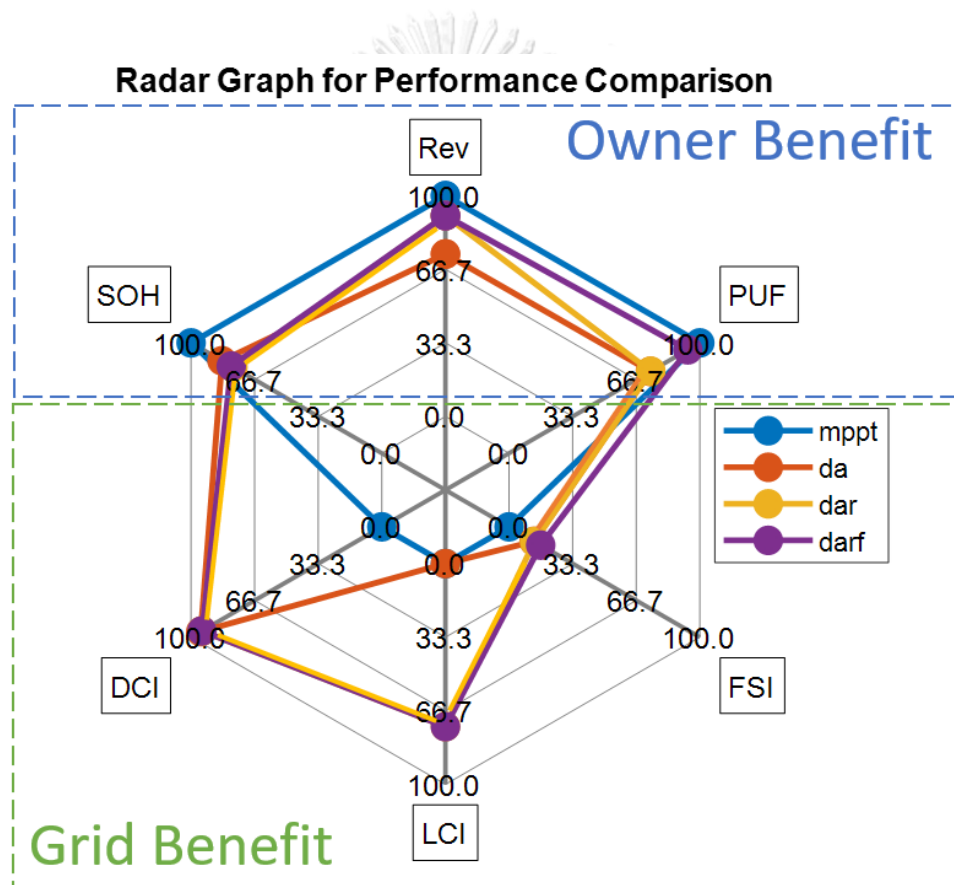


Figure 6-19 Radar graph for performance comparison

Figure 6-19 covers the owner and grid benefit contribution. The higher area shows a better performance of the strategy, which can provide benefits to both sides. Even mppt has the highest benefit on Rev and PUF, but it does not provide grid benefit. While da, dar, and darf can provide

grid benefit. When comparing holistic benefit, including both grid and owner benefit, the best performance of all cases is that using the proposed method (GFDS) because the area of this case is maximum in the radar chart.



# Chapter 7

## Conclusion

### 7.1 Conclusion

High PV penetration reduces system inertia and system ramp capability as a result in lower network stability tolerance, as shown in the simulation results of Chapter 4. The critical ramp capability obtained by the method in Chapter 4 can help system operators prepare sufficient system ramp capability to handle expected contingency.

This dissertation proposes a grid-friendly dispatch strategy (GFDS) to mitigate uncertainty and stability issues from PVPP while considering both grid and owner benefits, as described in Chapter 5. GFDS divides PV power at maximum power point into 4 components (DSC, LRC, BRC, and FSC) to satisfy the designed objective. DSC and LRC aim to sell more reliable power and operating reserve for load frequency regulation, respectively. BRC aims to restore BES energy as a reserve for compensating mismatch power between scheduled and actual power. FSC aims to reduce frequency deviation by the remaining power instead of curtailment. The results show that PVPP with GFDS can utilize resources for providing both owner and grid benefit.

For owner benefit, GFDS can give proper resource utilization for PVPP with BES. Curtailment can be reduced by assigning excess scheduled PV power for FSC. Furthermore, GFDS does not force BES to change rapidly for FSC. It assigns BES for compensating error from DSC and LRC with a lower operation cycle, instead. Thus, it is expected that BES degradation can be reduced.

For grid benefit, GFDS can reduce frequency deviation at low system inertia because it makes PVPP providing more smooth and reliable power as DSC, providing load frequency regulation as LRC and providing frequency support as FRC. Besides, it can compromise between the scheduled power and remaining reserve by adaptive BES power (ABA) to reduce sudden large unserved power. Even though the revenue of PVPP with GFDS compare to PVPP with MPPT is reduced, the integration to the network is better. The reduction of revenue can be seen as the cost of integration or the contribution for system synchronization.

In summary, the greener power system network of high PV penetration with healthy stability can be achieved by improving the PVPP dispatch strategy. The proposed GFDS is the one solution of many strategies that try to compromise owner and grid benefit with a good result.

## **7.2 Recommended Future Works**

There are rooms to increase revenue and reliability by improving solar power forecast accuracy and the dispatch strategy. The stochastic optimization and day ahead re-schedule with higher accuracy of solar power forecast might improve both issues. There is also room of improvement in frequency system security index (FSI) due to GFDS implementation in PVPP.

ABA can prevent the spike of frequency deviation base on the assumption that other fast-reacting resources are adequate for handling the reduced unserved power. Further study should consider re-dispatch of other generation resources to prevent unexpected large unserve event.



**Appendix A**

จุฬาลงกรณ์มหาวิทยาลัย  
CHULALONGKORN UNIVERSITY

### Test System Information

Test System is composed of PVPP with BES. This plant connects to the power network.

The specification of BES could be shown in Table A-1. 1-C rate is chosen with 20% of  $Cap_{PV}$  power output to compensate 20% solar power forecast error.

Table A-1 Battery energy storage (BES) parameters.

Parameters	Value
BES Capacity ( $Cap_{bat}$ )	2MW/2MWh
Maximum State of Charge ( $SOC_{max}$ )	20%
Minimum State of Charge ( $SOC_{min}$ )	80%
Discharge Efficiency	90%
Charge Efficiency	90%
Maximum BES Discharge Output ( $P_{bd,max}$ )	2 MW
Minimum BES Discharge Output ( $P_{b,min}$ )	0 MW
Maximum BES Charge Output ( $P_{bc,max}$ )	2 MW
Minimum BES Charge Output ( $P_{bc,min}$ )	0 MW

PVPP parameters could be shown in Table A-2.

Table A-2 PV power plant (PVPP) parameters.

Parameters	Value
PV Capacity ( $Cap_{PV}$ )	10 MW
Maximum PV Output ( $P_{PCC,max}$ )	10 MW
Minimum PV Output ( $P_{PCC,min}$ )	0 MW
Ramp Limit of $P_{pcc,sch}(R_{limit})$ [75]	0.1p.u./min

$R_{\text{limit}}$  is set equal to 0.1 p.u./min follow the standard of [75] and lower than critical ramp capability as shown in Figure 4-10 at 0.4 PVR of the sudden drop of 0.4 MRED PV power to prevent stability problem expected disturbance.

The specification of power system parameters could be shown in Table A-3.

Table A-3 Default values of network parameters [63].

Symbol	Meaning	Values
$H_0$	per unit system inertia	5 s
D	damping coefficient	0.8
$T_g$	governor time constant	0.2 s
$T_t$	turbine time constant	0.5 s
$\beta_0$	primary response gain	1/0.05
$K_s$	secondary response gain	0.005
$\alpha$	on-AGC ratio	0.5
RC	system ramp capability	0.1 p.u./min [86]

The simulation time step of input and output are shown in Table A-4.

Table A-4 Time step parameters.

Parameters	Value
System frequency time-step	1 s
Forecast PV power time step	60 min
PV power time step	5 min
Output time step	1 s



### Optimization Information

Price and the ramp cost coefficient are shown in Table A-5.

Table A-5 Price coefficients [100].

Parameters	Value
Hour-Ahead Capacity Price Coefficient ( $cp_{ha}$ )	20.31 \$/MW
Day-Ahead Energy Price Coefficient ( $ep_{da}$ )	27.23 \$/MWh
Non-Firm Energy Price Coefficient ( $ep_{nf}$ )	27.23 \$/MWh
Ramp Cost Coefficient ( $c_r$ )	27.23 \$/MW/h

To fairly compare non-firm PVPP with grid-friendly PVPP (GFPV), it is assumed that  $ep_{nf}$  is equal to  $ep_{da}$ .

Note:  $c_r$  could be arbitrarily chosen to adjust  $P_{sch,da}$  smoothness. For this simulation, it has valued equal to  $|ep_{da}|$ .

The reduction factor of day-ahead solar power forecast ( $r_{da}$ ) and hour ahead of the operating reserve ( $r_{ha}$ ) are set to be 0.8 and 1, respectively.

## REFERENCES



จุฬาลงกรณ์มหาวิทยาลัย  
**CHULALONGKORN UNIVERSITY**

1. Fu, R., D.J. Feldman, and R.M. Margolis, *US solar photovoltaic system cost benchmark: Q1 2018*. 2018.
2. IRENA, *Trends in Renewable Energy*. 2019.
3. Nathwani, J. and D.M. Kammen, *Affordable Energy for Humanity: A Global Movement to Support Universal Clean Energy Access*. Proceedings of the IEEE, 2019. **107**(9): p. 1780–1789-1780–1789.
4. Bueno, P.G., J.C. Hernández, and F.J. Ruiz-Rodriguez, *Stability assessment for transmission systems with large utility-scale photovoltaic units*. IET Renewable Power Generation, 2016. **10**(5): p. 584–597-584–597.
5. Flynn, D., et al., *Technical impacts of high penetration levels of wind power on power system stability*. Wiley Interdisciplinary Reviews: Energy and Environment, 2017. **6**(2): p. e216-e216.
6. Miller, N.W., et al., *Eastern frequency response study*. 2013.
7. You, S., et al., *Impact of high PV penetration on the inter-area oscillations in the US eastern interconnection*. IEEE Access, 2017. **5**: p. 4361–4369-4361–4369.
8. Hou, Q., et al., *Probabilistic duck curve in high PV penetration power system: Concept, modeling, and empirical analysis in China*. Applied Energy, 2019. **242**: p. 205–215-205–215.
9. Obi, M. and R. Bass, *Trends and challenges of grid-connected photovoltaic systems—A review*. Renewable and Sustainable Energy Reviews, 2016. **58**: p. 1082–1094-1082–1094.
10. Kundur, P., N.J. Balu, and M.G. Lauby, *Power system stability and control*. Vol. 7. 1994: McGraw-hill New York.
11. Wang, Q. and B.-M. Hodge, *Enhancing power system operational flexibility with flexible ramping products: A review*. IEEE Transactions on Industrial Informatics, 2016. **13**(4): p. 1652–1664-1652–1664.
12. Miller, N.W., M. Shao, and S. Venkataraman, *California ISO (CAISO) frequency response study*. GE Energy, 2011. **9**.
13. Miller, N.W., K. Clark, and M. Shao. *Frequency responsive wind plant controls: Impacts on grid performance*. in *2011 IEEE Power and Energy Society General Meeting*.
14. Lawrence, E.O. and J. Undrill, *Power and Frequency Control as it Relates to Wind-Powered Generation*. 2010.
15. Atae, S., et al. *Investigating the impacts of wind power contribution on the short-term frequency performance*. in *2014 Smart Grid Conference (SGC)*.
16. Seneviratne, C. and C. Ozansoy, *Frequency response due to a large generator loss with the increasing penetration of wind/PV*

- generation—A literature review. Renewable and Sustainable Energy Reviews, 2016. 57: p. 659–668-659–668.*
17. Correa-Posada, C.M., et al., *Dynamic ramping model including intraperiod ramp-rate changes in unit commitment. IEEE Transactions on Sustainable Energy, 2016. 8(1): p. 43–50-43–50.*
  18. Morales-España, G., et al., *Power-capacity and ramp-capability reserves for wind integration in power-based UC. IEEE Transactions on Sustainable Energy, 2015. 7(2): p. 614–624-614–624.*
  19. Wang, C., P.B.-S. Luh, and N. Navid, *Ramp requirement design for reliable and efficient integration of renewable energy. IEEE Transactions on Power Systems, 2017. 32(1): p. 562-571.*
  20. Uriarte, F.M., et al., *Microgrid ramp rates and the inertial stability margin. IEEE Transactions on Power Systems, 2015. 30(6): p. 3209–3216-3209–3216.*
  21. Antonanzas, J., et al., *Review of photovoltaic power forecasting. Solar Energy, 2016. 136: p. 78–111-78–111.*
  22. Cabrera-Tobar, A., et al., *Review of advanced grid requirements for the integration of large scale photovoltaic power plants in the transmission system. Renewable and Sustainable Energy Reviews, 2016. 62: p. 971–987-971–987.*
  23. De la Parra, I., et al., *Control strategies to use the minimum energy storage requirement for PV power ramp-rate control. Solar Energy, 2015. 111: p. 332–343-332–343.*
  24. Alam, M.J.E., K.M. Muttaqi, and D. Sutanto, *A novel approach for ramp-rate control of solar PV using energy storage to mitigate output fluctuations caused by cloud passing. IEEE Transactions on Energy Conversion, 2014. 29(2): p. 507–518-507–518.*
  25. Ellis, A., et al. *PV output smoothing with energy storage. in 2012 38th IEEE Photovoltaic Specialists Conference.*
  26. Wang, T., H. Kamath, and S. Willard, *Control and optimization of grid-tied photovoltaic storage systems using model predictive control. IEEE Transactions on Smart Grid, 2014. 5(2): p. 1010–1017-1010–1017.*
  27. Crăciun, B.-I., et al., *Power ramp limitation capabilities of large PV power plants with active power reserves. IEEE Transactions on Sustainable Energy, 2016. 8(2): p. 573–581-573–581.*
  28. Entsoe, *The Network Code on Requirements for Generators. 2016.*
  29. Etxegarai, A., et al., *Review of grid connection requirements for generation assets in weak power grids. Renewable and Sustainable Energy Reviews, 2015. 41: p. 1501–1514-1501–1514.*

30. Entsoe, *Frequency Containment Reserves (FCR)*.
31. Teleke, S., et al., *Rule-based control of battery energy storage for dispatching intermittent renewable sources*. IEEE Transactions on Sustainable Energy, 2010. **1**(3): p. 117–124-117–124.
32. Brenna, M., et al., *Energy Storage Control for Dispatching Photovoltaic Power*. IEEE Transactions on Smart Grid, 2018. **9**(4): p. 2419-2428.
33. Conte, F., et al., *Day-Ahead and Intra-Day Planning of Integrated BESS-PV Systems providing Frequency Regulation*. IEEE Transactions on Sustainable Energy, 2019.
34. Goggin, M., et al., *Customer Focused and Clean, Power Markets for the Future*. Wind Solar Alliance, 2018.
35. Mishra, S., et al., *Single-phase synchronverter for a grid-connected roof top photovoltaic system*. IET Renewable Power Generation, 2016. **10**(8): p. 1187-1194.
36. Zhong, C., Y. Zhou, and G. Yan, *A Novel Frequency Regulation Strategy for a PV System Based on the Curtailment Power-Current Curve Tracking Algorithm*. IEEE Access, 2020. **8**: p. 77701-77715.
37. Hoke, A.F., et al., *Rapid active power control of photovoltaic systems for grid frequency support*. IEEE Journal of Emerging and Selected Topics in Power Electronics, 2017. **5**(3): p. 1154-1163.
38. Zhong, C., et al., *Flexible power-point-tracking-based frequency regulation strategy for PV system*. IET Renewable Power Generation, 2020. **14**(10): p. 1797-1807.
39. Liang, L., Y. Hou, and D.J. Hill, *Design guidelines for MPC-based frequency regulation for islanded microgrids with storage, voltage, and ramping constraints*. IET Renewable Power Generation, 2017. **11**(8): p. 1200–1210-1200–1210.
40. Chen, S., et al., *Penetration rate and effectiveness studies of aggregated BESS for frequency regulation*. IEEE Transactions on Smart Grid, 2015. **7**(1): p. 167-177.
41. Xie, X., et al., *Improving AGC performance of coal-fueled thermal generators using multi-MW scale BESS: A practical application*. IEEE Transactions on Smart Grid, 2016. **9**(3): p. 1769-1777.
42. Ma, H., et al., *Optimal scheduling of an regional integrated energy system with energy storage systems for service regulation*. Energies, 2018. **11**(1): p. 195.
43. Bullich-Massagué, E., et al., *Active power control in a hybrid PV-storage power plant for frequency support*. Solar Energy, 2017. **144**: p. 49–62-49–62.

44. Yan, G., et al., *Novel adapted de-loading control strategy for PV generation participating in grid frequency regulation*. The Journal of Engineering, 2019. **2019**(16): p. 3383-3387.
45. Xin, H., et al., *A new frequency regulation strategy for photovoltaic systems without energy storage*. IEEE Transactions on Sustainable Energy, 2013. **4**(4): p. 985-993.
46. Akram, U., et al., *A review on rapid responsive energy storage technologies for frequency regulation in modern power systems*. Renewable and Sustainable Energy Reviews, 2020. **120**: p. 109626-109626.
47. Cabrera-Tobar, A., et al., *Active and reactive power control of a PV generator for grid code compliance*. Energies, 2019. **12**(20): p. 3872-3872.
48. Hu, Z., *Energy Storage for Power System Planning and Operation*. 2020: John Wiley & Sons.
49. Chowdhury, B.H. and S. Rahman, *A review of recent advances in economic dispatch*. IEEE transactions on power systems, 1990. **5**(4): p. 1248–1259-1248–1259.
50. Lorca, A. and X.A. Sun, *Adaptive robust optimization with dynamic uncertainty sets for multi-period economic dispatch under significant wind*. IEEE Transactions on Power Systems, 2014. **30**(4): p. 1702-1713.
51. Foley, A.M., et al., *Current methods and advances in forecasting of wind power generation*. Renewable Energy, 2012. **37**(1): p. 1-8.
52. Wang, Z., C. Shen, and F. Liu, *A conditional model of wind power forecast errors and its application in scenario generation*. Applied energy, 2018. **212**: p. 771-785.
53. Zhang, S., et al. *Robust optimization method based on scenario analysis for unit commitment considering wind uncertainties*. in *2011 Ieee Power and Energy Society General Meeting*. 2011. IEEE.
54. Sharma, K.C., P. Jain, and R. Bhakar, *Wind power scenario generation and reduction in stochastic programming framework*. Electric Power Components and Systems, 2013. **41**(3): p. 271-285.
55. Miñambres-Marcos, V.c.M., et al., *A grid connected photovoltaic inverter with battery-supercapacitor hybrid energy storage*. Sensors, 2017. **17**(8): p. 1856-1856.
56. Donnellan, B.J., D.J. Vowles, and W.L. Soong. *A review of energy storage and its application in power systems*. in *2015 Australasian Universities Power Engineering Conference (AUPEC)*.

57. Jiang, W., et al., *Research on power sharing strategy of hybrid energy storage system in photovoltaic power station based on multi-objective optimisation*. IET Renewable Power Generation, 2016. **10**(5): p. 575–583-575–583.
58. Wu, D., et al., *Autonomous active power control for islanded ac microgrids with photovoltaic generation and energy storage system*. IEEE Transactions on energy conversion, 2014. **29**(4): p. 882–892-882–892.
59. Perez, E., et al., *Predictive power control for PV plants with energy storage*. IEEE Transactions on Sustainable Energy, 2012. **4**(2): p. 482–490-482–490.
60. Marcos, J., et al., *Storage requirements for PV power ramp-rate control*. Solar Energy, 2014. **99**: p. 28–35-28–35.
61. Daud, M.Z., et al., *Heuristic optimization of state-of-charge feedback controller parameters for output power dispatch of hybrid photovoltaic/battery energy storage system*. Measurement, 2014. **49**: p. 15–25-15–25.
62. Li, X., et al., *Application of fuzzy wavelet transform to smooth wind/PV hybrid power system output with battery energy storage system*. Energy Procedia, 2011. **12**: p. 994–1001-994–1001.
63. Saadat, H., *Power system analysis*. 1999: McGraw-hill companies.
64. Zheng, Q., et al. *Overview of grid codes for photovoltaic integration*. in *2017 IEEE Conference on Energy Internet and Energy System Integration (EI2)*.
65. Nanou, S.I., A.G. Papakonstantinou, and S.A. Papathanassiou, *A generic model of two-stage grid-connected PV systems with primary frequency response and inertia emulation*. Electric Power Systems Research, 2015. **127**: p. 186–196-186–196.
66. EGAT, *EGAT Connection Code 2019*. 2019.
67. Greenwood, D.M., et al., *Frequency response services designed for energy storage*. Applied Energy, 2017. **203**: p. 115–127-115–127.
68. Dowling, A.W. and V.M. Zavala, *Economic opportunities for industrial systems from frequency regulation markets*. Computers & Chemical Engineering, 2018. **114**: p. 254–264-254–264.
69. Grid, N., *Enhanced frequency response*. 2016.
70. Cui, M., et al., *Characterizing and analyzing ramping events in wind power, solar power, load, and netload*. Renewable energy, 2017. **111**: p. 227–244-227–244.
71. Kakimoto, N., et al., *Ramp-rate control of photovoltaic generator with electric double-layer capacitor*. IEEE Transactions on Energy Conversion, 2009. **24**(2): p. 465–473-465–473.

72. Akatsuka, M., et al. *Estimation of battery capacity for suppression of a PV power plant output fluctuation*. in *2010 35th IEEE Photovoltaic Specialists Conference*.
73. Tesfahunegn, S.G., et al., *PV fluctuation balancing using hydrogen storage—a smoothing method for integration of PV generation into the utility grid*. *Energy Procedia*, 2011. **12**: p. 1015–1022-1015–1022.
74. Sukumar, S., et al., *Ramp-rate control approach based on dynamic smoothing parameter to mitigate solar PV output fluctuations*. *International Journal of Electrical Power & Energy Systems*, 2018. **96**: p. 296–305-296–305.
75. Noone, B., *PV integration on Australian distribution networks*. The Australian PV Association, UNSW, Australia, 2013.
76. PEA, *Regulation on the Power Network System Interconnection Code*. 2016.
77. Rodrigues, E.M.G., et al., *Grid code reinforcements for deeper renewable generation in insular energy systems*. *Renewable and Sustainable Energy Reviews*, 2016. **53**: p. 163–177-163–177.
78. On, E., *Grid code high and extra high voltage*. Requirements on generating plants, 2015.
79. Shi, G., *A Data Driven Approach to Solar Generation Forecasting*. 2017.
80. DiOrio, N., P. Denholm, and W.B. Hobbs, *A model for evaluating the configuration and dispatch of PV plus battery power plants*. *Applied Energy*, 2020. **262**: p. 114465-114465.
81. Ahmadian, A., et al., *Plug-in electric vehicle batteries degradation modeling for smart grid studies: Review, assessment and conceptual framework*. *Renewable and Sustainable Energy Reviews*, 2018. **81**: p. 2609–2624-2609–2624.
82. Young, K., et al., *Electric vehicle battery technologies*, in *Electric vehicle integration into modern power networks*. 2013, Springer. p. 15–56-15–56.
83. You, S., et al., *Comparative Assessment of Tactics to Improve Primary Frequency Response Without Curtailing Solar Output in High Photovoltaic Interconnection Grids*. *IEEE Transactions on Sustainable Energy*, 2018. **10**(2): p. 718–728-718–728.
84. Wang, Y., V. Silva, and M. Lopez-Botet-Zulueta, *Impact of high penetration of variable renewable generation on frequency dynamics in the continental Europe interconnected system*. *IET Renewable Power Generation*, 2016. **10**(1): p. 10–16-10–16.



85. Yan, R., T.K. Saha, and others, *A new tool to estimate maximum wind power penetration level: In perspective of frequency response adequacy*. Applied energy, 2015. **154**: p. 209–220-209–220.
86. Pan, C.T. and C.M. Liaw, *An adaptive controller for power system load-frequency control*. IEEE Transactions on Power Systems, 1989. **4**(1): p. 122–128-122–128.
87. Ploskas, N. and N. Samaras, *Linear Programming Using MATLAB*. 2017: Springer.
88. MATLAB. *Linear Programming Algorithms*. [cited 2020 17 August]; Available from: <https://www.mathworks.com/help/optim/ug/linear-programming-algorithms.html>.
89. Eto, J.H., *Use of frequency response metrics to assess the planning and operating requirements for reliable integration of variable renewable generation*. 2011.
90. Saadat, H., *Power system analysis*. Vol. 232. 1999: WCB/McGraw-Hill Singapore.
91. Tran, D. and A.M. Khambadkone, *Energy management for lifetime extension of energy storage system in micro-grid applications*. IEEE Transactions on Smart Grid, 2013. **4**(3): p. 1289-1296.
92. Koller, M., et al. *Defining a degradation cost function for optimal control of a battery energy storage system*. in *2013 IEEE Grenoble Conference*. 2013. IEEE.
93. Musallam, M. and C.M. Johnson, *An efficient implementation of the rainflow counting algorithm for life consumption estimation*. IEEE Transactions on reliability, 2012. **61**(4): p. 978-986.
94. He, G., et al., *Optimal bidding strategy of battery storage in power markets considering performance-based regulation and battery cycle life*. IEEE Transactions on Smart Grid, 2015. **7**(5): p. 2359-2367.
95. Xu, B., et al., *Factoring the cycle aging cost of batteries participating in electricity markets*. IEEE Transactions on Power Systems, 2017. **33**(2): p. 2248-2259.
96. Yao, M., R.R. Shoults, and R. Kelm, *AGC logic based on NERC's new control performance standard and disturbance control standard*. IEEE Transactions on Power Systems, 2000. **15**(2): p. 852-857.
97. NREL, *Solar Power Data for Integration Studies*. 2006, NREL.
98. PEA, *load profile*. 2019.
99. National grid, E.S.O., *Historic frequency data*. 2019, national grid ESO.

100. Monitoring Analytics, L.L.C., *State of the Market Report for PJM*. 2019.



## VITA

**NAME** Sarute Srisontisuk

**DATE OF BIRTH** 17 May 1988

**PLACE OF BIRTH** Khonkaen

**INSTITUTIONS ATTENDED** Chulalongkorn University

**HOME ADDRESS** 191/59 Decah Village Soi.9  
Maliwan Rd. Muang District  
Khonkaen 40000

**PUBLICATION**

1. S. Srisontisuk and N. Hoonchareon, "PV and Battery Sizing for User's Defined Energy Independence", Auckland, New Zealand, 7th of Conference of ISGT ASIA , December 2017.
2. S. Nitisanon, S. Srisontisuk and N. Hoonchareon, "Modeling of Solar PV Generation System Using Artificial Neural Network", Chulalongkorn University, Bangkok, Thailand, IEEJ P&ES-IEEE PES Joint Symposium, March 2016.